DEVELOPMENT OF RAPID LABEL-FREE CELLS DISCRIMINATOR FOR DENGUE-INFECTED HEPATIC CELLS UTILIZING DIELECTROPHORESIS

BASHAR MOHAMMED SHAHER YAFOUZ

FACULTY OF ENGINEERING
UNIVERSITY OF MALAYA
KUALA LUMPUR

2016

DEVELOPMENT OF RAPID LABEL-FREE CELLS DISCRIMINATOR FOR DENGUE-INFECTED HEPATIC CELLS UTILIZING DIELECTROPHORESIS

BASHAR MOHAMMED SHAHER YAFOUZ

THESIS SUBMITTED IN FULFILMENT OF THE REQUIREMENTS FOR THE DEGREE OF DOCTOR OF PHILOSOPHY

FACULTY OF ENGINEERING
UNIVERSITY OF MALAYA
KUALA LUMPUR

2016

UNIVERSITY OF MALAYA

ORIGINAL LITERARY WORK DECLARATION

Name of Candidate: BASHAR MOHAMMED SHAHER YAFOUZ

Registration/Matric No: KHA110073

Name of Degree: Doctor of Philosophy

Title of Thesis: Development of Rapid Label-Free Cells Discriminator for Dengue-Infected Hepatic Cells Utilizing Dielectrophoresis

Field of Study: BioMEMS

I do solemnly and sincerely declare that:

(1) I am the sole author/writer of this Work;
(2) This Work is original;
(3) Any use of any work in which copyright exists was done by way of fair dealing and for permitted purposes and any excerpt or extract from, or reference to or reproduction of any copyright work has been disclosed expressly and sufficiently and the title of the Work and its authorship have been acknowledged in this Work;
(4) I do not have any actual knowledge nor do I ought reasonably to know that the making of this work constitutes an infringement of any copyright work;
(5) I hereby assign all and every rights in the copyright to this Work to the University of Malaya ("UM"), who henceforth shall be owner of the copyright in this Work and that any reproduction or use in any form or by any means whatsoever is prohibited without the written consent of UM having been first had and obtained;
(6) I am fully aware that if in the course of making this Work I have infringed any copyright whether intentionally or otherwise, I may be subject to legal action or any other action as may be determined by UM.

Candidate's Signature Date:

Subscribed and solemnly declared before,

Witness's Signature Date:

Name:

Designation:

ABSTRACT

This thesis presents the development of a label-free cell discriminator for dengue-infected cells using Dielectrophoresis (DEP). DEP, the induced movement of dielectric particles in a non-uniform electric field, has been used as a potential technique for the manipulation and separation of many biological samples without destructive consequences to the cell. Because cells of the same genotype in different physiological and pathological states have unique morphological and structural features, it is possible to differentiate normal and infected cells using their DEP responses. The proposed lab-on-a-chip platform consisted of five layers and employs microarray dot electrodes that utilize both positive and negative DEP effects. The geometry of the electrode design was optimized with numerical modeling using COMSOL Multiphysics 4.2a®. The testing and proof of feasibility for this device were performed by conducting size-dependent manipulation and separation experiments on 1, 5 and 15 μm polystyrene particles. A total of 120 samples (60 samples of normal WRL-68 cells and 60 samples of Dengue-infected WRL-68 cells) were used to conduct the DEP experiments to discriminate between normal and infected cells. The DEP responses of the cells were quantified by analyzing the light intensity shift of the captured images before and after the application of the electric field. The differences in dielectric properties between normal and infected cells were exploited by plotting a unique DEP spectrum for each set of cells and obtaining the DEP crossover frequency at which no resultant movement occurs to the cells in response to the DEP force.

ABSTRAK

Tesis ini membentangkan pembangunan satu sistem diskriminasi sel tanpa label untuk sel-sel yang dijangkiti denggi dengan menggunakan *Dielektroforesis* (*DEP*). *DEP*, pergerakan zarah dielektrik dalam medan elektrik yang tidak seragam, telah digunakan sebagai satu teknik yang berpotensi untuk manipulasi dan mengasingkan sampel-sampel biologi tanpa meninggalkan kesan kerosakan pada sel. Oleh sebab sel-sel genotip yang sama di dalam keadaan fisiologi dan patologi yang berbeza mempunyai ciri-ciri morfologi dan struktur yang unik, terdapat kemungkinan di mana teknik *DEP* boleh menunjukkan perbezaan antara sel-sel tersebut. Sistem yang dicadangkan ini terdiri daripada lima lapisan dan terdapat elektrod titik mikrotatasusunan yang menggunakan kedua-dua kesan *DEP* positif dan negatif. Geometri reka bentuk elektrod telah dioptimumkan menggunakan pemodelan berangka *COMSOL Multiphysics* 4.2a®. Ujian dan bukti kelayakan bagi peranti ini telah dilakukan dengan menjalankan eksperimen memanipulasi dan pengasingan zarah polistirena yang bergantung pada saiz 1, 5 dan 15 µm. Sebanyak 120 sampel (60 sampel normal sel, WRL-68 dan 60 sampel sel yang dijangkiti Denggi,WRL-68 sel) telah digunakan untuk menjalankan eksperimen DEP bagi tujuan membezakan antara sel-sel normal dan sel-sel yang dijangkiti. Maklumbalas *DEP* daripada sel-sel tersebut telah dinilai dengan menganalisis perubahan keamatan cahaya imej yang dirakam sebelum dan selepas penggunaan medan elektrik. Perbezaan sifat dielektrik antara sel-sel normal dan yang telah dijangkiti dieksploitasi dengan memplot spektrum *DEP* yang unik bagi setiap set sel, dan mendapatkan frekuensi titik silang *DEP* di mana tiada sebarang pergerakan yang berlaku oleh sel-sel semasa daya *DEP* dikenakan.

ACKNOWLEDGEMENTS

First and foremost, all praise belongs to Almighty Allah, the Lord of the Universe, who has enabled me to accomplish and complete this work successfully.

I would like to extend my sincere gratitude to my supervisors Prof. Ir. Dr. Fatimah Ibrahim and Associate Prof. Dr. Nahrizul Adib Kadri for their constant support, patience and constructive comments. The guidance you have bestowed has been truly beneficial beyond an academic perspective. You have provided many opportunities for me to expand my knowledge and experience that have been crucial to my academic career. You have challenged me and never let me settle for anything other than my best; for that I am grateful.

The constant support and encouragement my family has given throughout this process has been a blessing. I would like to thank my parents for their support in my pursuit of a PhD degree. The unconditioned love, support and encouragement of my wife has been my biggest motivation to finish this thesis. Therefore, I dedicate this work to them.

I would like to thank my fellow labmates in the Centre for Innovation in Medical Engineering (CIME). Time spent in the lab wouldn't have been as enjoyable without you. Specifically, I would like to thank Lina, Wisam and Gilbert.

Finally, I would like to acknowledge the University of Malaya High Impact Research Grant UM-MOHE UM.C/625/1/HIR/MOHE/05 from Ministry of Higher Education Malaysia (MOHE) for supporting my studies and research financially.

TABLE OF CONTENTS

LIST OF FIGURES

LIST OF TABLES

LIST OF SYMBOLS AND ABBREVIATIONS

AC	Alternative current
Ω	Angular frequency
DEP	Dielectrophoresis
F_{DEP}	Dieletrophoretic force
ε^*	Complex permittivity
σ_p	Conductivity of particle
σ_m	Conductivity of surrounding medium
CMIS	Cumulative Modal Intensity Shift
DMEM	Dulbecco's Modified Eagle's Medium
∇E	Electric field gradient
ELISA	Enzyme-linked immunosorbent assay
G	Gram
WRL-68	Hepatic fetal human epithelial cell line
ITO	Indium tin oxide
I_2	Iodine
LOC	Lab-on-a-chip
I	Light intensity shift
µm	Micrometer
mm	Millimeter
MOI	Multiplicity of infection
N	Number of pixels
ε_o	Permittivity of free space
ε_p	Permittivity of particle
ε_m	Permittivity of surrounding medium

PBS	Phosphate buffered saline
POC	Point-of-Care
PMMA	Polymethyl methacrylate
KCl	Potassium chloride
KI	Potassium iodide
R	Radius of particle
Re [K(ω)]	Real part of the Clausius-Mossotti factor
ROI	Region of interest
rpm	Revolutions per minute
3D	Three dimensional
2D	Two dimensional

LIST OF APPENDICES

CHAPTER 1: INTRODUCTION

1.1 Overview

The trend toward point-of-care (POC) systems has grown dramatically in the past two decades. New diagnostic tools are needed to meet the increasing demand for fast, reliable and cost-effective diagnostic devices. These new tools would replace currently available tests that can only be conducted in fully equipped diagnostic laboratories. Real-time test results from POC devices can lead to rapid therapeutic interventions and enhance patients' clinical outcomes (Ritzi-Lehnert, 2012).

Many research groups have proposed models for POC systems that are implemented in microfluidic-based platforms, based on a wide range of available technologies (Fang *et al.*, 2010; Ferguson *et al.*, 2011; Hsieh *et al.*, 2012; Sista *et al.*, 2008). Miniaturized laboratory equipment has been designed to achieve a better reaction efficiency and faster results, while being more portable and consuming fewer reagents.

One of the platforms used in microfluidic devices is the lab-on-a-chip (LOC) platform, which has great potential for use in automated bio-microfluidic diagnostic systems. Various diagnostic techniques have been employed to effectively integrate multiple microfluidic components into fully automated LOC systems that can perform sophisticated biomedical analyses (Haeberle *et al.*, 2012). Specifically, capillary driven microfluidics, multilayer soft lithography, multiphase microfluidics, electrowetting-on-dielectric mechanisms, electrokinetics, and centrifugal microfluidics are the platforms with the most potential for incorporating microfluidics into a variety of biomedical engineering applications (Sin *et al.*, 2011). Each approach has unique advantages and disadvantages. Dielectrophoresis (DEP) (in the category of electrokinetics) offers a number of positive features that many other available techniques are unable to provide. The advantages of DEP include non-invasiveness, high selectivity and efficacy on small

scales, label-free manipulation, low costs and well-established fabrication techniques (Pethig, 2010). DEP has proven to be a promising technique for the manipulation of micro and nanoscale objects, including cells, viruses, DNA, bacteria and proteins, in aqueous suspensions (Cheng *et al.*, 2009; del Moral Zamora *et al.*, 2015; Madiyar *et al.*, 2013; Sabuncu *et al.*, 2015; Sonnenberg *et al.*, 2014; Yahya *et al.*, 2014). However, very few studies have exploited the DEP technology to investigate the changes in the electrophysiological properties of virus-infected cells. The currently available diagnostic methods for viral diseases are virus isolation, nucleic acid detection, and antigen (NS1) or antibody (IgG or IgM) detection via enzyme-linked immunosorbent assay (ELISA) (WHO, 2014). Virus separation and nucleic acid detection are more sensitive and specific than ELISA, but these examinations are not commonly offered due to their high cost. Furthermore, ELISA requires bulky instruments and highly trained personnel to perform the test, and it takes time to obtain a result (Yager *et al.*, 2006). Therefore, the development of an inexpensive, accurate and rapid tool for diagnosing viral diseases is in high demand. The aim of this thesis is to develop an LOC platform to discriminate between normal and dengue-infected cells based on DEP in a step toward developing POC diagnostic devices for viral diseases.

Previous studies have shown that the physical and electrical properties of cells change when cells transform from a healthy to a pathological state (An *et al.*, 2009; Chandramohanadas *et al.*, 2011; Gascoyne *et al.*, 1997a; Li & Lim, 2011). This result is in line with the findings confirming a morphological alteration in cells after infection with the dengue virus (McCormick *et al.*, 2012; Wu *et al.*, 2000). Because cells of the same genotype in different physiological and pathological states have unique morphological and structural features, it is possible to discriminate between these cells using their DEP responses (Gascoyne *et al.*, 2002). The electrophysiological properties, namely conductivity and permittivity, of the cellular cytoplasm and membrane can be

used as biomarkers for detecting dengue virus. In the current project, an LOC platform based on microarray dot electrodes was developed and optimized to conduct the DEP experiments. Size-dependent manipulation and separation DEP experiments were conducted on mixtures of different-size polystyrene microparticles to test the proposed LOC platform. Furthermore, the developed LOC platform was applied on the dengue virus, which is estimated to infect between 50 and 100 million people worldwide annually and threaten more than 2.5 billion people in tropical countries (WHO, 2014). Normal and dengue-infected WRL-68 cells were discriminated utilizing the LOC platform developed in this project. The DEP forces applied to the cells were quantified by analyzing the light intensity shift within the electrode's dot region based on the Cumulative Modal Intensity Shift (CMIS) image analysis technique. The differences in dielectric properties between infected and uninfected cells were exploited by plotting a unique DEP spectrum for each set of cells and obtaining the DEP crossover frequency at which no resultant movement occurs to the cells in response to the DEP force.

1.2 Research Objectives

The main objective of this project is to develop an LOC platform to differentiate rapidly between normal and dengue-infected cells in a label-free manner. To achieve this end, the following sub-objectives must be met:

i. Design and optimize electrode geometry parameters to generate highest electric field strength based on simulation analysis.
ii. Design and develop simple and cost-effective LOC platform for microfluidics applications.
iii. Conduct rapid DEP manipulation and separation experiments on polystyrene microparticles.

iv. Discriminate between normal and dengue-infected cells based on DEP spectrum and crossover frequencies.

1.3 Scope of Work

This project focuses on the design and development of a LOC platform to be used for the discrimination between normal and Dengue-infected cells in a label-free manner. Dengue-infected hepatic cells were chosen to demonstrate the functionality of the developed platform. 120 samples (60 samples of normal cells and 60 samples of infected cells) were used to conduct the studies of the dengue-infected cells discrimination. The dynamic behaviors of the polystyrene microparticles in response to the DEP force were recorded with a CCD camera, and the images were captured and stored on a personal computer to be processed offline. System automation was not in the scope of the current study. The discrimination between the normal and infected cells was based on their DEP spectra and crossover frequencies. The characterization of the cells (i.e., calculating the conductivity and permittivity values of the membrane and cytoplasm) is out of the scope of this thesis.

1.4 Thesis Organization

The rest of the thesis is organized as follows:

Chapter 2 presents a literature review on the microfluidic LOC platforms, DEP theory and electrode geometries, followed by a concise assessment of the previous DEP investigations on biological samples.

Chapter 3 describes the research methodology and procedures followed to accomplish the defined objectives. Particularly, the chapter explains the design, simulation and fabrication of the microarray electrode, and the design and fabrication of the LOC platform's layers. Moreover, the chapter outlines the experimental setup used

to conduct the DEP experiments and the sample preparation procedures. Finally, a brief explanation of the image analysis technique used for analyzing the results is provided.

Chapter 4 discusses the results that were obtained in this project. Specifically, the chapter includes the simulation results and a discussion of the microarray dot electrode, followed by the results of the experiments that were conducted to test the proposed LOC platform. Finally, the DEP experiments on normal and dengue-infected WRL-68 cells are explained and discussed.

Finally, Chapter 5 presents an overall conclusion based on the work undertaken in this project, along with a summary of the original contribution undertaken towards the completion of this project. After that, few limitations that were faced in the current project are highlighted. Finally, few suggestions for possible future work are proposed.

CHAPTER 2: LITERATURE REVIEW

2.1 Introduction

This chapter covers the relevant background information concerning the microfluidic LOC platforms and the development process of the LOC design arrangements. Furthermore, a critical review is presented for the DEP theory, electrode geometries, and the microarray dot electrode and its advantages. Finally, a concise assessment of DEP investigations of biological samples is highlighted.

2.2 Lab-on-a-Chip (LOC)

Several automated systems have been presented for diseases diagnosis in order to enable fast sample collection and robust analysis for a high number of samples that medical centers handle every day. Yet, such instrumentations are not practical to be implemented as point-of-care (POC) diagnostic devices or in small biochemistry laboratories in rural areas. This is due to their high cost, not portable and often involves highly trained technicians to operate them (Whitesides, 2006; Yeo *et al.*, 2011). Therefore, various LOC designs have been developed in the past three decades for use in several different applications (Cheng *et al.*, 2007; Ho *et al.*, 2011; Jing *et al.*, 2015; Lin *et al.*, 2013; Ramji *et al.*, 2015; Warkiani *et al.*, 2014; Wei Hou *et al.*, 2012). The strengths of such systems include a reduced requirement for samples and reagents, fast and high-throughput results, low power consumption, a reduced contamination risk and a high degree of parallelization (Chaudhuri *et al.*, 2015; Haeberle & Zengerle, 2007; Ritzi-Lehnert, 2012; Sin *et al.*, 2011). These designs take advantage of the great developments occurring in microfabrication techniques. An example of these designs is shown in Figure 2.1.

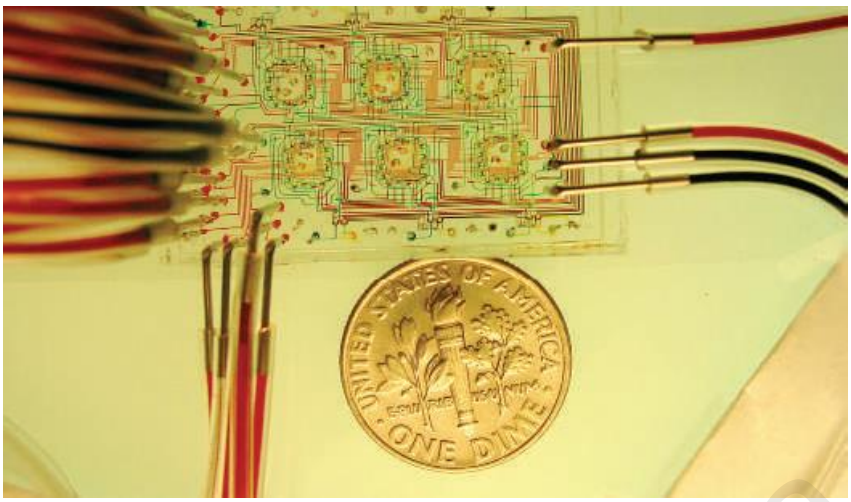

Figure 2.1: Lab-on-a-chip device.
This device was used to investigate the growth of microbial populations offering an alternative approach for existing microbial biofilms which involve complex plumbing. Adapted from (Balagaddé *et al.*, 2005).

LOC technology was emerged from the field of microfluidics which is the science of systems that deal with small volumes of fluids (10^{-9} to 10^{-18} liters) using channels with dimensions of a few micrometers to hundreds of micrometers (Lacaze, 2012). LOC is an approach that has a potential to make microfluidics has pronounced accomplishments like what the transistor did for microelectronics. An example of a microfluidic platform is presented in Figure 2.2.

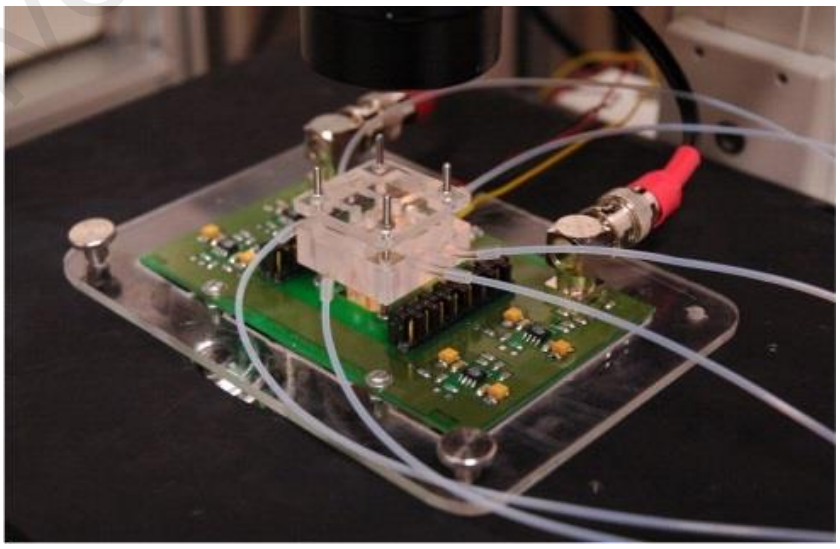

Figure 2.2: Microfluidic platform integrated with Lab-on-a-chip.
This platform was used to perform as a flow cytometer to sort normal and *Babesia Bovis* infected erythrocytes. Adapted from (Nascimento *et al.*, 2008).

Besides miniaturization and integration, LOC features the possibility of conducting experiments in parallel for high-throughput analysis. High-throughput biological analysis can be achieved either by the parallel examination of several test samples for a specific element, or by investigating one test sample for several targets concurrently, or by a combination of the two methods (Situma *et al.*, 2006). Sato *et al*. (2002) developed a microchip for screening several specimens for interferon-γ concurrently, while Kartalov *et al*. (2006) demonstrated a LOC platform for the simultaneous identification of several targets in one sample.

Diverse diagnostic approaches have been exploited to manipulate particles using LOC platforms; however, Dielectrophoresis (DEP) as the sample preparation stage of a POC device, presents unique features. The main advantage of the DEP technique is that the differentiation between particles is based merely on the particles' dielectric properties (electrical conductivity and permittivity) determined by the phenotype of the respective particles. In addition, DEP features high selectivity and efficacy of particles manipulation on micro/nano levels (Foudeh *et al.*, 2012).

Masuda *et al*. (1989) were one of the first groups to use DEP in an LOC device. They designed a "fluid integrated circuit," which was used to manipulate cells and separate them into different outlets. The proposed tool enabled automated single cell manipulation and device miniaturization by combining multiple cell-handling components, such as micropumps and cell-fusion electrodes, onto one substrate.

Gascoyne *et al*. (1997b) described a device for separating certain cancerous cells from blood in a dielectric affinity column. The device involved two parallel glass walls, in which the lower portion of the glass contained an interdigitated electrode. Three holes were drilled in the top chamber wall to play the roles of inlet and outlet ports for cell suspensions and elution buffers. A gasket chamber of a 100 μm thickness was

manufactured using Teflon. This technique, when integrated with other diagnostic or cell separation applications, increased the overall efficiency and sensitivity of the device.

MDA-435 cells, which are human breast cancer cells, and peripheral blood mononuclear cells were separated according to their dielectric properties by a device developed by Gasperis *et al*. (1999). That device combined 2-dimensional (2D) DEP forces with field flow fractionation to manipulate cells efficiently. The device consisted of a 250-µm thick latex gasket sandwiched between top and bottom plastic plates. The electrical connections to the electrodes were linked via pressure-loaded metal wires. This device could be integrated with other microfluidic elements, such as a micro polymerase chain reaction (micro-PCR) system and capillary electrophoresis systems, to create a preliminary stage for sample preparation.

Li *et al*. (2002) proposed a highly accurate device to manipulate *Listeria innocua* bacteria with DEP. The DEP effect took place in a rectangular electrode chamber, which was built by attaching silicone rubber to a glass substrate equipped with interdigitated microelectrodes. Such accurate yet simple LOC arrangements have great potential to be implemented in diagnostic applications.

A device developed by Fatoyinbo *et al*. (2011) rapidly determined the dielectric properties of biological cells. The device consisted of a 4 × 4 dot-patterned gold microarray with a parallel ground ITO microelectrode on top. The microarray was designed so that each dot could be energized separately. The gasket chamber was fabricated using a UV-curing photopolymer resin. Overall, their design measured cell electrophysiology at a nearly real-time speed.

The previous reviewed LOC platforms are capable of successfully manipulating and separating their intended cell populations; however, most of them are contained by laboratories and have yet to gain worldwide recognition by the biotechnology industry. Their limitations are due to fabrication constraints and difficulties, primarily cost factors. Therefore, there is a great need to develop a LOC designs that combine the efficiency, ease of fabrication and cost effective for POC diagnostic devices.

2.3 Dielectrophoresis (DEP)

2.3.1 Theory

The Dielectrophoresis (DEP) phenomenon describes the movement mechanism of particles in a non-uniform electric field. This phenomenon occurs when polarizable particles move according to the applied electric field (Pohl, 1951). DEP has been used as a low-cost technique for the potential manipulation and separation of many biological samples without destructive consequences to the cell (Voldman, 2006). DEP was chosen among other various approaches to manipulate cells due to several advantages. Features of DEP include non-invasiveness, high selectivity and efficacy on small scales, label-free manipulation, low costs and well-established fabrication techniques (Bousse *et al.*, 2000). Furthermore, one of the core strengths of DEP is that the characterization of different cells depends only on their dielectric properties, which are controlled by the cell's individual phenotype. Hence, DEP experiments do not require specific tags or involve any chemical reactions that may alter the properties of the target cells. Furthermore, it was reported that cell manipulation using DEP does not affect cell morphology, cellular oxidative respiration or cell cycle dynamics (Archer *et al.*, 1999).

The DEP force is generated from the difference in polarizability between the particles and the surrounding medium placed in the non-uniform electric field (Pohl, 1978). The strength and the direction of the DEP force are determined by the complex

dielectric properties of both the particles and the surrounding medium (Gascoyne & Vykoukal, 2002). The governing equation for DEP force applied to a spherical particle of a radius *r* that is surrounded by a medium of a relative permittivity ε_m can be expressed as follows:

$$\left\langle \vec{F}_{DEP} \right\rangle = 2\pi r^3 \varepsilon_o \varepsilon_m \, \mathrm{Re}[K(\omega)] \nabla E^2 \qquad (2.1)$$

where ε_o and ε_m represent the permittivity values of the free space and surrounding medium, respectively; ∇E denotes the electric field gradient; and Re[*K(ω)*] is the real part of the Clausius-Mossotti factor. The Clausius-Mossotti factor is calculated as follows:

$$K(\omega) = \frac{\varepsilon_p^* - \varepsilon_m^*}{\varepsilon_p^* + 2\varepsilon_m^*} \qquad (2.2)$$

where ε^* is the complex permittivity and subscripts *p* and *m* denote the particles and the medium, respectively. The complex permittivity ε^* can be expressed by the following equation:

$$\varepsilon^* = \varepsilon - j\frac{\sigma}{\omega} \qquad (2.3)$$

where ε represents the permittivity, $j = \sqrt{-1}$, σ is the conductivity and ω denotes the angular frequency of the applied AC electric field.

The value of the Clausius-Mossotti factor *K(ω)* can be positive or negative depending on the relative polarizability between the particle and the suspending medium. In the case that particles are more polarizable than the suspending medium, the $K(\omega)$ value will be positive, and the particles will be attracted to the region with a high electric field gradient (i.e., the electrode edge) as a result of a positive DEP (p-DEP) effect. In contrast, if the particles are less polarizable than the suspending medium, the

value of $K(\omega)$ will be negative, and the particles will be induced to travel away from the high electric field gradient in response to a negative DEP (n-DEP) effect. This mechanism is illustrated schematically in Figure 2.3. The relative polarisability of the particles and medium, and hence the DEP response, can be controlled by carefully selecting the appropriate frequency of the applied electric field.

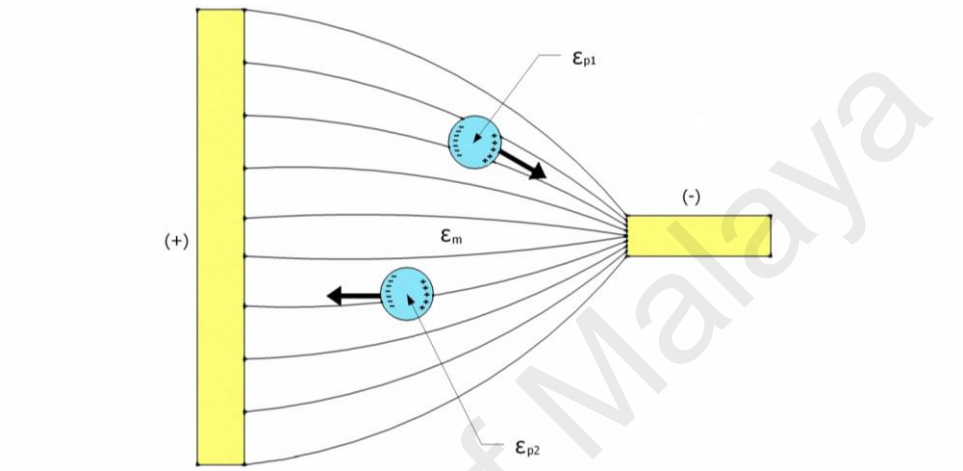

Figure 2.3: Schematic illustration of the responses of polarizable particles to a non-uniform electric field.
Particle 1 undergoes a p-DEP effect and travel to the high electric field gradient, while particle 2 undergoes an n-DEP effect and travel to the low electric field gradient. $\varepsilon_{p1} > \varepsilon_m > \varepsilon_{p2}$; ε_m, ε_{p1} and ε_{p2} are the complex permittivities of the medium, particle 1 and particle 2, respectively.

By studying carefully Equations 2.2 and 2.3, it was established that the conductivity controls the low frequency DEP behavior, while the permittivity controls the high frequency behavior (Ghallab & Badawy, 2004). Therefore, there are two main cases that govern the relationship between applied signal frequency and *Re[K(ω)]*. The first case occurs when $\sigma_p < \sigma_m$ and $\varepsilon_p > \varepsilon_m$; making *Re[K(ω)]* negative at low frequencies and positive at high frequencies. On the other hand, the second case is when $\sigma_p > \sigma_m$ and $\varepsilon_p < \varepsilon_m$, then Re[K(ω)] becomes positive at low frequencies and negative at high frequencies (Ghallab & Badawy, 2004). Figure 2.4 illustrated the relationship between the applied signal frequency and *Re[K(ω)]* with respect to the particle and surrounding medium permittivity and conductivity.

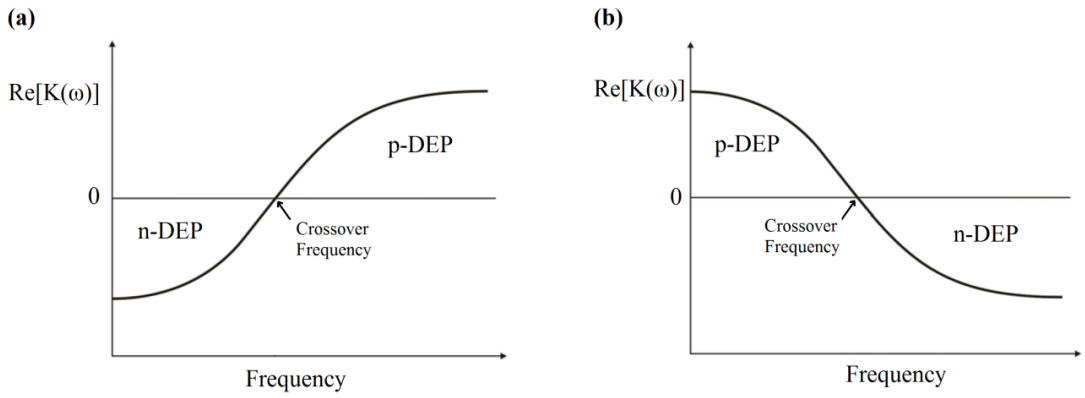

Figure 2.4: DEP spectrum (*Re[K(ω)]* vs. frequency) of a polarizable particle. (a) when $\sigma_p < \sigma_m$ and $\varepsilon_p > \varepsilon_m$, (b) when $\sigma_p > \sigma_m$ and $\varepsilon_p < \varepsilon_m$.

2.3.2 Electrode Geometries

The non-uniform electric field required to develop the DEP effect is generated by either electrode or electrodeless (insulator-based) DEP devices. Electrodeless DEP employs spatially non-uniform insulating constriction to generate a high electric field gradient with a local maximum (Lapizco-Encinas *et al.*, 2005). The advantage of such electrodeless devices is found in the fact that its structure is mechanically robust and chemically inert (Chou *et al.*, 2002). However, these devices require a high voltage supply and the channel length is limited (~10 mm) (Khoshmanesh *et al.*, 2011). On the other hand, electrode-based DEP devices provide large trapping areas for cell aggregation and do not require high driving voltage; since the electric field is produced by electrodes on the micron scale. Another advantage of miniaturizing the electrodes is the corresponding decrease in the temperature rise caused by joule heating; $\nabla T \sim L^2|E|^2$, where L is the length that characterizes the electric field variations, so a smaller L means a smaller ∇T provided that the applied electric field is fixed (Castellanos *et al.*, 2003).

Various electrode geometries have been proposed in the literature, but they can generally be categorized into two main groups: planar and 3-dimensional (3D)

electrodes. Planar electrodes are typically patterned on the bottom of a microchannel using conventional lithography techniques. Examples of planar electrode designs include interdigitated (Liu *et al.*, 2009), castellated (Becker *et al.*, 1995), spiral (Wang *et al.*, 1997), curved (Khoshmanesh *et al.*, 2009a), oblique (Pommer *et al.*, 2008), quadrupole (Jang *et al.*, 2009) and matrix (Fatoyinbo *et al.*, 2011). On the other hand, 3D electrodes can be designed on the bottom, the bottom and top, or the sidewalls of a microchannel, but these designs require complicated fabrication techniques. Examples of 3D electrode designs include a grid pattern (Junya & Ronald, 1998), microwells (Thomas *et al.*, 2009), DEP-wells (Hoettges *et al.*, 2008), extruded patterns (Iliescu *et al.*, 2008), a sidewall pattern (Wang *et al.*, 2009) and a top-bottom pattern (Dürr *et al.*, 2003). Selected electrode geometries and configurations used in the literature are represented schematically in Figure 2.5.

This variety in electrode geometry has evolved to address different research tasks. For example, the overall purpose of 3D electrode designs is to perform characterization studies on large populations of particles. Interdigitated electrodes are very popular for manipulating certain populations of particles depending on their characteristic electrical properties; on the other hand, a grid electrode is designed to precisely control the physical motions of individual particles. Hence, the electrode geometry to be used is determined by the goal of the study.

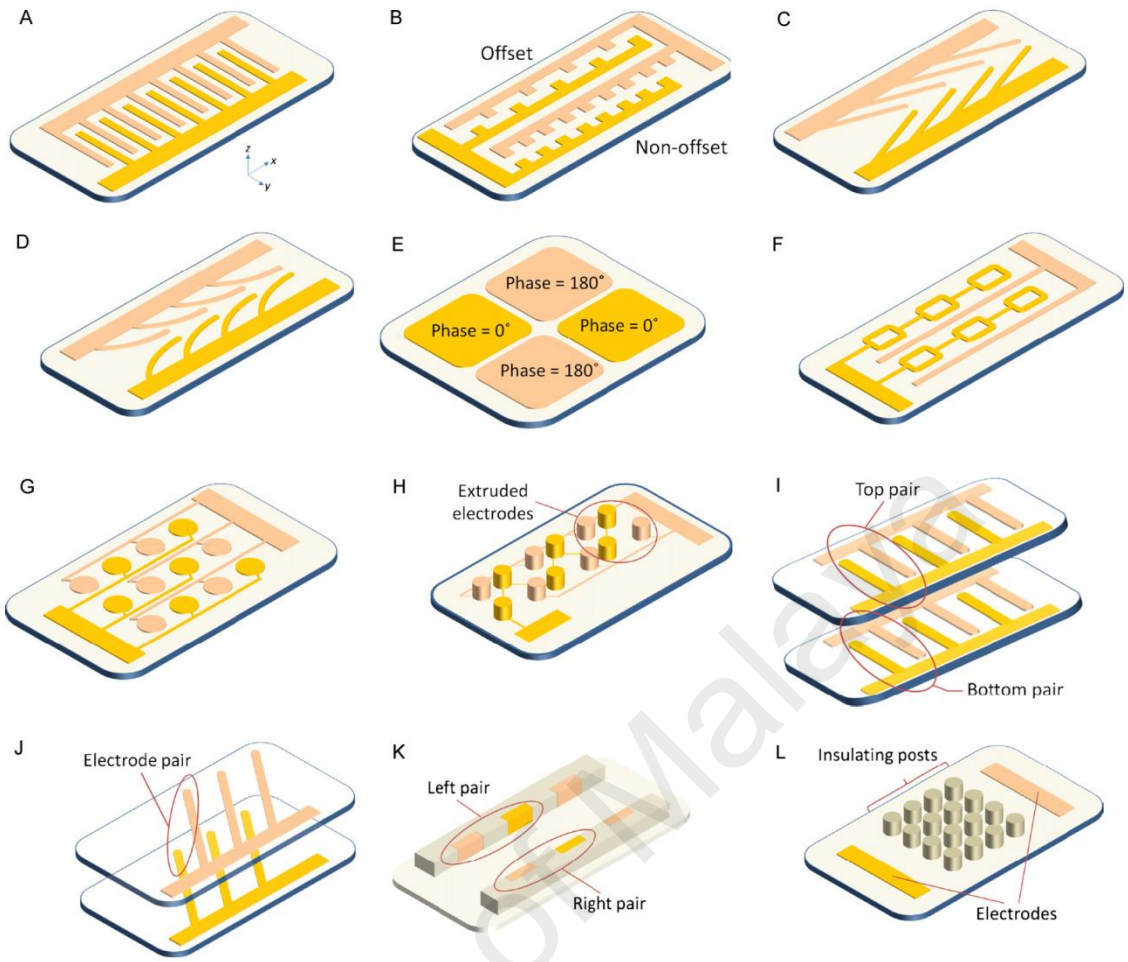

Figure 2.5: Schematic illustration of selected electrode geometries and configurations used in DEP applications.
(A) interdigitated, (B) castellated, (C) oblique, (D) curved, (E) quadrupole, (F) microwell, (G) matrix, (H) extruded, (I and J) top–bottom patterned, (K) sidewall patterned, (L) insulator-based or electrodeless. Adapted from (Khoshmanesh *et al.*, 2011).

One of the early non-uniform electric field designs of Herbert Pohl, the pioneer of DEP, was built by inserting a wire into a glass tube, with another wire surrounding the inner wall of the glass tube (Pohl & Plymale, 1960). However, this device required a high electric potential and could only manipulate particles larger than 1 micron due to the Joule heating effects. Another drawback to this design is that its electrodes only quantify p-DEP, since the target particles were manipulated to move only toward the wires not away of them.

A quadrupole electrode, made of four electrodes facing each other to form an inner defined area, has been a popular electrode configuration choice for particle trapping and DEP manipulation applications (Chung *et al.*, 2012; Michael & Hywel, 1998; Moghimi *et al.*, 2012). Recently, Guan *et al.* (2011) used a quadrupole electrode to trap charged particles in aqueous solution. This type of electrode has many advantages; however, it increases the applied electric field, resulting in a divergence of the targeted particles so that they travel away from the center of the four electrodes. To avoid this limitation, Voldman *et al*. (2003) proposed the extruded quadrupole electrode to manipulate particles using stronger DEP forces. However, these extruded quadrupole electrodes, similar to other 3D electrodes, include complex fabrication processes.

In general, most of these electrode geometries generate complicated and asymmetrical electric fields, making it difficult to measure the DEP force on the particles and extract their dielectric properties. Hence, there is a need to develop an electrode with simpler and more uniform geometry to address these challenges.

One of the potential electrode geometries to be applied in DEP applications is the circular "dot" electrode. The advantages offered by this type of microelectrode were reviewed by the author of this thesis in (Yafouz *et al.*, 2013). There are many advantages to this electrode design, making its configuration unique and more practical than other existing designs. These advantages can be summarized as following:

i. *Confined region of analysis*: The round structure of the dot electrode creates a well-defined and enclosed region of analysis. This attribute enables the holding and manipulation of individuals and populations of cells in defined locations.
ii. *Simple fabrication*: A dot electrode is a planar 2D electrode with a simple fabrication procedure that utilizes the standard lithography technique. This feature gives the dot electrode design a competitive advantage over existing 3D

electrode designs, which require complex fabrication steps. The dot gold electrode, for example, is fully fabricated in approximately 3 hours by the photolithography technique (provided that the photomask of the electrode pattern is available).

iii. *Strong electric field*: While other 2D electrode designs suffer from weak trapping forces, micro-array ring-dot electrodes allow for the creation of multiple capture sites, each with strong trapping (Taff & Voldman, 2005). Furthermore, previous simulation works were conducted to explore the electric field over the dot electrode using numerical analysis (Fatoyinbo *et al.,* 2008), and these works have confirmed its effective electric field penetration.

iv. *Integrity*: The round pattern of the dot electrode can be used for the probe surfaces of antibodies and biosensors in diagnostic devices. Piezoelectric, optical and electrochemical biosensors can be incorporated with DEP technology to better characterize and manipulate cells (Park *et al.*, 2009; Stevens & Jaykus, 2004). In addition, because the dot electrode geometry is simple (with the resultant image being circular), no registration is needed between the images and the electric field template (Fatoyinbo *et al.*, 2008).

v. *Scalability*: The number of dots in the electrode can be scaled up to create larger arrays, allowing more regions of analysis and reducing the time needed to generate the DEP spectrum.

vi. *Symmetry*: The dot electrode design is geometrically symmetrical. As a result, the electrode can manipulate cells regardless of the flow direction used for their injection.

vii. *Re-dispersion*: When removing the electric field from the dots, particles were observed to travel back across the dot, ending in a near-homogeneous distribution after a period much shorter than that predicted for diffusion alone

(Fatoyinbo *et al.*, 2008). This phenomenon enabled serial experiments to obtain a complete DEP spectrum to be conducted rapidly because there is no need for external intervention to redistribute the particles over the dots after each experiment.

Figure 2.6 illustrates a schematic diagram for the DEP effect caused by the dot electrode. When supplying the electrodes with low frequency signal (~10 kHz), cells exhibit n-DEP and accumulate at the center of the dot aperture. On the other hand, p-DEP occurs when applying high frequency signal (~1 MHz) causing the cells to be cleared from the center of the dot aperture and attracted to the electrode edge. This mechanism occurs when $\sigma_p < \sigma_m$ and $\varepsilon_p > \varepsilon_m$ as discussed in Figure 2.4.

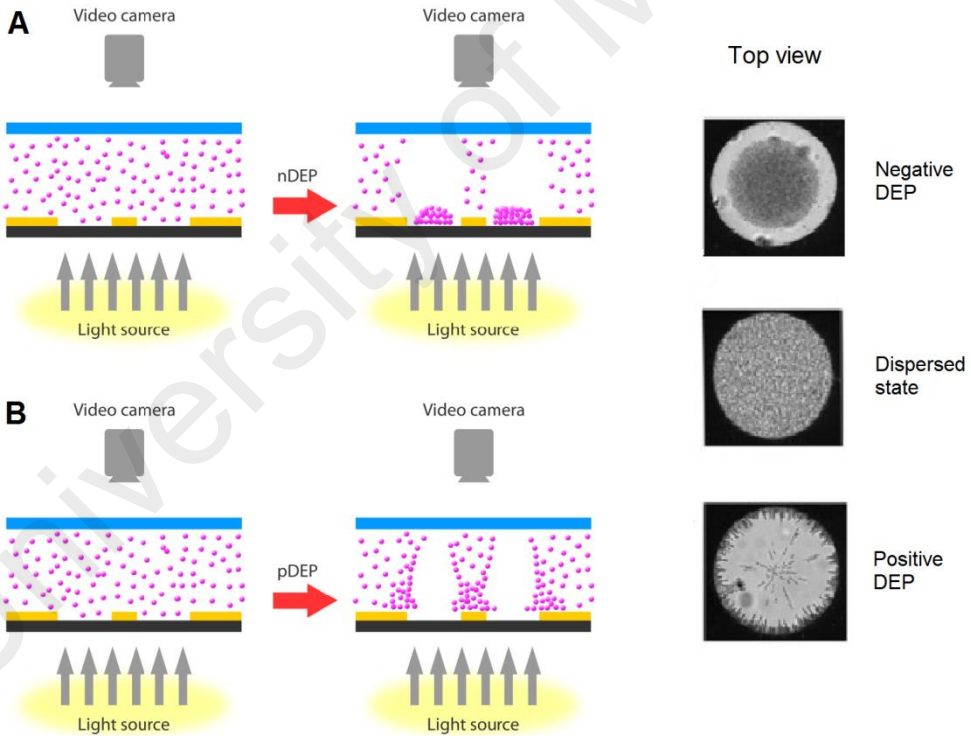

Figure 2.6: Schematic diagram of the movement of particles within the dot microelectrode device.
(A) n-DEP effect, and (B) p-DEP effect. Adapted from (Fatoyinbo *et al.*, 2008).

There are few works in the literature used circular electrodes to induce DEP effects on biological samples. The main drawback of these works is the long time needed to conduct the DEP experiments. This limitation is mainly due to the low electric field generated from the electrodes.

Cheng *et al.* (1998) separated *E. coli* bacteria from a mixture containing human blood cells by DEP. Platinum circular posts were used to isolate the bacteria by means of applying non-uniform electric field. The experiment took 4 minutes to separate the bacteria from other populations by attracting to the electrode edge in response to p-DEP effect.

Huang *et al.* (2002) developed a 5 × 5 circular posts array to separate five different cultivated cell lines and human peripheral blood mononuclear cells utilizing their distinct crossover frequencies. The separations were achieved 3-5 minutes after applying the electric field.

A circular "ring-dot" electrode geometry was proposed by Taff and Voldman (2005) for *HL-60* cells trapping and sorting using p-DEP. The ring-dot electrode geometry incorporates an outer ring electrode and an inner dot electrode that lies on a different metal layer. This electrode design maintains a strong and spatially localized electric field.

Fatoyinbo *et al*. (2008) developed a dot microsystem to determine the dielectric properties of biological cells. The device consisted of a dot-patterned gold microarray with parallel ground microelectrode on top, made of indium tin oxide (ITO) material. The electrical properties of the particles were linked to the shifts in light transmission through the dots and computed their results from an analysis of digital images. The final particles' positions were achieved 1 minute after applying the electric field.

Fatoyinbo *et al.* (2008) also reported a re-dispersion effect on the particles when the electric field was switched off. It was noted that this effect was significantly easier to observe when the size of the dot decreased and the particles stock concentration increased. This feature makes the dot electrode design a potential choice to develop a rapid and automated LOC device for biomedical applications.

Recently, Huang *et al.* (2012) developed an electric module for *HeLa* cells separation from RBCs using DEP. Indium-tin-oxide coated spiral electrodes were used to induce p-DEP effect on *HeLa* cells while RBCs did not move from their initial positions after applying the electric field. The separation of *HeLa* was achieved in approximately 3 minutes.

Table 2.1 summarizes the speed and mechanism of trapping target species utilizing DEP induced by circular-like electrodes for various on-chip applications.

2.3.3 Operating Strategies

There are several operating strategies that DEP devices can implement to manipulate particles. These strategies define how the induced forces in the DEP device affect each other to control the movement of the target particles. The most frequently implemented form of DEP is conventional DEP which is established on the theory discussed in Subsection 2.3.1. Besides the conventional DEP, the operating strategies can be categorized into four main groups: Field-flow Fractionation Dielectrophoresis (DEP-FFF), Traveling-wave Dielectrophoresis (twDEP), Electrorotation (ROT) and Insulator-based DEP (iDEP).

Table 2.1: Speed and mechanism of trapping target species utilizing DEP induced by circular-like electrodes.

Reference	Electrode	Target	Application	Mechanism	Speed
Cheng *et al.* (1998)	Circular posts	*E. coli*	Separation	p-DEP	4 minutes
Huang *et al.* (2002)	Circular posts	Mononuclear cells	Separation	p-DEP & n-DEP	3-5 minutes
Taff & Voldman (2005)	Ring-dot	*HL-60* cells	Sorting	p-DEP	Not reported
Fatoyinbo *et al.* (2008)	Dot microarray	Red blood cells & yeast cells	Characterization	p-DEP & n-DEP	1 minute
Huang *et al.* (2012)	Circular (spiral)	*HeLa* cells and RBCs	Separation	p-DEP	3 minutes

2.3.3.1 Field-flow Fractionation Dielectrophoresis (DEP-FFF)

DEP-FFF is a combination of DEP hydrodynamic forces. Particles are levitated by n-DEP force produced by electrodes at the bottom of a flow-through chamber. Particles with different dielectric properties and density are levitated to diverse heights within the chamber. Then, particles are transferred at different velocities because of the parabolic profile of flowing liquid, and therefore, particles are separated along the chamber (Gascoyne *et al.*, 2013).

2.3.3.2 Traveling-wave Dielectrophoresis (twDEP)

twDEP is an electric field generated by supplying parallel electrodes with a 90º phase shift signal sequence. It is not necessarily to push the fluid throughout the platform (i.e., using syringe pump) to generate horizontal motion. In twDEP, both real and imaginary part of the Clausius-Mossotti factor $K(\omega)$ have impact on particles transition. The role of the real part of the Clausius-Mossotti factor $\mathrm{Re}[K(\omega)]$ is to levitate the particles from the electrode plane. On the other hand, the imaginary part of the Clausius-Mossotti factor $\mathrm{Im}[K(\omega)]$ regulate the particles' parallel movement to the electrode plane (van den Driesche *et al.*, 2012).

2.3.3.3 Electrorotation (ROT)

Similar to twDEP, ROT DEP employs a phase shifted signal to exploit the imaginary part of the Clausius-Mossotti factor $\mathrm{Im}[K(\omega)]$ to induce circular movement of particles. The induced particles by ROT rotate around their central axis. The direction and the speed of the rotation can be used as indicators for the dielectric properties of the particles by obtaining the $\mathrm{Im}[K(\omega)]$ spectrum over a range of frequencies (Han *et al.*, 2013).

2.3.3.4 Insulator-based DEP (iDEP)

iDEP employs spatially non-uniform insulating structures to generate large field gradients in an electric field produced by remote electrodes. iDEP devices trap or focus particles nearby the narrowing area. The main advantage of such iDEP devices is the fact that it eliminates the necessity for complex device configurations and microelectrodes. Furthermore, iDEP offers the particles and medium to flow by electroosmosis generated from an applied DC voltage without the need for external pumping mechanism. However, in order to produce strong DEP force enough for particle manipulation, a high DC voltage is usually essential. Consequences of such high voltages include extreme Joule heating and electrothermal flow (Braff *et al.*, 2012).

2.3.4 Methods for Quantifying Dielectrophoretic Response

The DEP forces applied on a cell can be used to determine the cell's electrical properties (conductivity and permittivity) as a function of the applied signal frequency. Plotting the DEP force versus the applied frequency creates a plot known as a "DEP spectrum," making DEP a powerful tool for cell characterization studies. Cells have unique DEP responses depending on their electrical phenotypes, which can be considered as the cells' electrical fingerprints. The electrical phenotype of a cell is mainly governed by its total net charge and polarizability. Electrical phenotypes are important because they can reflect the biological variation in cells (Voldman, 2006).

It is not possible to directly quantify the DEP force applied to each cell. Researchers, however, have developed few alternative techniques to determine the forces generated on cells. These techniques depend on measuring the real part of Clausius-Mossotti factor $Re[K(\omega)]$ in Equation 2.1. There are five main techniques which are: collection rate measurement, crossover measurement, particle velocity measurement, levitation measurement and impedance measurement.

2.3.4.1 Collection Rate Measurement

This method is appropriate for studying sub-populations of particles on an electrode array, and works by counting the number of particles collected at the electrode's region of analysis in a particular period of time (Labeed *et al.*, 2006). Images of particles are captured before and after the application of an electric field, and particles' movements into and out of the region of p-DEP and n-DEP effects on the electrode are analyzed. The light output intensity increases when particles gather at the electrode edges by p-DEP. On the other hand, when particles are collected at the center of the electrode (away from the electrode edge) by n-DEP effect, light output intensity decreases. Shifts in the intensity of the transmitted light passing through the population of particles are calculated and used to represent the DEP force of the particles. The particles response to DEP effects is quantified by plotting the light intensity shift versus the frequency at which the images were captured, to construct the "DEP spectrum".

The electrophysiological properties of cells (i.e., the conductivity and permittivity of the cytoplasm and the membrane) can be extracted from the DEP spectrum by applying an appropriate best-fit model to line the DEP spectrum, as shown in Figure 2.7 (Bisceglia *et al.*, 2015; Duncan *et al.*, 2008; Labeed *et al.*, 2011; Mulhall *et al.*, 2011). Interpretation of the extracted properties can provide an evaluation of what state the cells were experiencing and; therefore, can help in diagnosing diseases, allowing replacement of bulky laboratory instrumentation with POC devices.

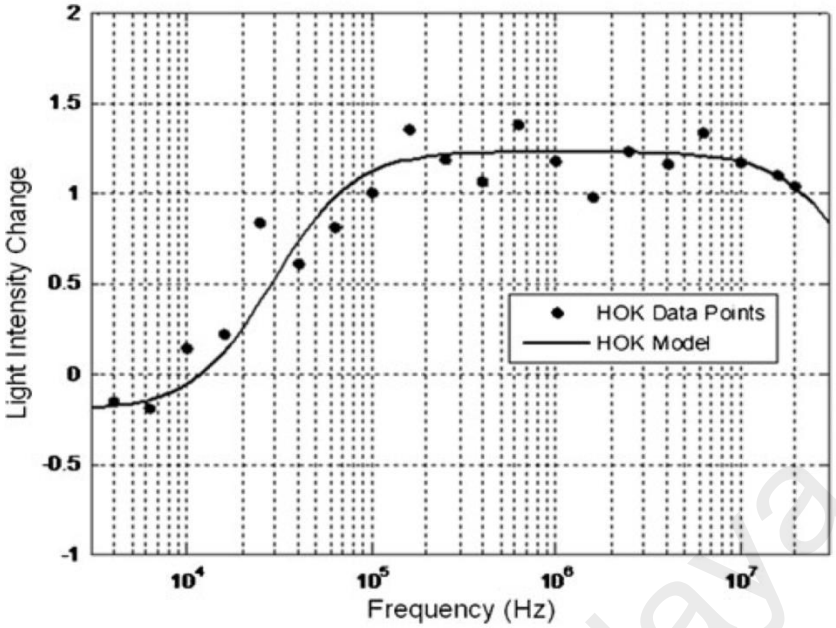

Figure 2.7: DEP spectrum of human oral keratinocytes (HOK) along with best-fit model.
Adapted from (Mulhall *et al.*, 2011).

2.3.4.2 Crossover Measurement

This method depends on monitoring the movement of particles placed in a non-uniform electric field using a microscope. Particles transfer either towards or away from the electrode edge under p-DEP or n-DEP effects, respectively. The DEP force becomes zero at a specific frequency and the particles do not move. This specific frequency is known as the *crossover frequency* or *zero force frequency* (Hughes *et al.*, 2002). This phenomenon takes place when the real part of the effective polarizabilities of the particle and the surrounding medium equal each other (i.e., $Re[K(\omega)] = 0$). If the $Re[K(\omega)]$ is identified, then the effective complex permittivity of the investigated particles can be obtained using Equation 2.2. Typically, the crossover frequency is obtained for several surrounding medium conductivities as shown in Figure 2.8. In practice, it is simple to measure the crossover frequency for particles with diameter down to 50 nm, provided they are able to be traced under the microscope. Cells have distinct crossover frequencies depending on their electrical phenotypes, which can be

considered as the cells' electrical fingerprints. The electrical phenotype of a cell is mainly governed by its total net charge and polarizability. Electrical phenotypes are important because they can reflect the biological variation in cells (Voldman, 2006).

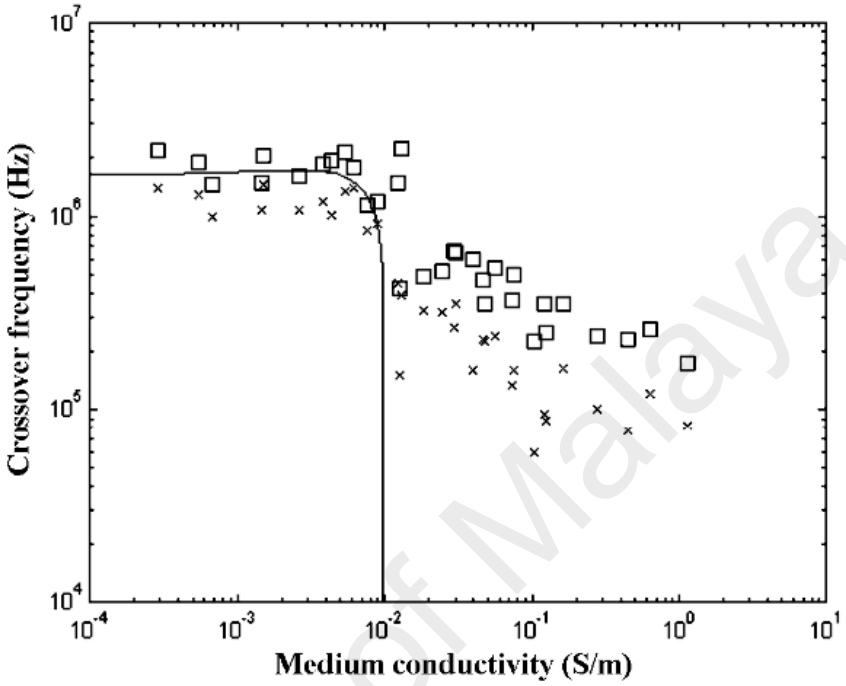

Figure 2.8: Crossover frequency vs. suspending conductivity for 557 nm diameter spheres in KCl.
(× and □ denote to frequencies which induced p-DEP and n-DEP, respectively). Adapted from (Green & Morgan, 1999).

2.3.4.3 Particle Velocity Measurement

This method compares the velocity and direction of the particles placed in a non-uniform electric field to predefined regions of the electric field strength. The velocity of single particles is monitored as they travel under p-DEP effect to the electrode edge, and then the instantaneous velocity is plotted versus the distance from the electrode edge as depicted in Figure 2.9. The DEP force experienced by particles is balanced by the Stokes force, in such a way particles travel in a constant velocity in the region of constant electric field gradient (Watarai *et al.*, 1997). This method can be utilized for identifying the dielectric properties of microparticles, provided that the effects of

Brownian motion are taking into consideration. This method, however, has a main challenge in differentiating between the DEP effect of the applied electric field on the particles and the secondary effects of electric field-induced fluid motion (i.e., AC electroosmosis) (Morgan & Green, 2003).

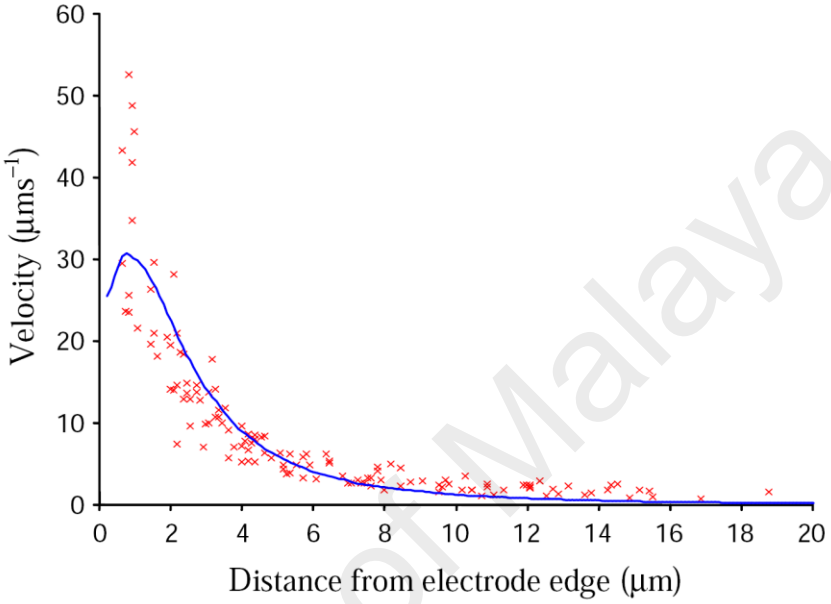

Figure 2.9: Instantaneous velocity of particles induced by p-DEP force plotted versus the distance from the electrode edge.
The solid line represents the theoretical velocity obtained from the electric field numerical modeling for the used electrode. Adapted from (Morgan & Green, 2003).

2.3.4.4 Levitation Measurement

Particles are repelled from the electrode surface under the n-DEP effect and travel to the region of electric field local minimum where the gravitational force equals the n-DEP force. The levitation height of the particle is plotted as a function of the applied voltage as shown in Figure 2.10, and used to calculate the n-DEP force applied on the particle (Cui *et al.*, 2001). Therefore, this method is suitable for measuring the dielectric properties of single large particles. The density of the particle, however, should be adequate to reach steady-state levitation within a sensible period of time.

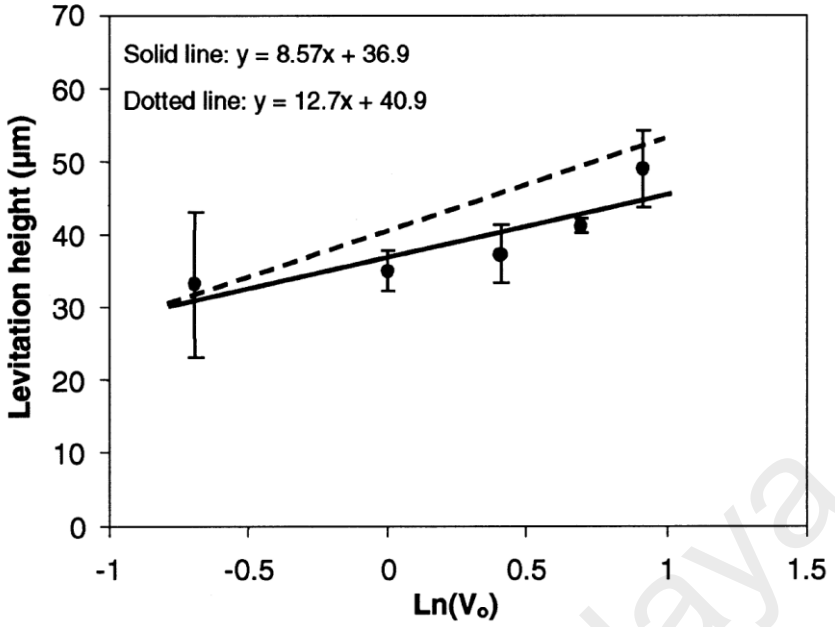

Figure 2.10: Average levitation height of 2.02, 4.66, and 9.76 μm diameter latex beads versus the applied voltage.
Particles were levitated by travelling wave DEP electrodes supplied by four-phases. Adapted from (Cui *et al.*, 2001).

2.3.4.5 Impedance Measurement

This method depends on the fact that the impedance of the electrodes changes when particles are attracted to the electrode edge under the effect of p-DEP (Sabounchi *et al.*, 2008). This impedance change can be utilized to measure the DEP response of the target particles. Zhiwei *et al*. (2008) developed a DEP microfluidic platform to characterized microparticles based on impedance spectroscopy.

2.4 Dielectrophoretic Investigations of Biological Particles

Most efforts to explore applications of DEP have been focused on addressing challenges in the biomedical field. DEP has been used to manipulate, separate and characterize various biological particles. Table 2.2 lists the biological particles that have been studied using DEP. These studies were mainly focused on understanding the fundamental response of the biological particles to DEP forces. Few studies tried to link the DEP behaviors of the biological particles to their electrophysiological properties.

However, there is still a high demand to integrate DEP with miniaturized LOC platforms to perform various biomedical applications such as tissue engineering, medical diagnostics and biosensors.

Table 2.2: DEP investigations on biological particles.

Bioparticle	Reference
DNA	Holzel (2009); Martinez-Duarte *et al.* (2013); Mohamad *et al.* (2014); Song *et al.* (2015)
Proteins	SuáKim & KwangáHahn (2010); Nakano *et al.* (2012); Javanmard *et al*. (2014)
Bacteria	Zhou *et al.* (2006); Braff *et al.* (2013); Jones *et al.* (2014)
Viruses	Grom *et al.* (2006); Park *et al.* (2007); Woon-Hong *et al.* (2013); Masuda *et al.* (2014)
Neurons	Prasad *et al*. (2004); Yu *et al*. (2004); Jaber *et al.* (2013)
Chromosome	Prinz *et al.* (2002)
Leukemia cells	Choongho *et al.* (2005), Imasato *et al.* (2012), Shafiee *et al.* (2010)
Blood cells	Pommer *et al*. (2008); Cheng *et al.* (2009); Hashimoto *et al.* (2009); Huang *et al*.(2012)
Cancer cells	Moon *et al*. (2011); Sano *et al.* (2011); Huang *et al.* (2014)
Sperm cells	Rosales-Cruzaley *et al.* (2013)

Limited DEP studies have been conducted for detecting biomarkers of viral diseases. Generally, there are certain implications that need to be considered when using DEP to study viruses. The main challenge when dealing with viruses is the fact that most viruses have diameters between 10 and 300 nm and are too small to be seen with the eye or with conventional optical microscopes (Morgan & Green, 2003). Consequently, viruses must be fluorescently labeled before they can be examined. The attachment of the fluorescent molecules to the virus alters its surface charge density. The labeling procedure, therefore, may cause a change in the particles' DEP responses (Morgan & Green, 2003). Furthermore, DEP studies on viruses are usually on populations collected

at high electric field regions, and it is relatively rare to study the DEP response at a single viral level. Additionally, unlike large particles, viruses, due to their small diameters, are relatively more influenced by Brownian or electrothermal forces (Khoshmanesh *et al.*, 2011).

Hughes et al. (2002) characterized successfully *Herpes simplex virus* by DEP. Polynomial gold electrodes were used to conduct the DEP experiments and extract the crossover frequencies at different medium conductivity values. However, fluorescent labels were attached to the viruses before the experiment can be monitored using complex inverted microscopy. Furthermore, the process of measuring the crossover frequency at different conductivity values is tedious and required the subjective assessments of the operators.

Grom *et al.* (2006) designed a microfluidic platform for trapping *Hepatitis A virus* by DEP and electrohydrodynamic flow. This platform was meant for sample concentration enhancement in biosensors applications. However, the main issue with this technique is the fact that it uses complex fluorescent microscope imaging detection to visualize the DEP response of the viruses. Furthermore, virus concentration experiment took 9 minutes before considerate quantity of viruses were aggregated.

Park *et al.* (2007) developed silicon nano-scale probe array for capture *Vaccinia* virus by p-DEP. Moreover, high electric field (10^7 V/m) was applied to lyse the virus particles. Yet, fluorescent microscopy was used in the experiment which took 30 minutes before a notable amount of the virus were collected.

Sonnenberg *et al*. (2012) isolated the T7 bacteriophage virus from blood samples. This was conducted by observing the fluorescent concentration of the blood with and without the virus. Fluorescent labeling still an issue and was not addressed in this work.

In addition, the DEP field had to be applied for 15 minutes before the microarray was washed with PBS and only then could the fluorescent images be taken.

Furthermore, Masuda *et al*. (2014) fabricated an LOC platform for virus enrichment using DEP. The influenza virus (A PR/8) was enriched using an n-DEP force, and then a single virus was transported to a cell chamber and attached to a selected cell. However, the limitation of using complex confocal microscope to track the virus fluorescently is yet to be addressed.

Recently, insulator-based DEP device for concentration of *Sindbis* virus has been fabricated by Ding *et al.* (2016). The device could collect the virus in a single step within 15 seconds; however, the virus needed to be labeled fluorescently to visualize the results, and voltages up to 600 V need to be applied.

Table 2.3 summarizes the limitations of the previous DEP investigations conducted on various types of viruses.

Table 2.3: DEP investigations on viruses.

Reference	Virus Type	Application	Limitation
Hughes *et al.* (2002)	*Herpes simplex virus*	Characterization	- Fluorescent labeling
Grom *et al.* (2006)	*Hepatitis A virus*	Capturing from aqueous suspension	- Fluorescent labeling - Takes 9 minutes
Park *et al.* (2007)	*Vaccinia virus*	Capturing from aqueous suspension	- Fluorescent labeling - Takes 30 minutes
Sonnenberg *et al.* (2012)	*T7 bacteriophage virus*	Isolation from blood	- Fluorescent labeling - Takes 20 minutes
Masuda *et al.* (2014)	*Influenza virus*	Virus enrichment	- Fluorescent labeling
Ding *et al.* (2016)	*Sindbis virus*	Virus concentration	- Fluorescent labeling - High voltage

Previous studies have shown that the electrical properties of cells change when cells transform from a healthy to a pathological state (An *et al.*, 2009; Gascoyne *et al.*, 1997a). Because cells of the same genotype in different physiological and pathological states have unique morphological and structural features, it is possible to discriminate between these cells using their DEP responses (Gascoyne *et al.*, 2002). Therefore, the electrophysiological properties (namely, conductivity and permittivity) of the cellular cytoplasm and membrane may be used as biomarkers for detecting viral diseases.

Researchers have begun to direct their efforts of diagnosing diseases caused by small particles (i.e., parasites) to studying the change in the DEP response of normal and infected cells. Nascimento *et al*. (2008) have successfully discriminated between normal and *Babesia bovis*-infected erythrocytes by DEP. They observed a change in the DEP response of normal and infected cells, which is caused by the morphological changes in the membrane and cytosol. These morphological changes are likely due to the high metabolic activity of *Babesia bovis*-infected erythrocytes compared to the simpler metabolism and biochemistry of the normal erythrocyte (Alkhalil *et al.*, 2007).

Findings of previous studies confirmed a morphological alteration in the cells after infection with the dengue virus (McCormick *et al.*, 2012; Wu *et al.*, 2000). These findings indicate a need to investigate the changes that occur in the electrophysiological properties of cells upon infection with the dengue virus. This could lead to the development of POC diagnostic devices for the dengue virus. To the best of the author's knowledge, there are no studies investigated the changes in the electrophysiological properties of the dengue-infected cells using DEP technology.

Even though DEP is yet to enjoy a worldwide recognition by the biochemistry society, a user-friendly DEP-based cell analysis system has been commercialized by Labtech International Ltd, Figure 2.11 ("Deptech 3DEP Reader," 2015). The device is

consisted of a disposal chip in which the sample is loaded into after being resuspended in the DEP medium. Then, the chip is inserted into a reader where DEP experiments are conducted and a complete DEP spectrum is plotted. *Deptech 3DEP* ® reader is capable of detecting cancer cells in a label-free manner.

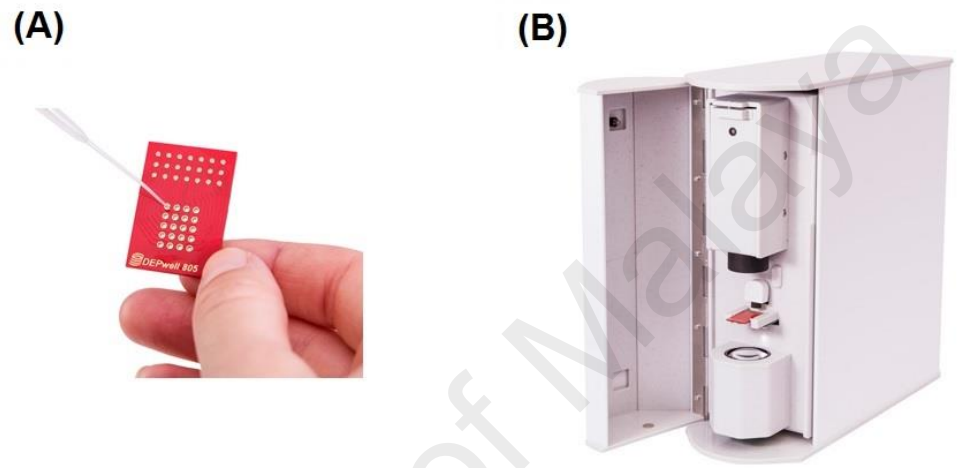

Figure 2.11: *Deptech 3DEP* ® system.
(A) chip where the sample is pipetted into,(B) reader to analyze the measurements and plot the DEP spectrum.. Adapted from ("Deptech 3DEP Reader," 2015).

2.5 Summary

In this chapter, literature related to this project was reviewed. First, LOC and microfluidic platforms were presented, highlighting their advantages and potential applications. Then, the different state-of-the-art LOC devices that have been proposed in the literature for DEP applications were critically reviewed, pointing out their limitations. After that, a detailed analysis of the theory of the DEP phenomenon and the electrode geometries was presented and the advantages offered by microarray dot electrode geometry were outlined. Additionally, a critical evaluation for several DEP platforms was defined; highlighting their limitations. Next, the operating strategies of the DEP devices were reviewed along with the methods of quantifying the DEP forces.

Then, the DEP investigations that were conducted on biological particles were discussed. Finally, an assessment for the DEP studies that were conducted on viruses was presented.

CHAPTER 3: METHODOLOGY

3.1 Introduction

This chapter outlines the design and development of the LOC platform used in this project. The chapter explains the design and simulation of the planar microarray dot electrode, the fabrication of the designed electrode utilizing photolithography process, and the design and fabrication of the LOC platform's components. Moreover, the chapter describes the experimental setup used to conduct the DEP experiments and the sample preparation procedures. Finally, a brief explanation of the image analysis technique used for analyzing the results is provided, along with a description of the statistical analysis test that was used. A flowchart of the key steps in the research methodology of this project is summarized in Figure 3.1.

3.2 Lab-on-a-chip Design and Development

In this section, the methodology of the LOC development is explained. The LOC platform was designed in a way to achieve the objectives of the current thesis. The design specifications of the LOC platform were summarized in Table 3.1. The LOC platform is consisted of five layers: the microarray dot electrode, ITO electrode, spacer and top and bottom covers. Because the geometry of the electrode, used to generate the non-uniform electric field for DEP, is of great importance, the following subsections explain the development of the microarray dot electrode separately, and then the development of the other LOC layers is described.

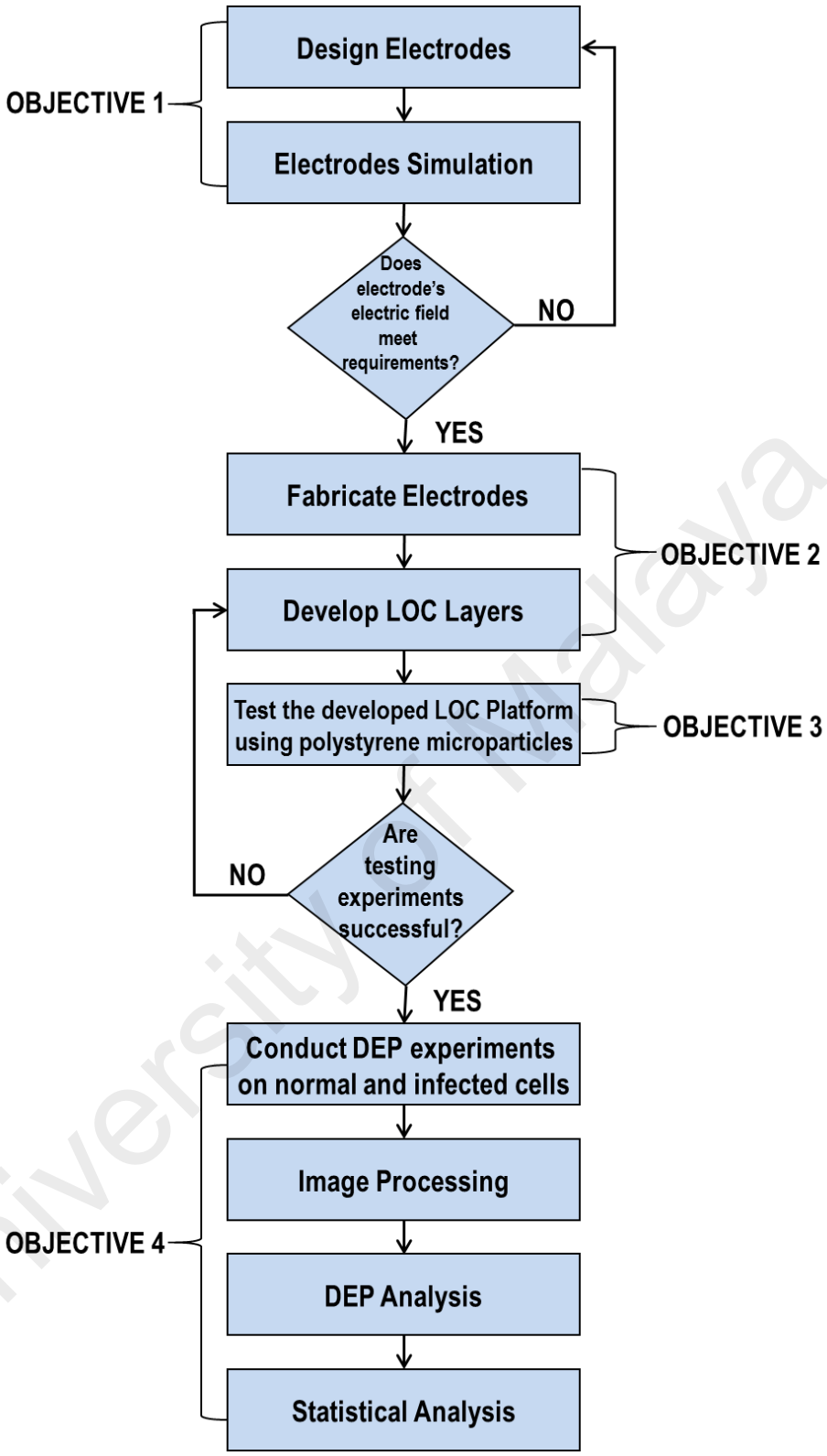

Figure 3.1: Flowchart of the key steps implemented in the research methodology.

Table 3.1: Design specifications of the developed LOC platform.

Parameter	Design Specification
Fabrication Method	Simple photolithography
Electric Field Strength	$> 1 \times 10^5$ V/m
Experiment Duration	< 10 Seconds
Lab-on-a-Chip Platform	- Simple fabrication - Leakage-free flow - Reusability
Cells Manipulation Mechanism	Label-free
DEP Mechanism	p-DEP & n-DEP
Results Analysis	No need for image registration

3.2.1 Electrode Design and Operation Principle

The electrode is needed to generate the non-uniform electric field required to develop the DEP effect. The electrode design of choice for the current project is based on the microarray dot electrodes. The advantages of such electrode geometry were highlighted in Subsection 2.3.2. Mainly, microarray dot electrodes can be fabricated using standard photolithography process; avoiding the use of complex fabrication methods (i.e. reactive ion etching, laser ablation, plasma etching, hot embossing or injection molding). Furthermore, previous simulation work conducted on microarray dot electrodes confirmed its effective electric field penetration (Fatoyinbo *et al.*, 2008). When this electric field is maximized via electrode geometry optimization, rapid DEP experiments could be conducted. Furthermore, since the resulting image of the microarray dot electrode is circular, no registration is needed between the images and the electric field template.

In this project, the electrode geometry parameters were optimized using numerical modeling to strengthen the electric field gradient generated from the electrode and

therefore to strengthen the DEP forces (discussed in Subsection 3.2.2). Furthermore, a ground plane has been added between adjacent dots to avoid the overlapping between the electric fields generated by adjacent dots as shown in Figure 3.2. The purpose of inserting a ground plane between adjacent dots is to increase the efficiency of the microelectrode by producing stronger electric fields (as proven in the simulation results in Subsection 4.2.1).

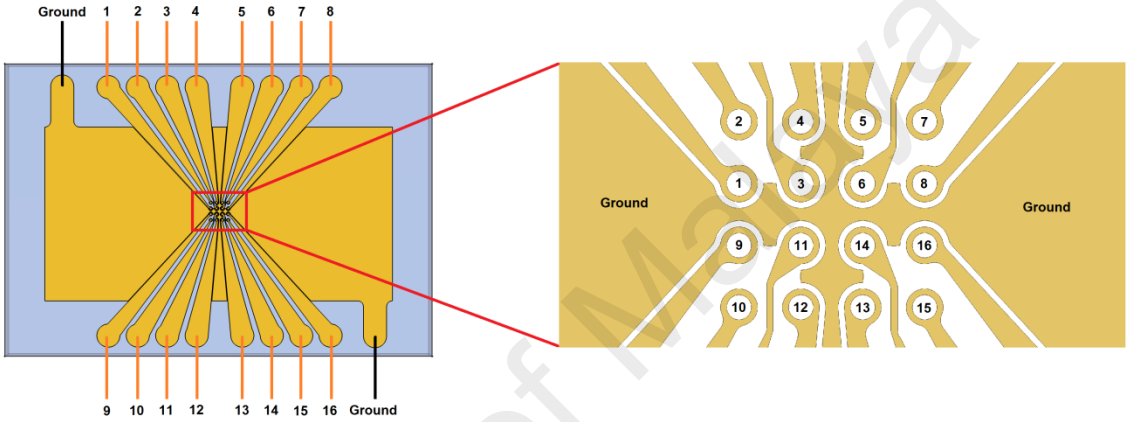

Figure 3.2: Schematic diagram of the 4 × 4 microarray dot electrode.
Sixteen individual inputs can be supplied simultaneously.

The main advantage of using such circular electrode geometry is the simplicity of interpreting and processing the results to obtain the DEP spectrum (Fatoyinbo *et al.*, 2011). Cell motion can be measured by analyzing the light intensity shift in the central region of the dot (discussed in detail in Section 3.5). The operation principle of the dot electrodes is illustrated schematically in Figure 3.3. Before the electrical signal is applied, cells are homogenously distributed over the dot area (no DEP effect, reference state). However, when the cells experience p-DEP force, they clear the central part of the dot aperture and move to the region with a high electric field gradient (i.e., the dot edge). In contrast, if the cells are induced by n-DEP effect, they collect at the dot center, where the electric field gradient is at its lowest value.

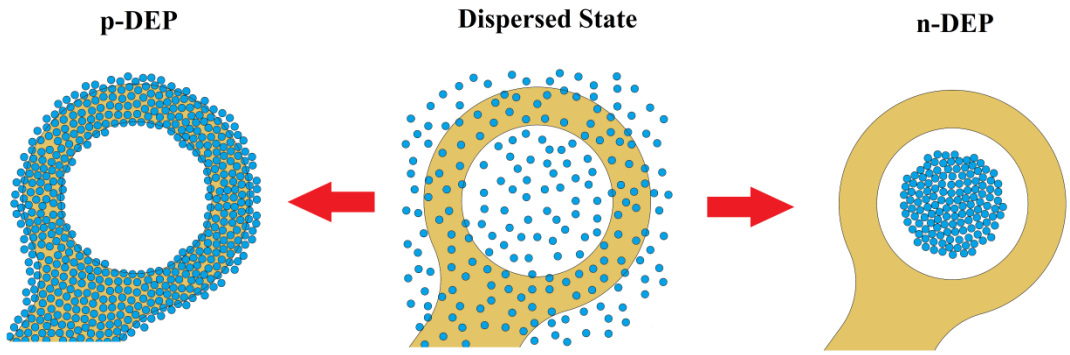

Figure 3.3: The operation principle of the dot electrodes.
Particles distributed homogenously over the dot area before the electrical signal is applied (middle), particles experiencing p-DEP effect and thus being attracted to the dot electrode edge (left), and particles collected at the dot center under the effect of n-DEP (right).

3.2.2 Electrode Simulation

Since electric fields up to 10^5 V/m are required to produce a suitable DEP force (Martinez Duarte, 2010), the parameters of microarray dot electrode were optimized using numerical modeling to create the highest possible electric field strength. The reference parameters that were used as a start point for the electrode design optimization was based on the electrode array used by Fatoyinbo *et al.* (2008). Then, various dot diameters, ring width and distance between adjacent dots were studied for generating the height possible electric field strength. Furthermore, a numerical analysis of the electric field generated by the microarray dot electrode was conducted also to study the effect of inserting a ground plane between adjacent dots on the generated electric field. This modification was meant to avoid the overlapping between the electric fields generated by adjacent dots.

To optimize the size of the dots, the electrodes were numerically analyzed, and their electric field strength and distribution were compared for different dot diameters. Moreover, the effect of adding a ground plane between dot apertures was evaluated.

AC/DC module of COMSOL Multiphysics 4.2a® (COMSOL Inc, Palo Alto, USA) was used to conduct the simulation. Two 3D models were designed in order to perform the objective of the simulation as shown in Figure 3.4. The designed 3D model represents a gasket chamber sandwiched between a bottom patterned electrode and a top "ground" electrode, as shown in Figure 3.4(A). Adding ground plane between dots apertures leads to the second design, which is shown in Figure 3.4(B). Furthermore, Figure 3.4(C) and (D) illustrate the bottom patterned electrodes without and with ground plane respectively, with a thickness of 0.1 mm. The top ground electrode and the gasket chamber were modeled as solid blocks, as depicted in Figure 3.4 (E) and (F). The size specifications of the three components forming the model are summarized in Table 3.2.

Table 3.2: Size specifications of the three components for the simulation models.

Component	**Dimension**
Microarray Dot Electrode	$22 \times 22 \times 0.1$ mm^3 (without ground plane) $30 \times 22 \times 0.1$ mm^3 (with ground plane)
Top Ground Electrode	$5 \times 5 \times 0.1$ mm^3
Gasket Chamber	$3 \times 3 \times 1$ mm^3

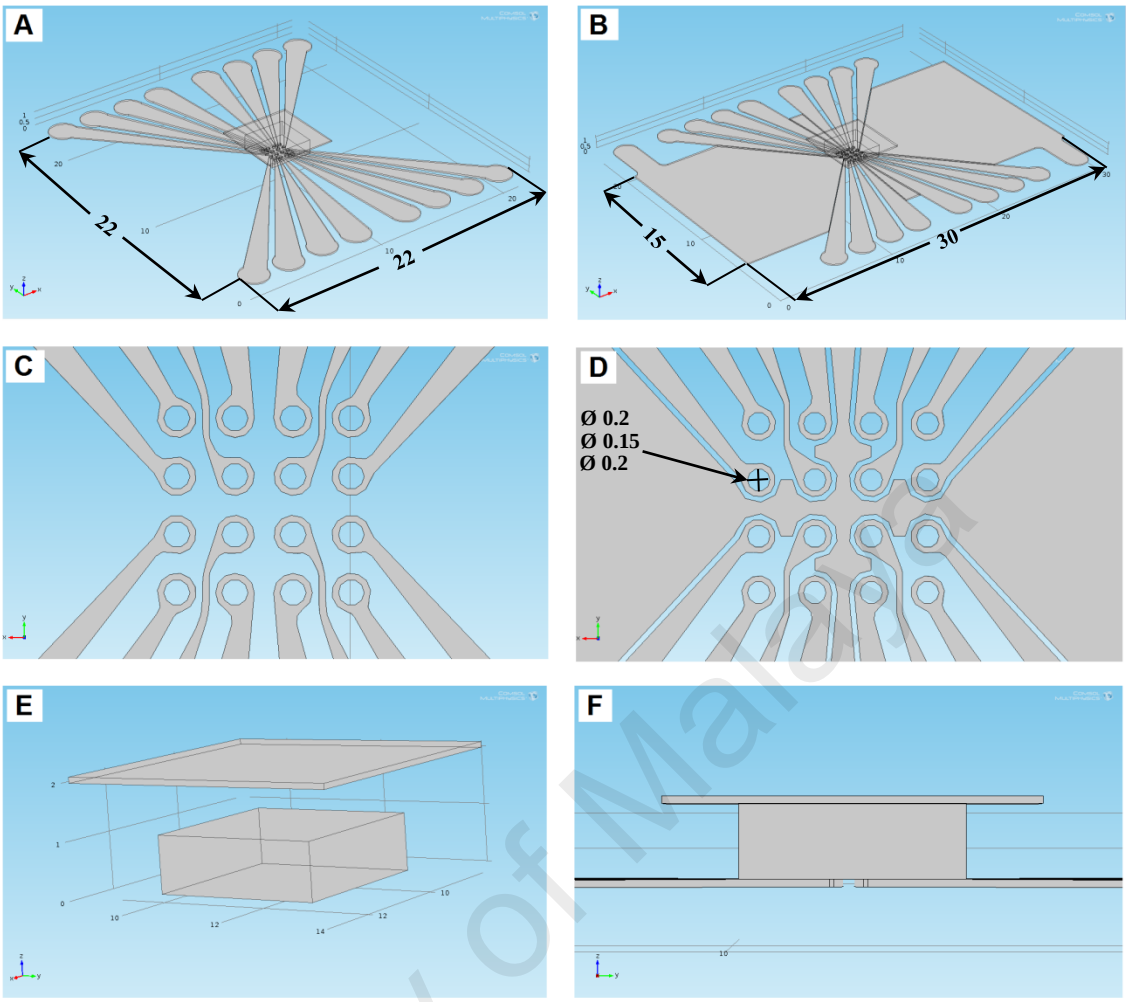

Figure 3.4: Designs of the microarray dot electrode in COMSOL Multiphysics®. (A) The full design of the electrode without ground plane between adjacent dots, and (B) with ground plane. (C) The pattern of the 4 × 4 microarray dot electrode without ground plane, and (D) with ground plane. (E) 3D view of the counter "ground" electrode and the gasket chamber, while (F) shows a side view of the entire design. All dimensions in mm.

In order to optimize the size of the dots, dots were given diameters of 100, 150, and 200 µm for both electrode designs. The diameter of the dots was adjusted by changing either the ring width or the distance between adjacent dots as illustrated in Figure 3.5. First, the size of the dots was modified by varying the ring width 100, 75 and 50 µm, for the dots diameters of 100, 150, and 200 µm, respectively. The distances between adjacent dots and between the centers of the dots were fixed at 150 and 450 µm, respectively. Second, in order to investigate whether the ring width variation has an effect on the electric field strength, other simulations were conducted such that the

width of the rings was fixed at 50 µm for all sizes of the dots, while varying the distances between adjacent dots (distance between dots centers remained fixed at 450 µm).

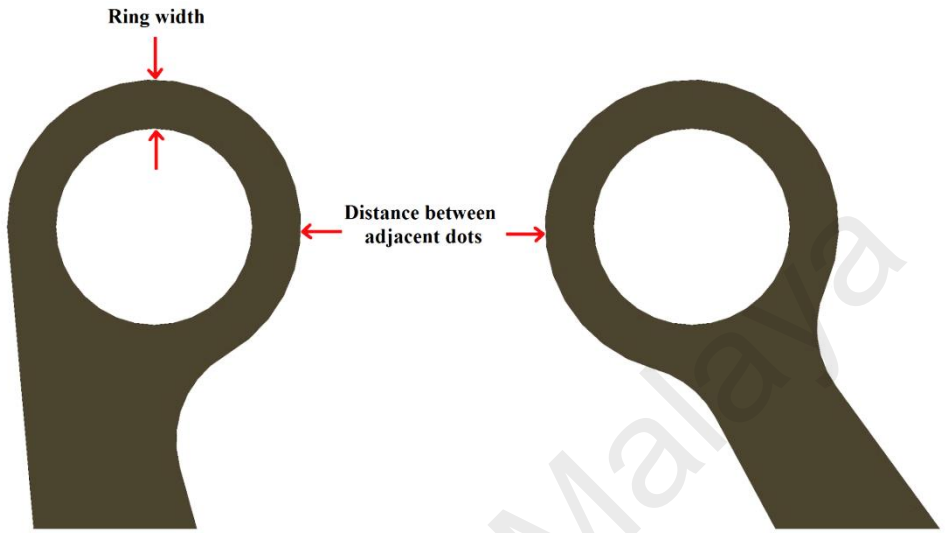

Figure 3.5: Schematic illustration for the ring width and distance between adjacent dots which were manipulated to change the dots diameter.

The patterned dot electrode and the ground plane between dots apertures were given gold properties, the ground top electrode was given material properties of indium tin oxide (ITO). Finally, the gasket chamber, which represents the suspending medium, was given the material properties of deionized water. Table 3.3 shows the values of the conductivities and permittivities assigned to respected materials of the designed models (Serway, 1998).

Table 3.3: Values of the electrical properties (conductivity and permittivity) given to the materials of the designed models.

Material	Conductivity σ (S/m)	Permittivity ε_r
Gold	4.1×10^{7}	1
ITO	1.3×10^{4}	10
DI Water	2×10^{-4}	78

The entire geometries were meshed using tetrahedral elements with maximum and minimum element sizes of 5 and 0.05 mm, respectively. The meshed models are shown in Figure 3.6. Boundary conditions for the top electrode and ground plane between the apertures of the dots were defined as ground, while the patterned electrode was supplied with 10 V_p sinusoidal electrical signal. A range of frequencies was applied to observe any changes in the generated electric field strength and distribution over the designed electrodes. The applied frequencies were 100 Hz, 1 kHz, 10 kHz, 50 kHz, 100 kHz, 500 kHz, 1 MHz and 2 MHz.

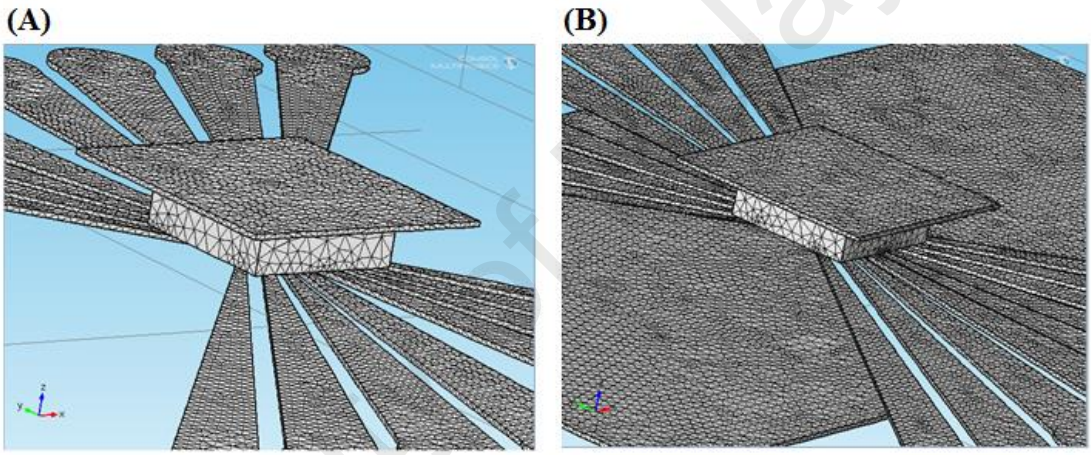

Figure 3.6: Electrode models after meshing.
(A) Electrode without ground plane, and (B) with ground plane between adjacent dots.

3.2.3 Electrode Fabrication

The uniqueness of dot electrodes is in their planar geometry nature. Its flat geometry gives the dot electrode a crucial advantage over 3D electrodes because it is easier to fabricate. There are number of techniques exist for the fabrication of microfluidic devices, including wet etching, reactive ion etching, conventional machining, soft lithography, hot embossing, injection molding, laser ablation, in situ construction, and plasma etching (Fiorini & Chiu, 2005). However, photolithography is considered the basis for most of these processes. 2D microelectrodes such as the dot microelectrode

can be fabricated using the simple photolithography technique. The overall photolithography process requires only 3 hours to fabricate planar electrodes, assuming the photomask which carries the electrode pattern is available.

Prior starting the electrode fabricating procedure, gold-coated glass slides (24K gold-coated microscopic glass slides, Fisher Scientific, Malaysia) were cut into two halves using glass cutter, generating dimensions of 38 × 26 mm^2. The stages that the electrode substrate underwent before becoming an electrode are briefly described here.

3.2.3.1 Photomask Design

The microarray dot electrode geometry was designed using AutoCAD® software (Autodesk Inc, California, USA) in a way compatible with positive photoresist (i.e., transparency mask). The designed microarray dot electrode features 200 µm dot diameter and with ground plane between adjacent dots. The photomask was produced by JD photo-tools (Oldham, UK) on emulsion film with a resolution of 128,000 dpi. The photomask design parameters and the printed photomask are shown in Figure 3.7.

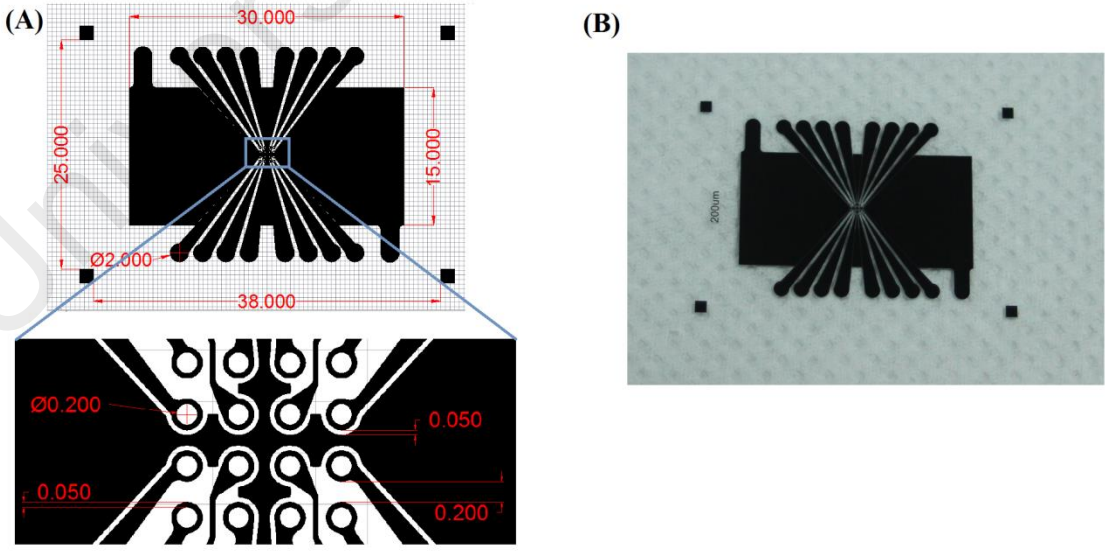

Figure 3.7: The electrode design parameters.
(A) The photomask design in AutoCAD® (all dimensions in mm), and (B) a digital photo of the printed photomask.

3.2.3.2 Substrate Preparation

The gold-coated glass slides were cleaned to remove any contaminants that may be stuck to their surfaces. This step promotes the photoresist adhesion to the substrate surface which is important for transferring the photomask pattern to the photoresist. Gold-coated glass slides were placed in acetone, methanol and DI H_2O, respectively, for 5 minutes each step with ultrasonic agitation.

3.2.3.3 Spin Coating

Positive photoresist (MICROPOSIT™ S1818™, MicroChem, Massachusetts, USA) was used in the fabrication of the electrode because it offers better process control for small geometry features compared to negative photoresists. Several drops of the photoresist were dispensed onto the substrate and was spun using spin coater (WS-650, Laurell Technologies, Pennsylvania, USA) at high speed to generate uniform partially dried layer of the photoresist.

3.2.3.4 Soft Bake

In order to get rid of the residual solvent in the photoresist, the gold-coated slides were "*soft baked*". This step also helps to stabilize the coated photoresist on the slides. Soft baking the slides were performed by placing the slides in a convection oven.

3.2.3.5 UV Exposure

The electrode pattern is transferred from the photomask to the photoresist by exposing the slides to UV light through the patterned photomask. The soft baked gold-coated slides were exposed to UV using vacuum UV exposure unit (AZ210, Mega Electronics, Cambridge, England) for 40 seconds. The slide was arranged with the photomask in a UV light box, as depicted in Figure 3.8(C). It is important to make the opaque side of the photomask to face the slide in the contact exposure mode to

minimize the distance between the photomask and the photoresist; enabling the pattern to be transferred efficiently.

3.2.3.6 Developing

After the slides were exposed to UV, the developing process is responsible for dissolving the areas of the photoresist that were exposed to UV (positive photoresist). The slides were immersed into the developer solution and quickly rinsed with DI H_2O. A longer developing time has an adverse effect on the unexposed photoresist areas. At this stage, the slides were examined under the microscope to ensure that the overall structure was adequately created and to confirm that the exposed photoresist material washed away.

3.2.3.7 Hard Bake

The goal of the hard bake process is to stabilize and harden the developed photoresist to withstand the harsh environment of the etching solution. Furthermore, hard bake step removes any residuals of the coating solvent or the developer. However, it must be noted that longer or hotter hard bake make the photoresist removal more complicated.

3.2.3.8 Etching

The uncovered gold regions were etched using a gold etching solution, until the glass slide appears. The photoresist material withstands the harsh acidic environment of the etching solution and, therefore, protects the beneath gold areas. The gold etching solution was based on potassium iodide solution. The protocol of preparing the gold etching solution was summarized in Table 3.4.

Table 3.4: The protocol of preparing the gold etching solution.

Step	Action
Step 1	Measure 8 g of Potassium Iodide (KI) using digital balance.
Step 2	Measure 2 g of Iodine (I_2) using digital balance.
Step 3	Fill an appropriate beaker with 80 mL DI water.
Step 4	Dissolve the KI and I_2 in the DI water and mix the solution carefully by a magnetic stirrer.

3.2.3.9 Seed Layer Removal

The goal of this step is to remove the seed layer of the glass slide. By removing the seed layer, the glass slide became clear and transparent except for the gold patterned areas. This will facilitates the monitoring the particles under examination when conducing DEP experiments. The seed layer was removed by dipping the slides into boiling 18% HCL solution.

3.2.3.10 Stripping

Finally, any remaining photoresist covering the gold areas of the electrode was removed. The conductivity of the electrodes was checked using Digital Multimeter to ensure the functionality of resulting gold-coated glass electrode.

Figure 3.8 illustrates the stages that the gold-coated glass slide underwent before becoming an electrode. The protocol used in fabricating the electrode was summarized in Table 3.5.

Table 3.5: Summary of the main steps implemented in the electrode fabrication process using photolithography technique.

Step	Actions
Surface Preparation	Soak the gold-coated glass slides first in acetone, then in methanol and then in DI H_2O with 5 minutes of ultrasonic agitation at each step. Then, dry the slides on a hotplate at 120°C for 10 minutes.
Photoresist Coating	Coat the slides with a positive photoresist using a vacuum spin coater. Set the spin coater parameters to 3,000 rpm and 30 seconds.
Soft Bake	Place the slides in a convection oven for 30 minutes at 90°C.
UV Exposure	Expose the slides to UV light through the photomask for 40 seconds.
Developing	Immerse the exposed slides into the developer solution for a few seconds only, and then rinse the slides with DI H_2O to avoid an overreaction.
Hard Bake	Place the slides in a convection oven for 30 minutes at 120°C.
Etching	Dip the slides into gold etchant and remove them once the exposed gold is washed away. Rinse the slides with DI H_2O.
Seed Layer Removal	Place the etched slides in a boiling 18% HCl until the seed layer is bubbled away. Rinse the slides with DI H_2O.
Stripping	Remove any leftover photoresist using a positive photoresist stripper solution or Acetone. Rinse the slides with DI H_2O and dry them.

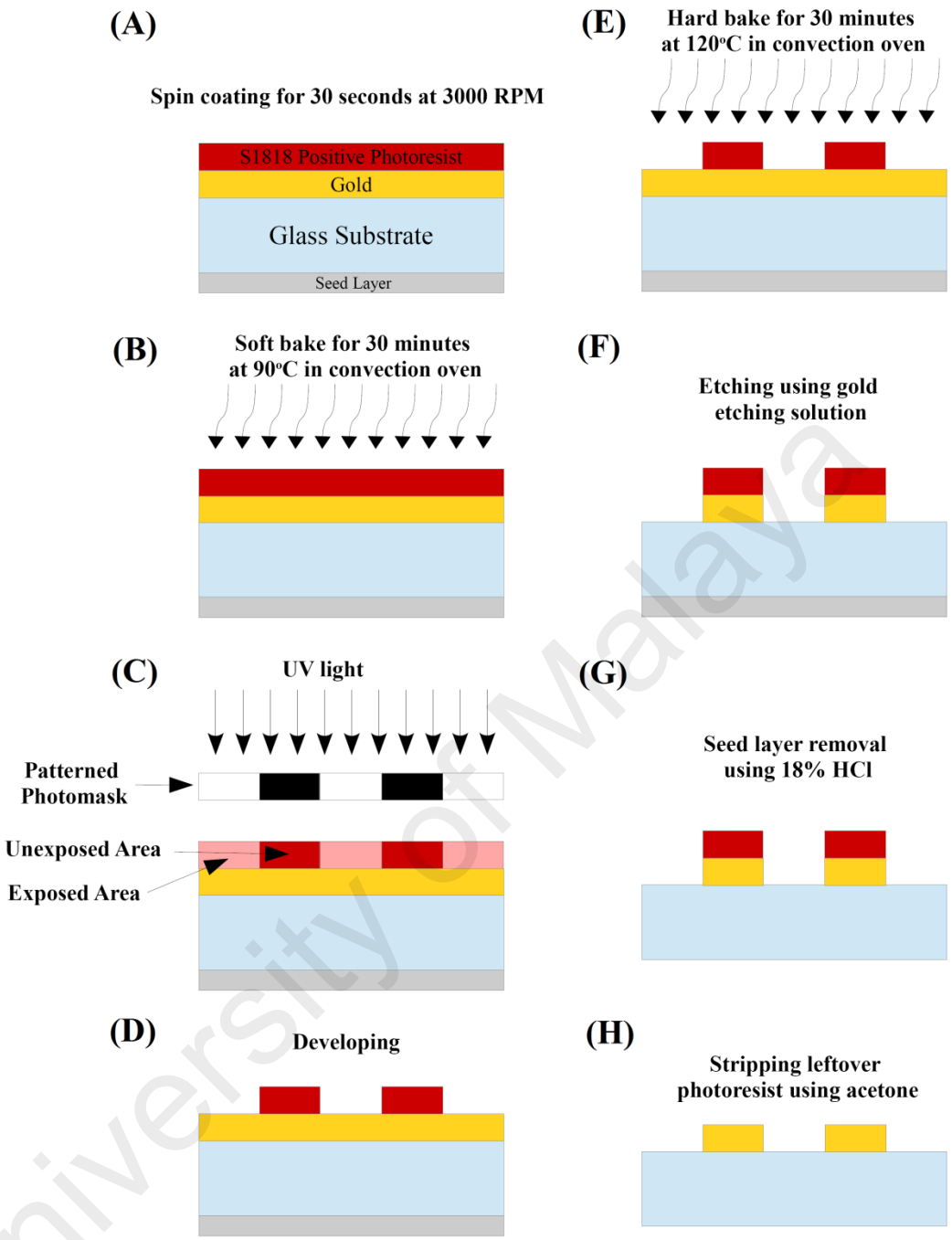

Figure 3.8: Main steps in the fabrication process of the 4 × 4 microarray gold electrode by photolithography.

The process includes (A) photoresist coating, (B) soft bake, (C) UV exposure through the photomask of the electrode design, (D) developing the exposed photoresist, (E) hard bake, (F) etching the uncovered gold layer, (G) removing the seed layer of glass substrate, and (H) stripping the leftover photoresist.

3.2.4 Design and Fabrication of Lab-on-a-chip Layers

A novel Lab-on-a-Chip (LOC) platform was designed to be compatible with the microarray dot electrode configuration. The proposed LOC design in this project consisted of five layers: top and bottom covers, ITO electrode, spacer and gold electrode, as shown in Figure 3.9. Detailed specifications on the dimensions and materials for each layer are described in Table 3.6. The proposed platform was designed to meet the following criteria: cost effectiveness, simple fabrication, leakage-free flow, reusability, ability to change any component at any time, and compatibility with different gasket heights.

Indium tin oxide (ITO)-coated glass slides (15-30 Ω ITO-coated glass slide, SPI Supplies, USA) plays the role of a ground electrode. Unlike opaque metallized electrodes, a unique advantage of ITO electrodes is their transparency, which facilitates DEP assay monitoring. Two 3-mm-diameter holes were drilled to provide inlet and outlet ports for microfluidic injections and ejections.

A spacer, where the DEP effect takes place, is another component of the LOC device. The spacer was cut using a cutter plotter (PUMA II, GCC, Taiwan). A 3-mm channel was introduced at the middle of the spacer to create space for the fluid to flow. It is of great importance to fix the distance between the positive and ground electrodes throughout the microchannel, creating a symmetrical electric field distribution and avoiding any possible fluid leakage.

The top and bottom covers were produced using a Computer Numerical Control (CNC) machine (VISION 2525, Vision Engraving and Routing Systems, USA). Rectangular holes (10×6 mm^2) were introduced through the top and bottom layers to allow better light transmission for observing and recording the DEP effects of the cells under the microscope.

The gold and ITO electrodes were connected to the function generator via flexible wires and silver-loaded epoxy. Specific areas in the top and bottom PMMA covers were engraved to provide a space for these connections.

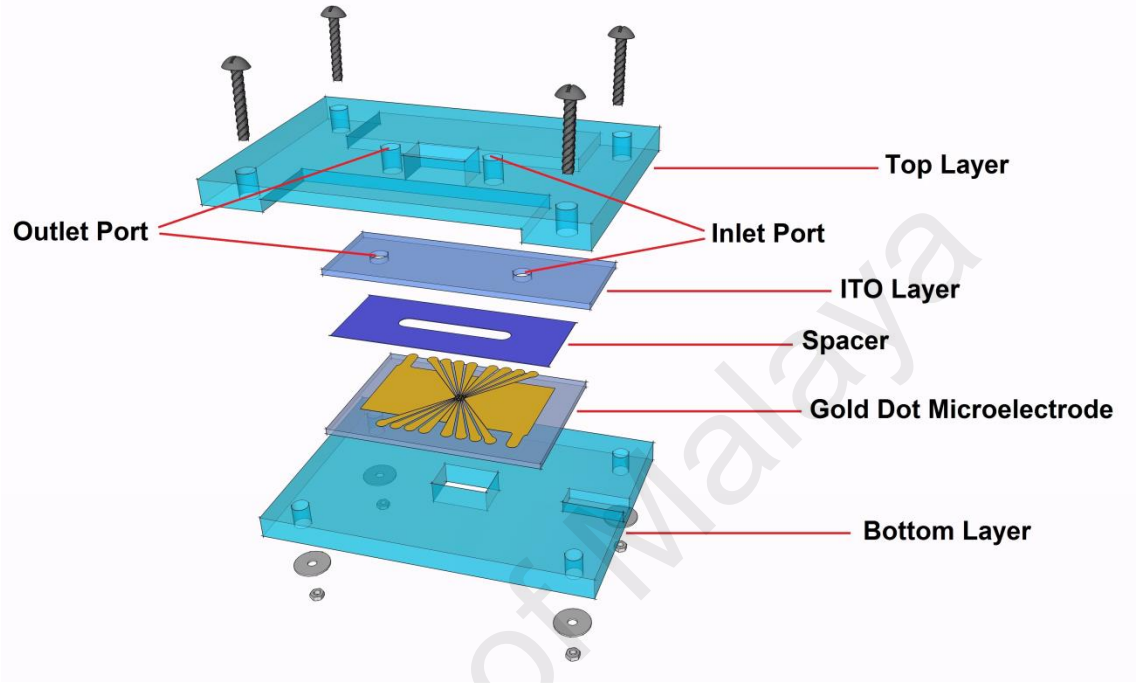

Figure 3.9: Schematic diagram of the proposed LOC platform.
The platform consisted of top and bottom covers, ITO electrode, spacer and gold electrode.

Table 3.6: Design specifications of the layers of the proposed LOC platform.

Component	**Material**	**Dimension (mm)**		
		Long	*Width*	*Thickness*
Top Layer	*PMMA*	60	40	4
ITO Layer	*ITO*	45	15	1
Spacer	*PET Polyester*	38	15	0.1
Electrode	*Gold*	38	26	1
Bottom Layer	*PMMA*	60	40	4

3.3 Lab-on-a-chip Testing

To test the proposed LOC platform, size-dependent manipulation and separation DEP experiments were conducted on mixtures of different-sized microparticles. As polystyrene microparticles have been widely used to evaluate the performance of DEP systems (Çetin *et al.*, 2009; Chiou *et al.*, 2013; Choi & Park, 2005; Khoshmanesh *et al.*, 2010; Khoshmanesh *et al.*, 2009b; Morgan *et al.*, 1999), polystyrene microparticles were used in the testing experiments in the current project. Descriptions of the experimental setup and the sample preparation procedure are presented in the following subsections.

3.3.1 Polystyrene Microparticles Preparation

Particles with diameters of 1, 5 and 15 µm (Microparticles based on polystyrene, 10%, Sigma-Aldrich, Munich, Germany) were used as the microparticles for the validation of the proposed device. The aqueous microparticles suspensions of 1, 5 and 15 µm polystyrene particles were diluted with deionized (DI) water in volume ratios of 1:60, 1:40 and 1:20, respectively. Prior experimentations, samples were ultrasonicated for 15 minutes to generate homogenous microparticle distributions. In each experiment, ten microliter of the particles suspension was pipetted into the spacer channel through the input port.

3.3.2 Experimental Setup

The LOC device was place on the stage of an optical microscope (BX51, Olympus, Pennsylvania, USA), as shown in Figure 3.10. A function generator (GFG-8255A, Good Will Instrument, New Taipei City, Taiwan) was used to supply the microelectrodes with AC signal. The dynamic behaviors of the polystyrene microparticles in response to the DEP force were recorded with a CCD camera (UC30, Olympus, Pennsylvania, USA) mounted on the top of the microscope. The images were

captured and stored on a personal computer (PC). A schematic diagram of the system design is illustrated in Figure 3.11.

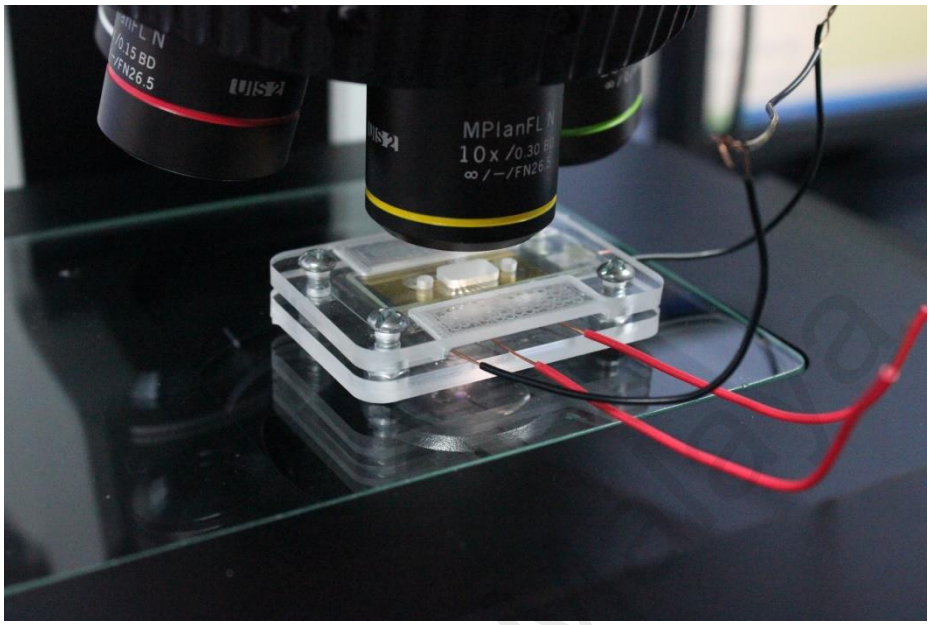

Figure 3.10: The LOC device placed on the microscope stage during DEP experiments.

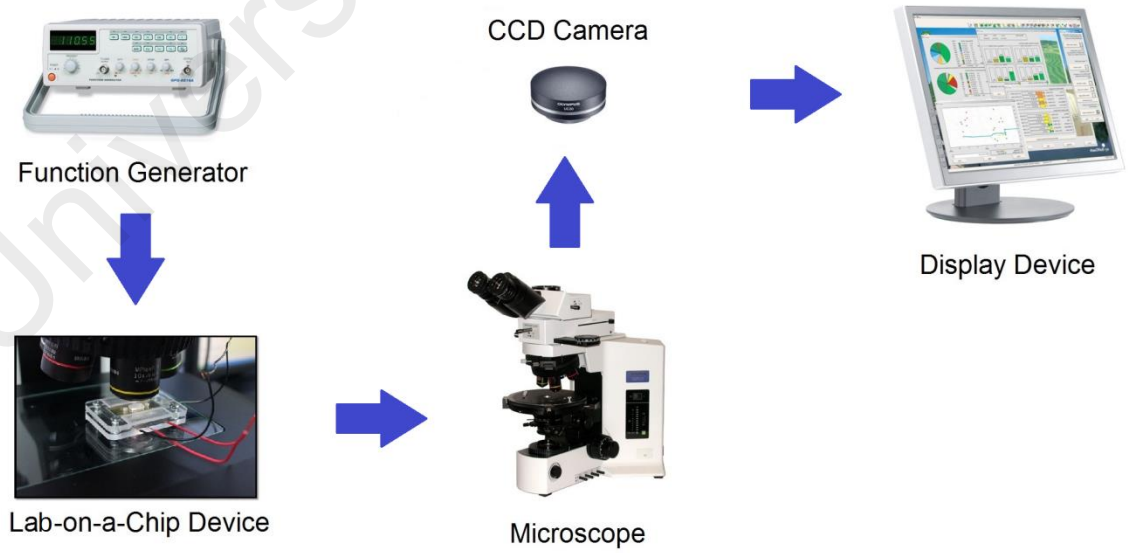

Figure 3.11: The system design used in the current project.

3.3.3 Polystyrene Microparticles Conductivity Calculation

Prior to conducting manipulation and separation experiments on the polystyrene microparticles, the DEP response (i.e., Re[K(ω)]) of the 1, 5 and 15 μm polystyrene microparticles must be plotted over a frequency range between 1kHz and 10 MHz. These plots will facilitate choosing the right frequency to conduct the manipulation and separation experiments.

To plot DEP response (i.e., Re[K(ω)] versus frequency) of the polystyrene microparticles using Equation 2.2, the conductivity and permittivity values of the microparticles and the suspending medium must be known. In the case of the crossover frequency (in which the DEP effect changes from positive to negative or *vice versa*), the Clausius-Mossotti factor $K(\omega)$ becomes zero. Then, Equation 2.2 can be rewritten as follows:

$$\varepsilon_p^* - \varepsilon_m^* = 0$$

$$\text{or } \varepsilon_p^* = \varepsilon_m^* \qquad (3.1)$$

The values of the complex permittivity of the particles ε_p^* and the medium ε_m^* in Equation 2.3 were substituted in Equation 3.1, resulting:

$$\varepsilon_p - j\frac{\sigma_p}{\omega} = \varepsilon_m - j\frac{\sigma_m}{\omega} \qquad (3.2)$$

$\varepsilon_p, \varepsilon_m, \sigma_m$ and ω are known. Hence, Equation 3.2 was solved to get the unknown parameter (particles conductivity σ_p).

$$-j\frac{\sigma_p}{\omega} = \varepsilon_m - j\frac{\sigma_m}{\omega} - \varepsilon_p$$

$$\sigma_p = -\frac{\omega}{j}[\varepsilon_m - j\frac{\sigma_m}{\omega} - \varepsilon_p]$$

$$\sigma_p = \sigma_m + j\omega(\varepsilon_m - \varepsilon_p) \quad (3.3)$$

where $\varepsilon = \varepsilon_r \times \varepsilon_o$, in which ε_r is the relative permittivity and ε_o is the permittivity of free space and equals to $8.854187817\times10^{-12}$ F/m.

As discussed in Subsection 4.3.1., the measured crossover frequency of 1, 5 and 15 µm polystyrene particles are 1100 kHz, 180 kHz and zero, respectively. The DI water (medium) conductivity σ_m and relative permittivity $\varepsilon_{r.m}$ are 2×10^{-4} S/m and 78, respectively. The relative permittivity of the polystyrene particles $\varepsilon_{r.p}$ is 2.5. Then, the conductivity values σ_p can be calculated for respected particles using Equation 3.3.

i. 1 µm particles

First, the angular frequency ω is calculated as follows:

$\omega = 2\pi f = 2 \times 3.14159 \times 1.1\times10^6$

$\omega = 6.9115\times10^6$ rad/s

Then, the conductivity value of 1 µm particles is calculated using Equation 3.3 as follows:

$\sigma_{p,1\mu m} = 2 \times 10^{-4} + j \times 6.9115\times10^6 \times 8.854187817\times10^{-12} \times (78 - 2.5)$

$\sigma_{p,1\mu m} = 2 \times 10^{-4} + j\ 4.6 \times 10^{-3}$

$|\sigma_{p,1\mu m}| = 4.6 \times 10^{-3}$ S/m

i. 5 µm particles

First, the angular frequency ω is calculated as follows:

$$\omega = 2\pi f = 2 \times 3.14159 \times 180 \times 10^{3}$$

$$\omega = 1.13097 \times 10^{6} \text{ rad/s}$$

Then, the conductivity value of 5 µm particles is calculated using Equation 3.3 as follows:

$$\sigma_{p,5\mu m} = 2 \times 10^{-4} + j \times 1.13097 \times 10^{6} \times 8.854187817 \times 10^{-12} \times (78 - 2.5)$$

$$\sigma_{p,5\mu m} = 2 \times 10^{-4} + j\ 7.5604 \times 10^{-4}$$

$$|\sigma_{p,5\mu m}| = 7.8 \times 10^{-4} \text{ S/m}$$

i. 15 µm particles

First, the angular frequency ω is calculated as follows:

$$\omega = 2\pi f = 2 \times 3.14159 \times 0$$

$$\omega = 0 \text{ rad/s}$$

Then, the conductivity value of 15 µm particles is calculated using Equation 3.3 as follows:

$$\sigma_{p,15\mu m} = 2 \times 10^{-4} + j \times 0 \times 8.854187817 \times 10^{-12} \times (78 - 2.5)$$

$$\sigma_{p,15\mu m} = 2 \times 10^{-4}$$

$$|\sigma_{p,15\mu m}| = 2 \times 10^{-4} \text{ S/m.}$$

3.4 Cells Discrimination Studies

The developed DEP device was utilized to discriminate between normal and dengue-infected WRL-68 cells. The following subsections explain the sample preparations and the experimental procedure for this step of the project.

3.4.1 Sample Preparation

3.4.1.1 DEP Experimental Medium

DEP experiments involving biological cells required the preparation of an appropriate medium with specific conductivity. In the current project, the DEP medium was prepared from 280 mM D-mannitol (Sigma-Aldrich Co., Munich, Germany). The medium was adjusted to a measured conductivity of 100 µS/cm by adding potassium chloride (KCl), as confirmed using a Hanna HI 991300 conductivity meter (Hanna Instruments, Michigan, USA). The procedure for preparing the DEP medium is outlined in Table 3.7.

Table 3.7: Procedure of preparing the DEP experimental medium.

Step	Action
Step 1	Measure 12.7 g of D-mannitol using digital balance.
Step 2	Fill an appropriate beaker with 250 mL DI water.
Step 3	Dissolve the D-mannitol in the DI water and mix the solution carefully by a magnetic stirrer.
Step 4	Prepare 100 mM KCl by dissolving 3.75 g of KCl into 500 mL DI water.
Step 5	Drip carefully few drops of KCl solution into the D-mannitol solution and measure its conductivity instantaneously. Stop dripping once the target conductivity is achieved.

3.4.1.2 WRL-68 Cells

Human hepatic fetal epithelial cells (WRL-68 cells) were cultured in a 24-well plate (1.5×10^5) and incubated for 24 hours at 37°C and 5% CO_2. The cells were infected with dengue virus (DENV2-isolate Malaysia M2, GenBank Taxonomy No.: 11062) by adding virus supernatant to the cells at a multiplicity of infection (MOI) of 0.2, followed by incubation for 2 hours with gentle shaking every 15 minutes for optimal virus-to-cell contact. The cells were washed twice with fresh serum-free Dulbecco's Modified Eagle's Medium (DMEM) media after removing the virus supernatant. New complete DMEM media were then added, and the cultures were incubated for 5 days. Afterward, the cellular supernatants were removed, and the cells were washed 3 times with Phosphate Buffered Saline (PBS) and trypsinized. Finally, the cells were resuspended in the DEP experimental medium by washing them twice by the DEP experimental medium and collecting them by centrifugation at 1500 RPM for 5 minutes.

3.4.1.3 Cell Count

To compare the DEP responses of normal and infected cells, it was important to maintain the same cell concentration in each sample. Therefore, cell counting tests were conducted for each sample prior the DEP experiments. In the current project, cell counting was conducted using a Laboroptik hemacytometer (LO - Laboroptik Ltd., Lancing, UK), as shown in Figure 3.12. Cells were maintained at 2×10^6 cells/mL in all of the DEP experiments on cells.

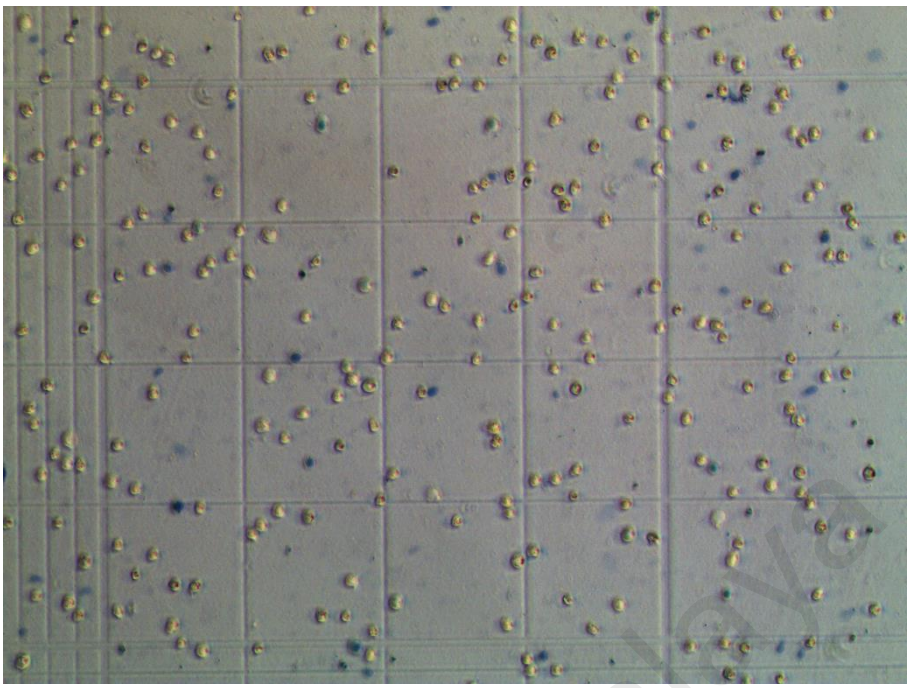

Figure 3.12: Microscopic image taken for a hemacytometer during cell counting procedure.

3.4.2 Experimental Setup

A similar setup to that used in the system validation experiments explained in Subsection 3.3.2 was used to conduct the application experiments. To study the DEP of normal and dengue-infected cells, 15 different frequencies over a range of 1 kHz to 5 MHz were supplied to each set of cells via the microarray dot electrodes. Each experiment (for each frequency and each sample) was repeated 4 times, and an image was captured before and after each signal application. A total of 120 samples (60 samples of normal WRL-68 cells and 60 samples of Dengue-infected WRL-68 cells) were used to conduct the DEP experiments to discriminate between normal and infected cells. A total of 240 images were saved on a personal computer and used in the analysis.

3.5 Image Analysis

Processing the acquired images was an important step to measure the DEP response of cell populations, as it is not possible to directly quantify the DEP force applied to

each cell population. Figure 3.13 shows a block diagram summarizing the image-processing steps that were conducted in the current work.

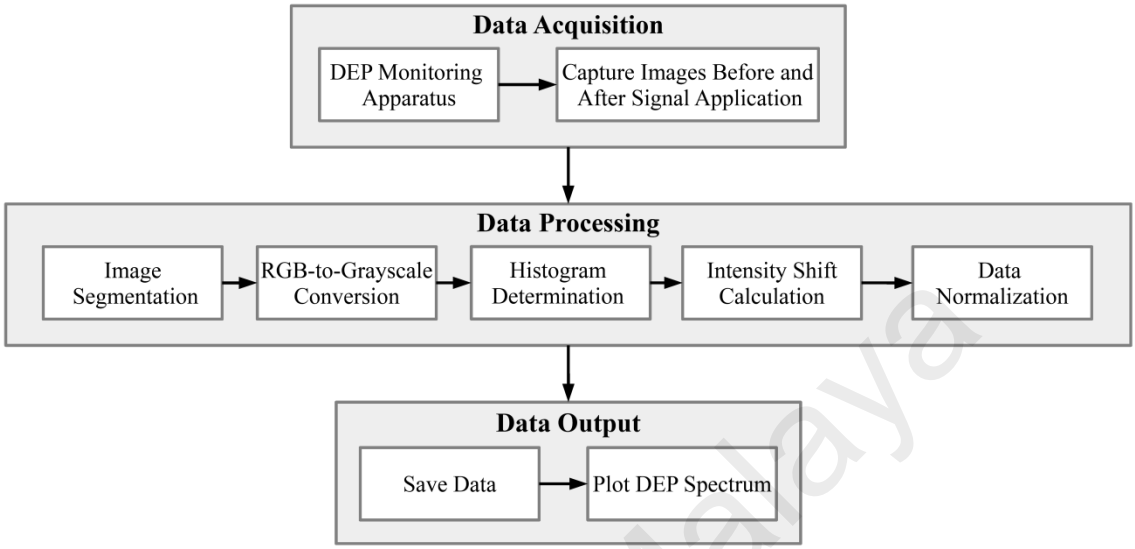

Figure 3.13: Block diagram showing the image-processing steps.
The diagram shows the steps from observing and capturing images of the cells movement to plotting the DEP spectrum.

3.5.1 Image Segmentation

The region of interest (ROI) was segmented out of the captured images before analyzing the results and plotting the DEP spectra of the respective cell populations. Instead of using a circular band to segment the circular area of the dot as conducted by Fatoyinbo *et al*. (2008), Kadri (2010) produced a good DEP spectra by segmenting the dot area using a square with a width of half of the radius of the dot. Therefore, the current project used a square with a width of 100 µm to segment the central part of the dot using digital processing software, as illustrated schematically in Figure 3.14. It is obvious that the analysis of these segmented areas will reflect the movement of the particles in response to the DEP forces.

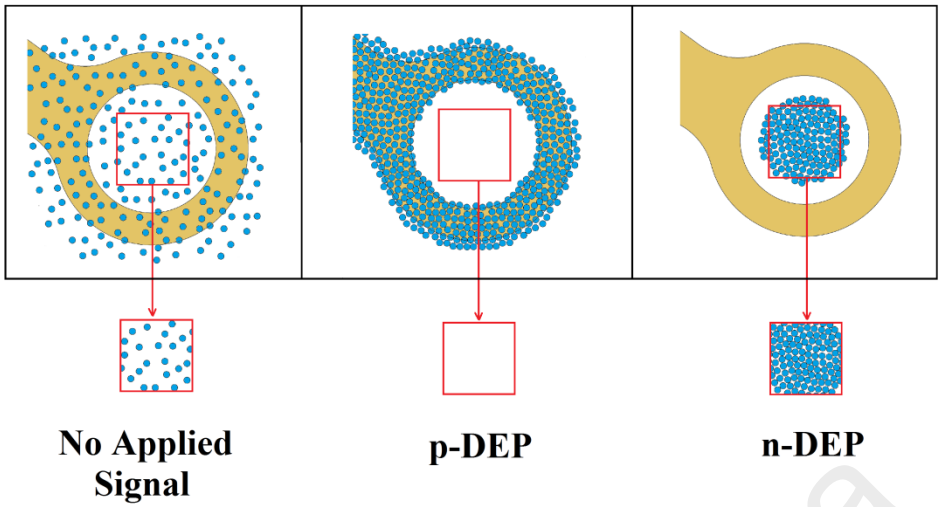

Figure 3.14: Illustration for image segmentation procedure.

3.5.2 RGB-to-Grayscale Conversion and Histogram Determination

At this stage, the segmented images were converted to the grayscale spectrum by using the *rgb2gray* function in MATLAB® software (Mathworks Inc.,Natick, Massachusetts, USA). Therefore, the images were represented by discrete values ranging from 0 (black) to 255 (white) (Gonzalez *et al.*, 2004). The histogram of the ROI for each dot was then calculated by counting all pixels with the same intensity values. This step was conducted by calling the *imhist* function in MATLAB®. Figure 3.15 shows a typical histogram generated from a segmented image.

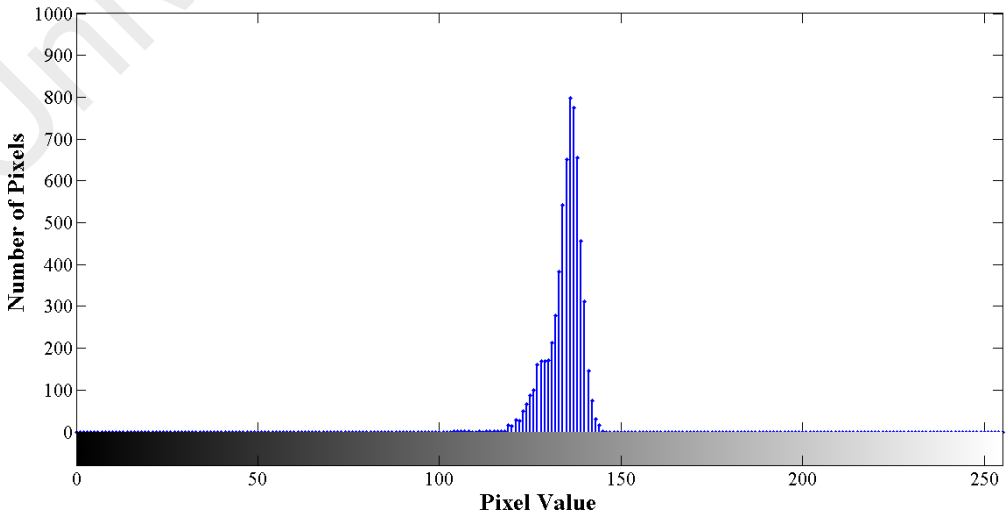

Figure 3.15: A typical histogram generated from a segmented image using MATLAB®.

3.5.3 Intensity Shift Calculation

Cells movements were measured by analyzing the light intensity shift within the ROI vicinity before and after the application of the electric field. This analysis was based on the Cumulative Modal Intensity Shift (CMIS) image analysis technique, which depends on the histogram's modal value of the processed image (Fatoyinbo *et al.*, 2008). Typically, this method computes the cumulative pixel intensity value by first finding the modal value of the captured image's ROI histogram (i.e., the peak value) and then summing the number of pixels (*N*) from this point to the maximum light intensity value of the histogram (i.e., 255 pixel value). The light intensity shift (*I*) at each frequency was calculated by subtracting the cumulative pixel value of the initial image (without a signal) from the cumulative pixel value of the final image (after signal application), as shown in the following equation (Fatoyinbo *et al.*, 2008):

$$I = \sum_{i=P_{\text{modal}}}^{255} N_A(i) - \sum_{j=P_{\text{modal}}}^{255} N_B(j) \qquad (3.4)$$

where N_B is the number of pixels in the image captured before signal application, N_A is the number of pixels in the image captured after signal application, and i and j represent the pixel values. The light intensity shifts were calculated for 240 images (120 images of normal cells and 120 images of infected cells) using Equation 3.1. The MATLAB code used to calculate the cumulative pixel intensity value of the images $\sum_{i=P_{\text{modal}}}^{255} N_A(i)$ and $\sum_{j=P_{\text{modal}}}^{255} N_B(j)$ is included in Appendix A.

3.5.4 Data Normalization

To make use of the light intensity shifts by plotting them against the respected frequencies, their values had to be normalized. All of the calculated light intensity shifts from the previous subsection were normalized by dividing all the values by 1000. Data resulted from the normalization procedure ranged from -1 to 1.

3.5.5 DEP Spectrum

The DEP behavior of each cell population can be examined by obtaining its DEP spectrum. Light intensity shifts, therefore, were plotted against the corresponding frequency at which the image was captured to construct the DEP spectrum using MATLAB®. The MATLAB code for plotting the DEP spectra of the normal and infected cells is included in Appendix B.

3.6 Statistical Analysis

Statistical analysis was conducted using SPSS version 16.0 (SPSS Inc., Chicago, Illinois, USA) to assess the difference in the DEP response of the healthy and infected cells. A parametric two independent sample Student's t test was carried out. The data introduced to the test were the individual data points of the light intensity shifts of the normal and infected cells at each frequency. The number of samples was 120 (60 samples of normal cells and 60 samples of infected cells). *P* value of < 0.05 was interpreted as statistically significant. The performance evaluation of the statistical test is included in Appendix C.

CHAPTER 4: RESULTS AND DISCUSSION

4.1 Introduction

This chapter presents the results that were obtained in this project. The chapter includes the simulation results and a discussion of the microarray dot electrode. After that, the fabrication results of the developed LOC layers are shown. Then, the results of the experiments that were conducted to test the proposed LOC platform are presented and discussed. After that, the DEP experiments on normal and dengue-infected WRL-68 cells are explained and discussed. Finally, a DEP analysis of the resulted figures was presented.

4.2 Lab-on-a-chip Design and Development

4.2.1 Electrode Simulation

To optimize the electrode geometry parameters, a numerical analysis of the electric field generated by the microarray dot electrode was conducted. The results of this analysis were published in Yafouz *et al.* (2012).

First, different experiments were run utilizing different frequencies; however, the change in the electric field strength (V/m) and distribution was negligible. Theoretically, this was expected because frequency plays a significant role only in the determination of the Clausius-Mossotti factor [K(ω)], which affects the DEP force, as expressed in equation (2.1) (Cao *et al.*, 2008). Therefore, the frequency of the applied signal controls the DEP force via the Clausius-Mossotti factor rather than the electric field strength.

The rest of the simulation experiments were conducted by applying a 10 V_p sinusoidal electrical signal with a frequency of 100 kHz. Figure 4.1 shows a typical result of the electric potential of the designed model. The electric potential at the bottom

microarray dot electrode is 10 V while degrading at the gasket chamber until it becomes 0 V at the top ground ITO electrode, as expected.

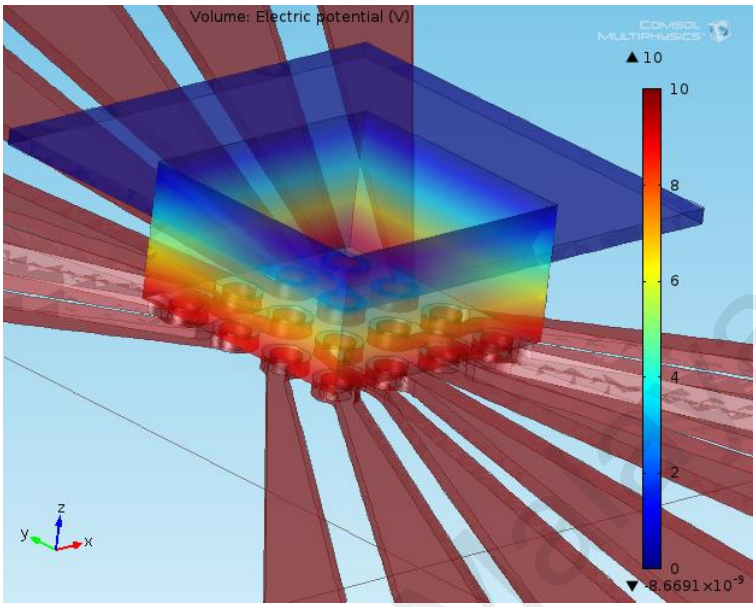

Figure 4.1: Typical electric potential (V) distribution generated from the designed model.

Figure 4.2 shows the distribution of the electric field strength generated from the electrode without a ground plane between the apertures of the dots, with dot diameters of 100, 150 and 200 µm. On the other hand, Figure 4.3 illustrates the distribution of the electric field strength of the electrode with a ground plane between the apertures of the dots, with dot diameters of 100, 150 and 200 µm. These results are associated with the adjustment of the ring width to change the diameters of the dots while maintaining the same distance between the adjacent dots (refer to Figure 3.5). The strength of the electric field is illustrated by colors ranging from blue (low strength) to red (high strength).

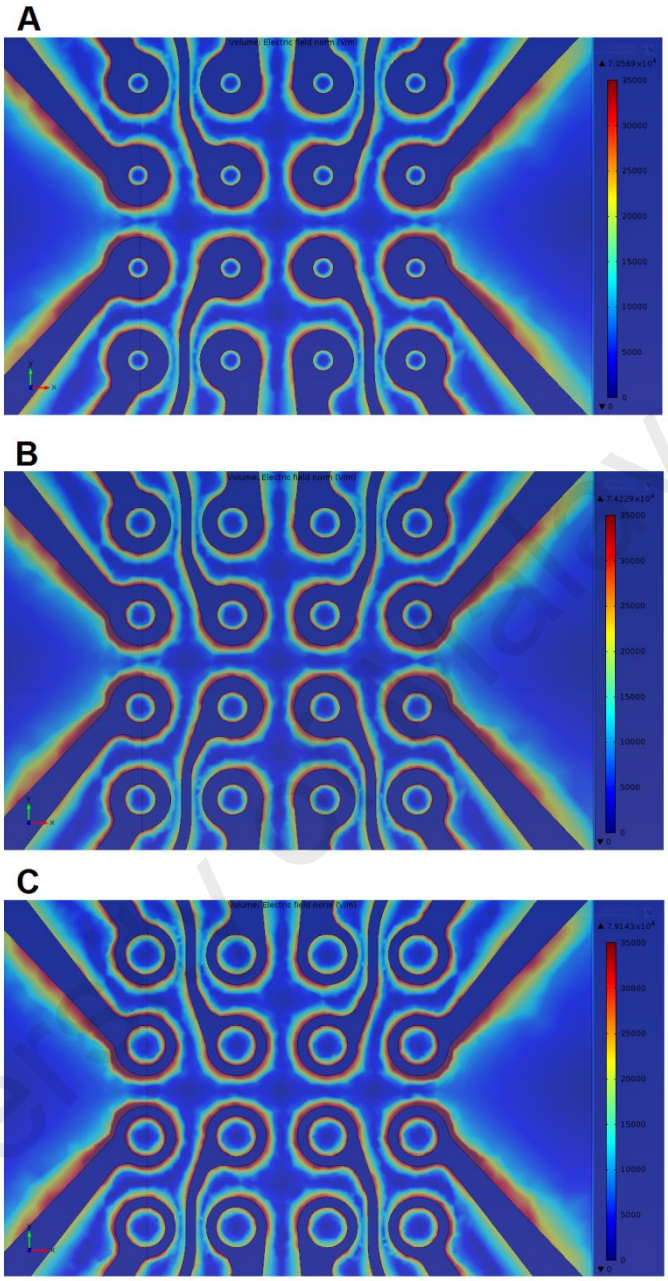

Figure 4.2: Electric field strengths of electrodes without ground plane between dots apertures.

Electrode dots diameters are (A) 100 µm, (B) 150 µm and (C) 200 µm. Dots diameters were adjusted by changing the ring width.

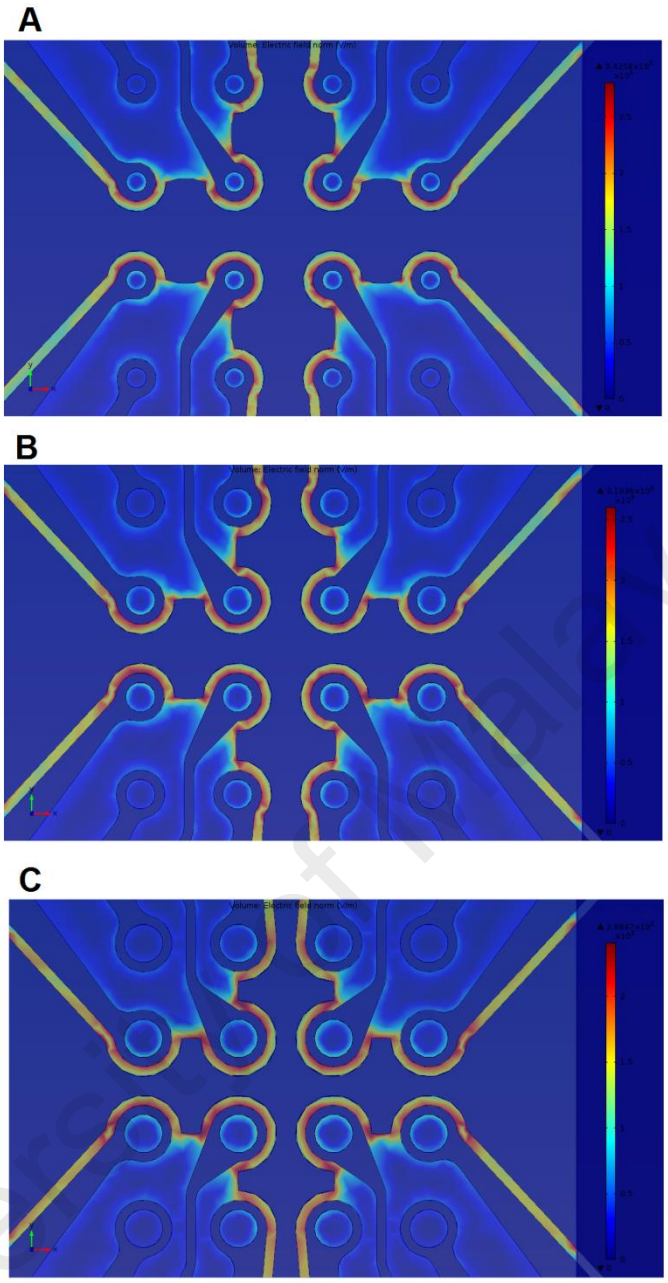

Figure 4.3: Electric field strengths of electrodes with ground plane between dots apertures.
Electrode dots diameters are (A) 100 µm, (B) 150 µm and (C) 200 µm. Dots diameters were adjusted by changing the ring width.

The results reveal that the values of the electric field strength at the edge of the dots are higher than that at the center of the dots for all electrode designs. This is aligned with previous simulations in the literature that show the electric field of planar electrodes increases near the electrode edge (Burgarella *et al.*, 2010; Cao *et al.*, 2008;

Cha *et al.*, 2011; Chuang *et al.*, 2011). Therefore, the DEP force is expected to be higher at the dot edges than at the dot centers.

Moreover, Figure 4.2 and Figure 4.3 depict that the electric field strengths are axisymmetric around the center of the aperture of the dots, which suggests that the DEP force is also axisymmetric within the dot volume. This indicates that the particles will undergo a homogenous radial movement. The direction of this movement will depend on whether the sign of the Clausius-Mossotti factor [$K(\omega)$] is positive or negative. In the case of p-DEP, particles would be attracted to the dot edge (i.e., the high electric field region), while they would be repelled to the dot center (i.e., the low electric field region) in the case of the n-DEP force. This finding is consistent with the work performed by Kadri (2010), in which K562 leukemic cells were enrich at the centers of the dots in the case of n-DEP and were attracted to the dot edges in the case of p-DEP.

The maximum values of the electric field strengths for the two electrode designs are summarized in Table 4.1 for the prescribed dot diameters. The results confirm that the strength of the electric field increases when a ground plane is introduced between the adjacent dots. According to Stulík *et al*. (2000), the gaps between adjacent electrodes should be wider than the diffusion layer thickness to prevent overlapping of the diffusion layers of the adjacent electrodes. Thus, the advantageous outcome of inserting a ground plane between adjacent dots in the proposed electrode is to avoid the overlapping that might occur between the electric fields generated by adjacent dots because the ground plane absorbs any charges in this area.

Table 4.1 also reveals that the values of the electric field strength decrease when the diameter of the dots increases with a ground plane between the dots. The highest electric field strength value is 3.426×10^5 V/m and this is associated with an electrode that has a dot diameter of 100 µm. On the other hand, the values of the electric field

strength increase as the diameters of the dots in the electrodes increase when there is no ground plane between the dots, as shown in Table 4.1: Maximum electric field strengths (V/m) of electrodes with and without ground plane between dot apertures for different dots diameters. Table 4.1. The maximum electric field strength was produced by an electrode that had a dot diameter of 200 μm.

Table 4.1: Maximum electric field strengths (V/m) of electrodes with and without ground plane between dot apertures for different dots diameters.

Dot Diameter (μm)	100	150	200
Electrodes without ground plane between dots	7.057×10^4	7.423×10^4	7.914×10^4
Electrodes with ground plane between dots	3.426×10^5	3.194×10^5	2.885×10^5

The dot diameters in the previous electrodes were changed by changing the ring width while maintaining the same distance between adjacent dots. To explore the effects the ring width may have on the electric field strength and distribution, electrodes with different dot diameters were designed with a fixed ring width (50 μm) for all sizes of dots, while varying the distances between adjacent dots. The results of the electric field strengths of these electrodes are shown in Figure 4.4. The results reveal that the distribution of the electric field over the dot electrodes is similar to that shown in Figure 4.2. Hence, ring width does not affect electric field distribution.

Table 4.2 depicts the maximum values of the electric field strengths of electrodes with fixed dot separation distances and electrodes with fixed rings. The findings show that there are insignificant differences between the two cases. Therefore, electrode ring width has no major effect on the induced electric field strength over the dot electrodes.

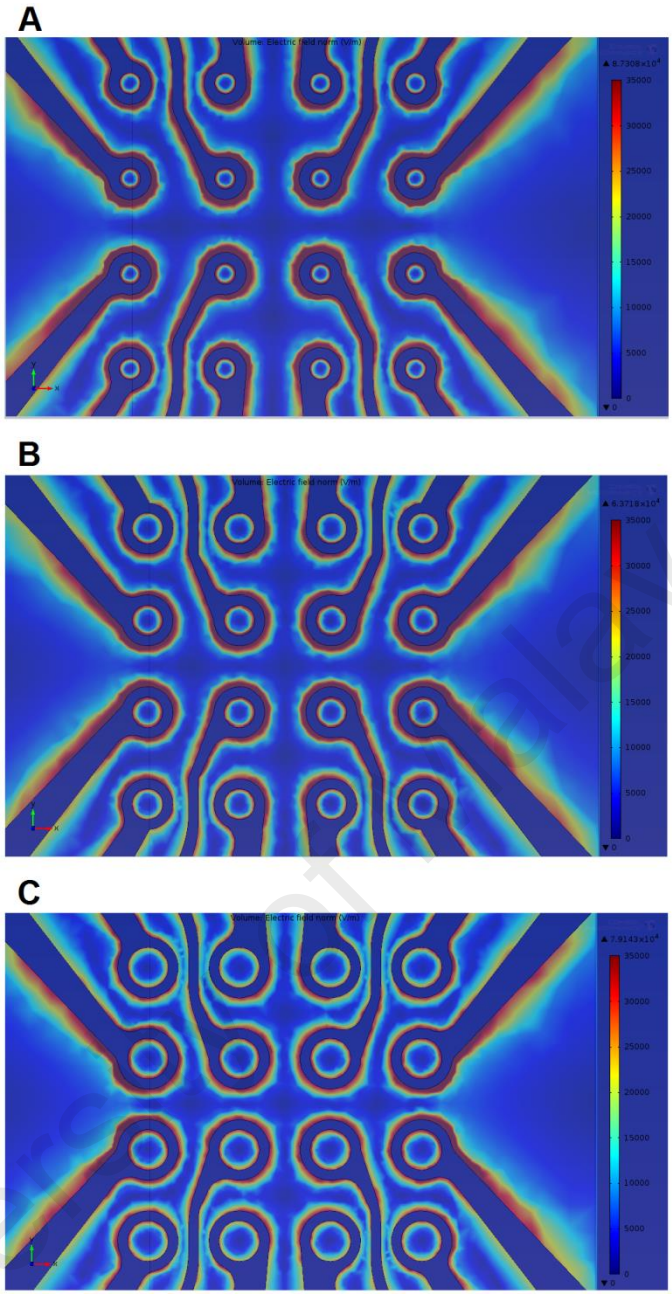

Figure 4.4: Electric field strengths of electrodes without ground plane between dots apertures.

Electrode dots diameters are (A) 100 µm, (B) 150 µm and (C) 200 µm. Dots diameters were adjusted by changing the distance between adjacent dots.

Table 4.2: Maximum electric field strengths (V/m) of electrodes without ground plane between dot apertures with fixed dots separation distance and with fixed ring width for different dots diameters.

Dot Diameter (µm)	**100**	**150**	**200**
Electrodes with fixed dots separation distance (150 µm)	7.057×10^4	7.423×10^4	7.914×10^4
Electrodes with fixed ring width (50 µm)	8.731×10^4	6.372×10^4	7.914×10^4

4.2.2 Electrode Fabrication

The microarray dot electrodes, needed to generate the non-uniform electric field for DEP, were fabricated using photolithography process as explained in Subsection 3.2.2. The final output of the fabricated gold-coated glass electrode is shown in Figure 4.5.

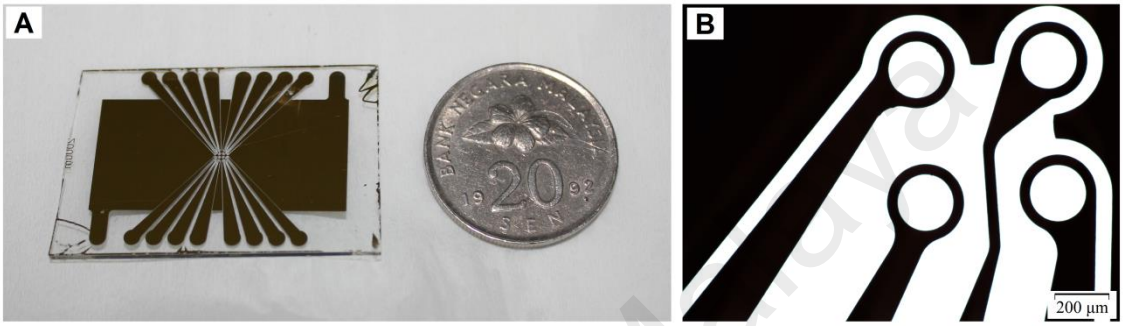

Figure 4.5: The fabricated gold 4 × 4 microarray dot electrode.
(A) Digital image with Malaysian 20 cents coin, (B) microscopic image showing the pattern was produced efficiently.

4.2.3 Design and Fabrication of Lab-on-a-chip Layers

A novel LOC design configuration was designed in the current project to be compatible with the microarray dot electrode. The detailed specifications and design criteria were fully explained in Subsection 3.2.4. The final result of the fabricated LOC components is shown in Figure 4.6.

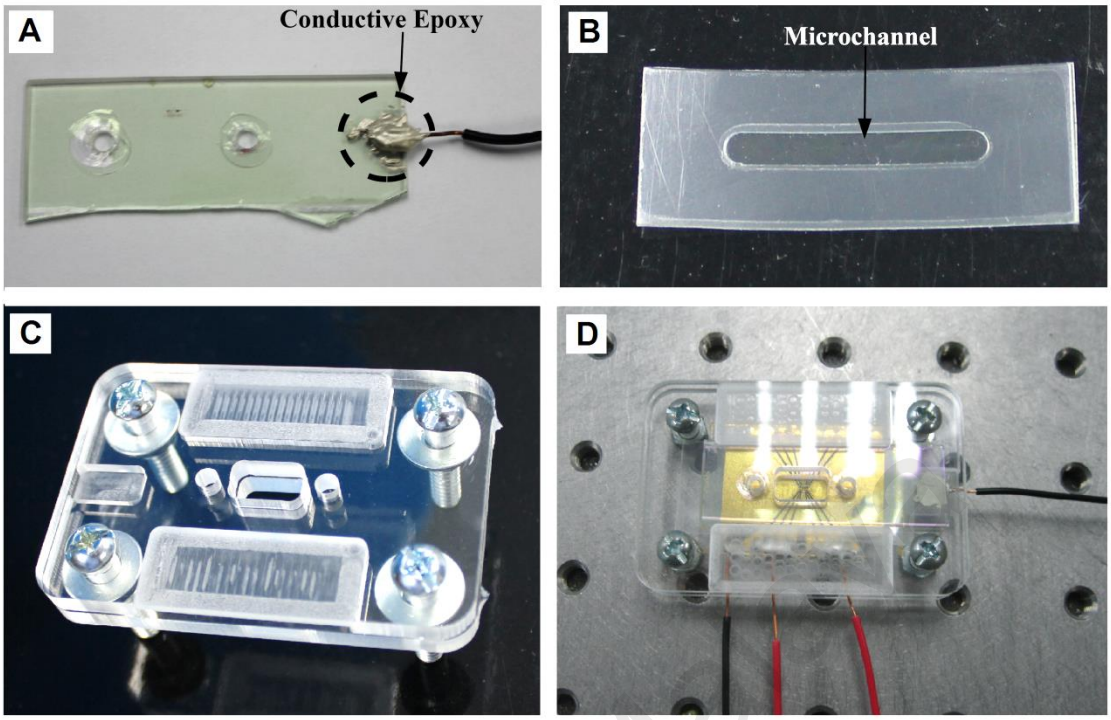

Figure 4.6: The final result of the fabricated LOC components.
(A) ITO layer, (B) spacer, (C) top and bottom covers, and (D) top view of the LOC device assembled.

4.3 Lab-on-a-chip Testing

Before the proposed LOC platform could be applied to study the DEP behaviors of biological cells, the functionality of the LOC platform needed to be tested. To achieve this, size-dependent manipulation and separation DEP experiments were conducted on mixtures of different-size polystyrene microparticles. The results of these expirements were published in (Yafouz *et al.*, 2014).

During each DEP experiment, particle movements were observed in the dot region of the electrodes. Signals with different frequencies can be applied to individual dots simultaneously in order to achieve multiple microparticle separations concurrently; however, each figure presented in the results focuses on a single dot aperture to closely examine the response of the particles to the DEP field inside the dot aperture.

In the case of a p-DEP response, particles travelled toward the high electric field gradient region (the dot edge) and away from the dot center. In contrast, in the n-DEP response, particles travelled away from the high electric field gradient region and collected at the dot center. This particle response to the DEP effect is aligned with DEP theory, microarray dot electrode simulations and previous DEP systems, in which particles are attracted to the electrode edge in p-DEP and repelled away from the electrode in n-DEP (Khoshmanesh *et al.*, 2010; Mulhall *et al.*, 2011; Yafouz *et al.*, 2012).

Furthermore, while observing particle migration in n-DEP, some of the microparticles were repelled from the electrode dots and collected between the dots, as indicated by the arrows in Figure 4.7. However, the focus was only on the dot centers, as illustrated in Figure 3.14. This is because the central part of the dot is the confined area where cell characterization can be conducted by studying the change in light intensity inside the dot aperture.

First, experiments were conducted using a 10 V_{p-p} sinusoidal signal; however, it was observed that this signal amplitude was not sufficient to generate a rapid DEP response. However, when the applied voltage was increased to 20 V_{p-p}, a faster microparticle response was obtained (final particles position was reached in less than 5 seconds). Therefore, the 20 V_{p-p} sinusoidal signal was used for the rest of the experiments.

The following subsections present the results and discussion of the manipulation and separation experiments of different mixture of samples based on polystyrene microparticles.

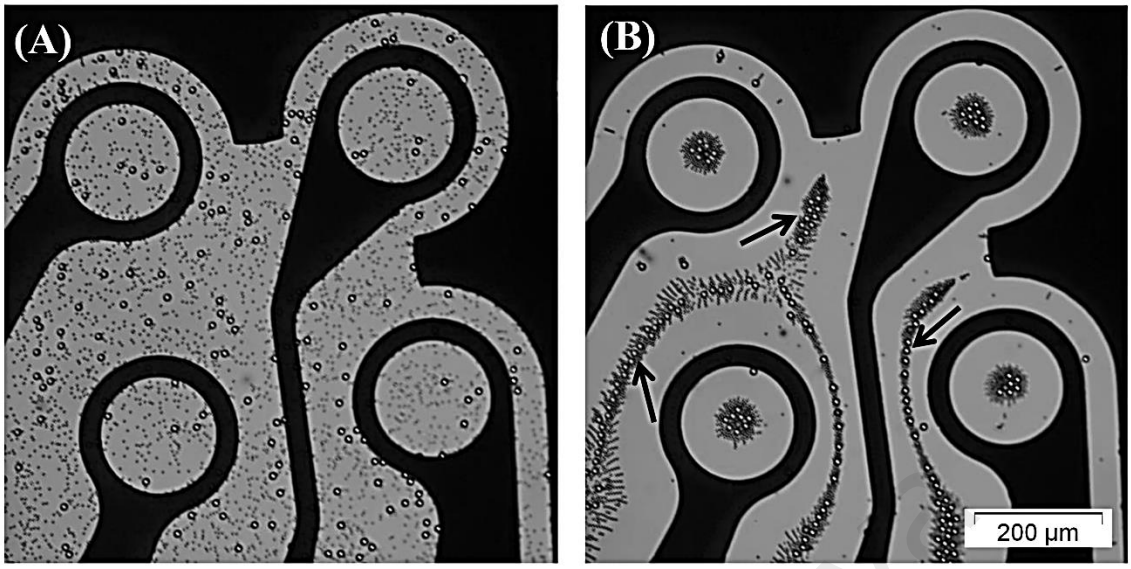

Figure 4.7: Typical experimental result for a mixture of microparticles under n-DEP effect.
(A) shows the microparticles distributed homogenously over the electrode area before the application of electric field, while (B) shows the microparticles were collected at the dot centers and in between adjacent dots as a result of n-DEP effect.

4.3.1 DEP Responses of 1, 5 and 15 µm Polystyrene Particles

Prior to conducting manipulation and separation experiments on the polystyrene microparticles, the DEP response (i.e., Re[K(ω)]) of the polystyrene microparticles had to be identified over a frequency range between 1kHz and 10 MHz. The Re[K(ω) of any suspending particle can be plotted versus the applied signal frequency using Equation 2.2. In the current project, the polystyrene microparticles were suspended in DI water as explained in Subsection 3.3.1.

The DI water had a conductivity and relative permittivity of 2×10^{-4} S/m and 78, respectively. The relative permittivity of the polystyrene particles was 2.5 (Khoshmanesh *et al.*, 2010). The overall conductivities of the 1, 5 and 15 µm polystyrene particles must be calculated before the DEP spectra can be acquired. To achieve this end, the crossover frequencies (the transition from p-DEP to n-DEP or *vice versa*) of polystyrene microparticles were experimentally measured in DI water. The measurements were performed by increasing the frequency of the applied signal in

incremental steps from a low value, at which all the microparticles of the same size clearly exhibited p-DEP, until the microparticles demonstrated an n-DEP response and were gathered at the dot centers. The crossover frequencies were 1100 ± 70 kHz and 180 ± 25 kHz for the 1 and 5 μm microparticles, respectively. Furthermore, the 15 μm particles exhibited an n-DEP in the frequency range of 1 kHz to 5 MHz. The obtained crossover values are in good agreement with the results reported by Khoshmanesh *et al.* (2010). Then, the overall conductivity of the particles was calculated using Equation 2.2 (provided that Re[$K(\omega)$] = 0 because the crossover frequency occurs when the Re[$K(\omega)$] changes its sign). The calculated overall conductivities of 1, 5 and 15 μm polystyrene particles equal to 4.6×10^{-3} S/m, 7.8×10^{-4} S/m and 2×10^{-4} S/m, respectively (refer to Subsection 3.3.3 for detailed calculations). Finally, these data were applied in Equation 2.2 for a frequency range of 1 kHz to 10 MHz to obtain the Re[$K(\omega)$] spectra as shown in Figure 4.8 (refer to Appendix D for the MATLAB code used to plot the Re[$K(\omega)$] spectra versus frequency). The DEP spectra indicate the DEP response of each microparticle population at a given frequency. Therefore, different size microparticles can be manipulated and separated merely by carefully selecting the appropriate frequency.

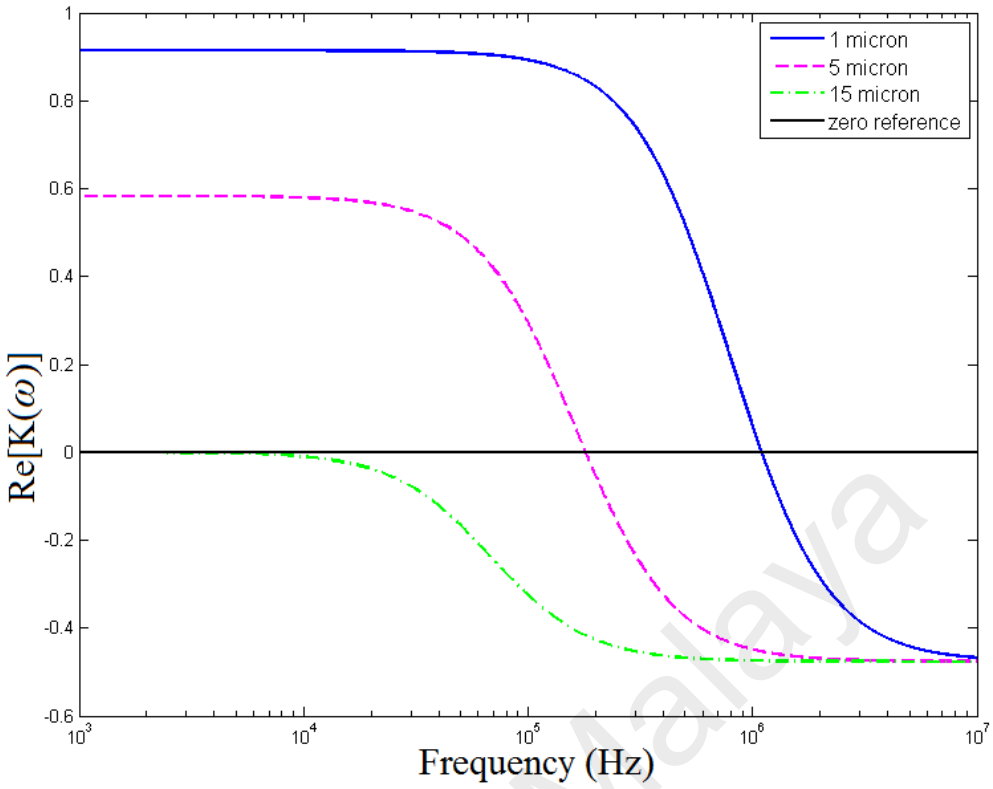

Figure 4.8: Re[K(*ω*)] *versus* frequency for 1, 5 and 15 µm polystyrene particles.

4.3.2 Manipulation of 1 µm Particles

Figure 4.9 illustrates the 1 µm polystyrene particle response when subjected to a DEP field. Before the application of the electric field, the microparticles were homogenously distributed over the dot aperture, as shown in Figure 4.9(A). When a 5 MHz signal was applied to one dot; the microparticles were repelled toward the dot center as depicted in Figure 4.9(B). This microparticle behavior was in response to the n-DEP effect, in which the microparticles travelled away from the high electric field gradient region.

Furthermore, a 100 kHz signal was applied to a different dot; the result is shown in Figure 4.9(C). In this case, the microparticles were cleared from the dot aperture and were attracted to the dot edge, marked by the arrows (the attracted microparticles were unseen in the electrode black zone). This microparticle behavior was in response to the p-DEP effect, in which microparticles migrate toward the high electric field gradient region.

Clearly, the microparticle populations form a cloud at the dot center in the case of n-DEP. This cloud of microparticles can be used to quantify the DEP force applied to the microparticles by assessing the light intensity change in the dot aperture before and after applying the electric potential. In p-DEP, it is not expected to observe a change in the light intensity passing through the dot aperture after applying the electric signal, as no microparticles are obstructing the light at the dot center.

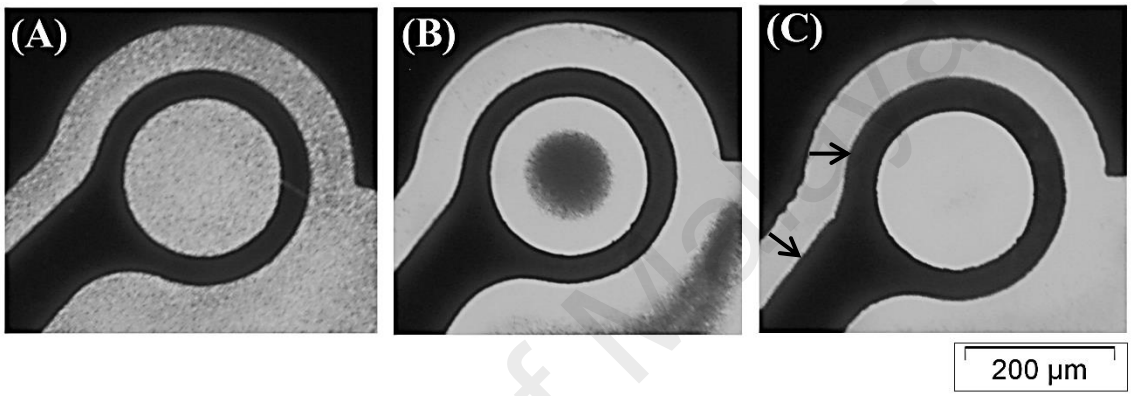

Figure 4.9: The manipulation of 1 µm particles under DEP field.
The microparticles demonstrated p-DEP and n-DEP depending on the applied frequency. Microparticles (a) before applying a non-uniform electric field (homogenously distributed over the dot aperture); (b) after applying 5 MHz signal (n-DEP) and (c) after applying 100 kHz signal (p-DEP).

4.3.3 Manipulation of 5 and 15 µm Particles

The developed device was further used to manipulate 5 and 15 µm particles. Equal volumes of 5 and 15 µm particle solutions, prepared as described in Subsection 3.3.1, were mixed and ultra-sonicated for 15 minutes to make a homogenous mixture of the microparticles.

Figure 4.10(A) demonstrates that both microparticle populations were homogenously mixed and uniformly distributed over the dot electrode before applying the signal. Then, 500 kHz was applied to induce an n-DEP response from both microparticle sizes according to their DEP responses as plotted in Figure 4.8. Figure 4.10(B) shows the 5

and 15 μm particle n-DEP responses. Both microparticle populations were repelled from the electrode edges and collected at the dot center.

Furthermore, it observed that the 15 μm particles experienced a stronger DEP force than the 5 μm particles. This result was visible because the 5 μm particles surrounded the 15 μm particles that occupied the dot center. This phenomenon agrees with the particles' DEP responses shown in Figure 4.8, in which the 15 μm particles had a higher Re[$K(\omega)$] value at 500 kHz than the 5 μm particles.

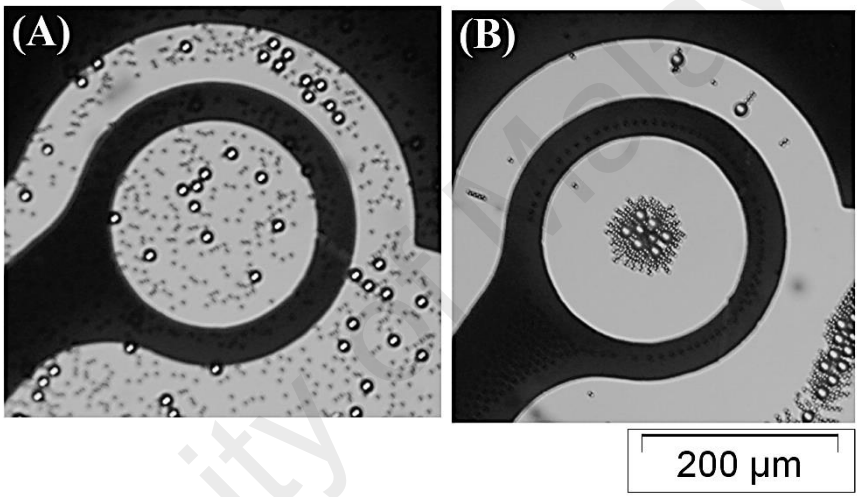

Figure 4.10: The manipulation of 5 and 15 μm particles under DEP field. The figure shows 5 μm particles (seen as the black points) and 15 μm particles (seen as the white circles) (A) before applying a non-uniform electric field (both sizes of microparticles were homogenously mixed and uniformly distributed) and (B) after applying 500 kHz signal (n-DEP on both microparticles).

4.3.4 Separation of 1 and 5 μm Particles

In addition to particle manipulation, the proposed LOC platform was employed to separate microparticles of different sizes as a step in testing the capabilities of the proposed DEP device. First, 1 and 5 μm particles were separated using the DEP effect at a frequency of 450 kHz. A mixture of the two microparticle populations was prepared with a procedure similar to that described in Subsection 4.3.3. Figure 4.11(A) depicts the mixture of 1 and 5 μm particles, in which the 1 μm particles were distributed over the entire electrode, and the 5 μm particles were observed as the black points. After

applying the signal, it was observed that the 1 μm particle population was repelled from the dot center and collected at the dot edge. In contrast, the 5 μm particles were collected at the dot center as shown in Figure 4.11(B). These behaviors were expected and corresponded to the DEP responses of the microparticles (Figure 4.8). At 450 kHz, the 1 μm particles undergo p-DEP; conversely, the 5 μm particles exhibit n-DEP.

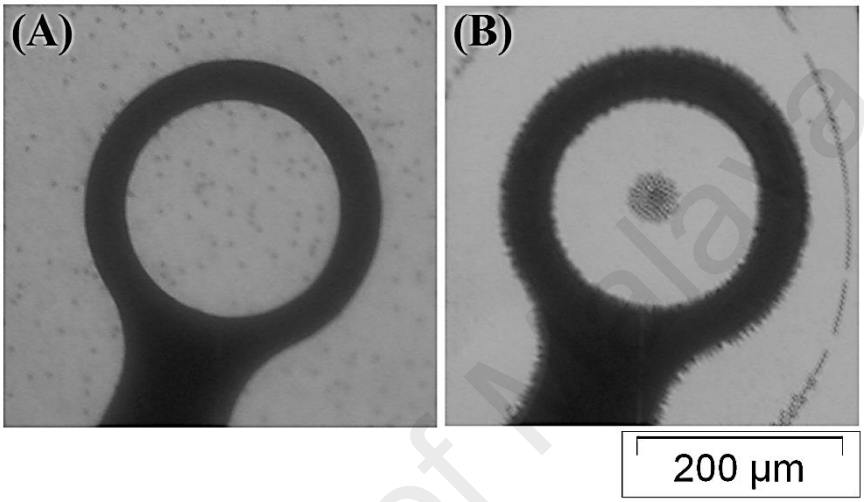

Figure 4.11: The separation of 1 and 5 μm particles under DEP field.
(A) A uniform mixture distribution of 1 and 5 μm particles is depicted (1 μm particles were distributed over the entire electrode; the 5 μm particles were seen as the black points). (B) After applying 450 kHz, the 1 μm particles were attracted to the dot edge (p-DEP), whereas the 5 μm particles were repelled to the dot center (n-DEP).

4.3.5 Separation of 5 and 15 μm Particles

The developed DEP device successfully demonstrated the separation of 5 and 15 μm particles. The samples were prepared with a procedure similar to those described in Subsections 4.3.3 and 4.3.4. Figure 4.12(A) illustrates the mixture of 5 and 15 μm particles distributed over the dot electrode at the beginning of the experiment. The electrode dot was then energized with a 12 kHz signal. The 5 μm particles were attracted to the electrode edge and left the dot aperture zone, while the 15 μm particles were attracted to the dot center (Figure 4.12(B)). These microparticle migration behaviors are in agreement with their corresponding DEP responses, as shown in

Figure 4.8. At 12 kHz, the 5 μm particles demonstrated p-DEP, while the 15 μm particles exhibited n-DEP.

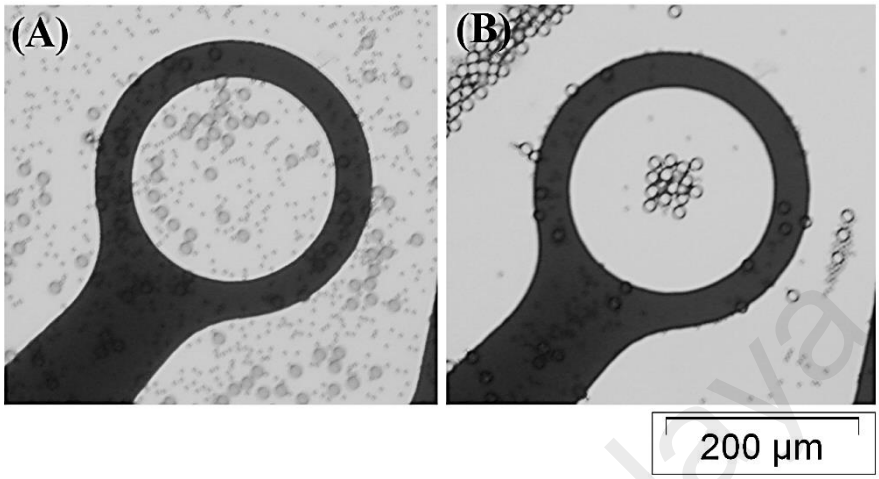

Figure 4.12: The separation of 5 and 15 μm particles under DEP field.
(A) A uniform mixture distribution of 5 and 15 μm particles is shown. (B) After applying 12 kHz signal, the 5 μm particles were attracted to the dot edge (p-DEP), while the 15 μm particles were repelled to the dot center (n-DEP).

It can be concluded from the previous results that the developed device successfully separated different sized polystyrene particles (1 micron mixed with 5 micron, and 5 micron mixed with 15 micron) by using p-DEP and n-DEP effects. In principle, the larger size particles were repelled and concentrate in the center of the dot electrode by n-DEP; however, the smaller sizes were attracted to and collected at the edge of the dot electrode by p-DEP. Hence, the different-sized microparticles could be successfully separated by supplying the electrodes with a suitable frequency that induces p-DEP and n-DEP simultaneously on the different-sized microparticles.

Although two different-sized microparticles can be individually separated using the proposed dot electrode, such electrode geometry will not be able to separate three sizes individually in three separated regions. However, this device can be used to separate one size of particles from a mixture of different sized particles provided that the target

particles undergo n-DEP and are concentrated in the center of the dot electrode, while other populations simultaneously exhibit p-DEP and collect by the electrode edge.

The time needed to conduct microparticles manipulation and separation experiments was reduced significantly in the current project to 5 seconds compared to previous works used similar electrode geometries (4 minutes (Cheng *et al.*, 1998) and 1 minute (Fatoyinbo *et al.*, 2008)). This is a result of the improvement in the electrode geometry and the LOC design.

Despite the fact that the DEP experiments often require skilled personnel to perform them, the proposed device in the current project can be used to measure experimentally the frequency-dependent dielectric properties of specific cells of interest after separating them from a heterogeneous mixture of biological particles, without the need for a skilled operator to take visual measurements . This is feasible because the polarizability of the cells within the dot region can be directly related to change shifts in light transmission through the dot aperture, and quantified from analysis of digital images without the need for field mapping or image registration. Such on-chip parallel DEP experiments show great potential in the development of integrated DEP analysis systems where cells are manipulated, separated and characterized automatically without the need for highly technical human intervention.

4.4 Cells Discrimination Studies

After the proposed device was optimized and tested, DEP experiments on normal and infected cells were conducted in order to achieve the final goal of the current project, which is to discriminate dengue-infected WRL-68 cells from normal ones. The results and discussion of the cell morphology of both normal and infected cells and their DEP experiments and spectra were published in (Yafouz *et al.*, 2015) and are presented in the following subsections.

4.4.1 Cell Morphology

To study the morphology of the WRL-68 cells before and after infection with the dengue virus, samples were examined under the microscope, as seen in Figure 4.13. It was noticed that the morphology of the WRL-68 cells was disturbed after infection. This observation is in line with the findings confirming a morphological alteration in cells after infection with the dengue virus (McCormick *et al.*, 2012; Wu *et al.*, 2000). The size of cells was measured using the public domain ImageJ software (National Institutes of Health). The measured diameters of the normal and infected cells are 17 and 8 µm, respectively. These physical changes are likely due to the cytopathic effect on the host cells induced by the dengue virus. The cytopathic effect is a physical alteration caused in the host cells after viral infection (Ball, 2010). Once a virus invades a cell, it destroys the host cell via modifications in the morphology and physiology of the cell. These changes enable viruses to replicate themselves effectively, causing the host cell destruction. The alteration in the cell's structure causes a change in the value of the Clausius-Mossotti factor in Equation 1. Hence, a unique DEP spectrum is expected for cells before and after dengue infection.

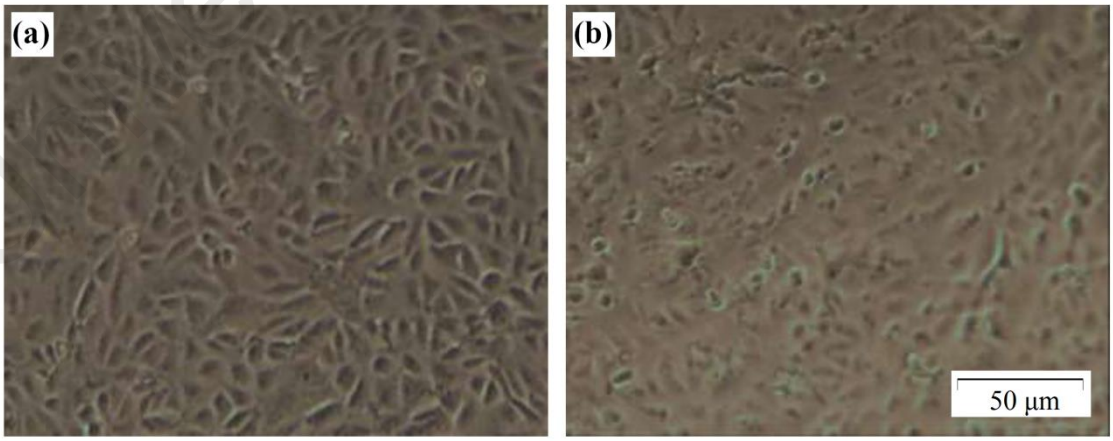

Figure 4.13: Microscopic images of cultured healthy and dengue-infected WRL-68 cells.
(A) Healthy cells, and (B) the morphological changes that appeared in the cells after infection because of the cytopathic effects (100x microscope power).

4.4.2 DEP Experiments

A total of 120 samples (60 samples of normal WRL-68 cells and 60 samples of Dengue-infected WRL-68 cells) were used to conduct the DEP experiments to discriminate between normal and infected cells. Before the application of the electric field, the cells were distributed homogenously over the dot area of the microelectrodes. When the electric signal was supplied to the microelectrode, the cells responded by either collecting at the dot center (in the case of n-DEP) or being attracted to the dot edge and clearing the dot center (in the case of p-DEP). The response of the cells to the applied electric field, exhibiting either the n-DEP or the p-DEP effect, is a function of the frequency of the applied electric field, which controls the permittivity and conductivity of the cells and the suspending medium (refer to Equation 2.3). This DEP mechanism of the dot electrode geometry is well established in (Fatoyinbo *et al.*, 2008; Fatoyinbo *et al.*, 2011; Mulhall *et al.*, 2011).

Selected images of the DEP response of the normal and dengue-infected WRL-68 cells on the dot electrode are presented in Figure 4.14 and Figure 4.15, respectively. Figure 4.14 shows the distribution of normal WRL-68 cells within the dot perimeter before the application of the electric field and after supplying the electrodes with 5 kHz and 5 MHz signals to induce the n-DEP and p-DEP effects, respectively. Similarly, Figure 4.15 depicts the dengue-infected WRL-68 cells before and after experiencing the n-DEP and p-DEP effects when supplied with 5 kHz and 5 MHz signals, respectively. In general, when applying a high-frequency electric field, cells became more polarizable than the suspending medium, resulting in the p-DEP effect. In contrast, when applying a low-frequency electric field, cells became less polarizable than the suspending medium, resulting in the n-DEP effect.

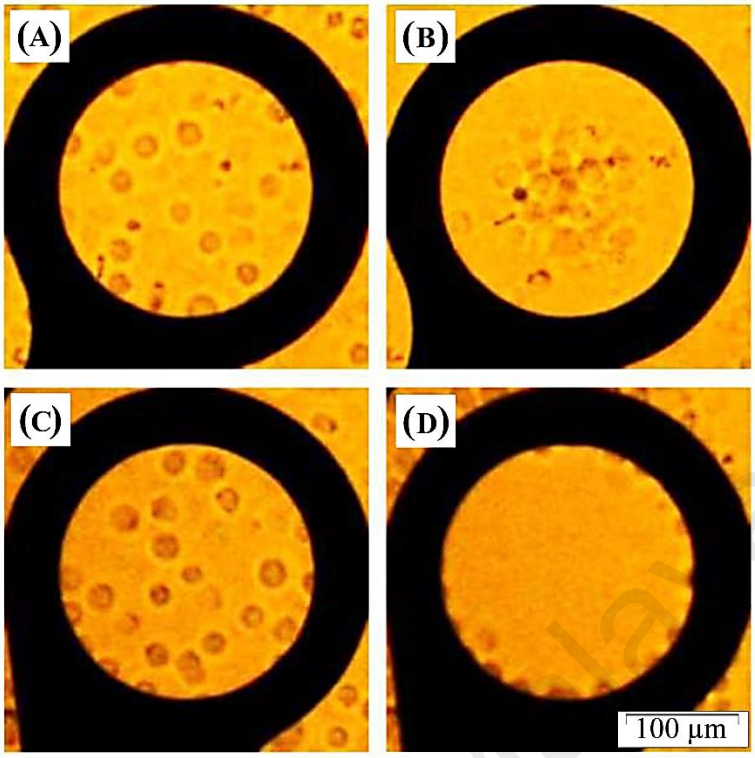

Figure 4.14: Selected images of the n-DEP and p-DEP effects among healthy WRL-68 cells.
(A) and (C) show the cells before the application of the electric field, (B) shows the cells after applying a 5 kHz signal (n-DEP effect), and (D) shows the cells after applying a 5 MHz signal (p-DEP effect).

The movement of the cells within the ROI was studied using the light intensity shift between the initial image and the final image (before and after the electric field application, respectively). The light intensity in the ROI is proportional to the cells concentration based on Beer-Lambert's law of light absorption as demonstrated in (Hoettges *et al.*, 2008). The best ROI to construct the Beer-Lambert area for the CMIS method is the central part of the dot (Fatoyinbo *et al.*, 2008). Moreover, a square with a width of half the radius of the dot was proved to produce good DEP spectra compared with a circular ROI (Kadri, 2010). Therefore, a 100 µm square was used to segment the central part of the dots in each captured image to form the ROI, as illustrated in Figure 3.14.

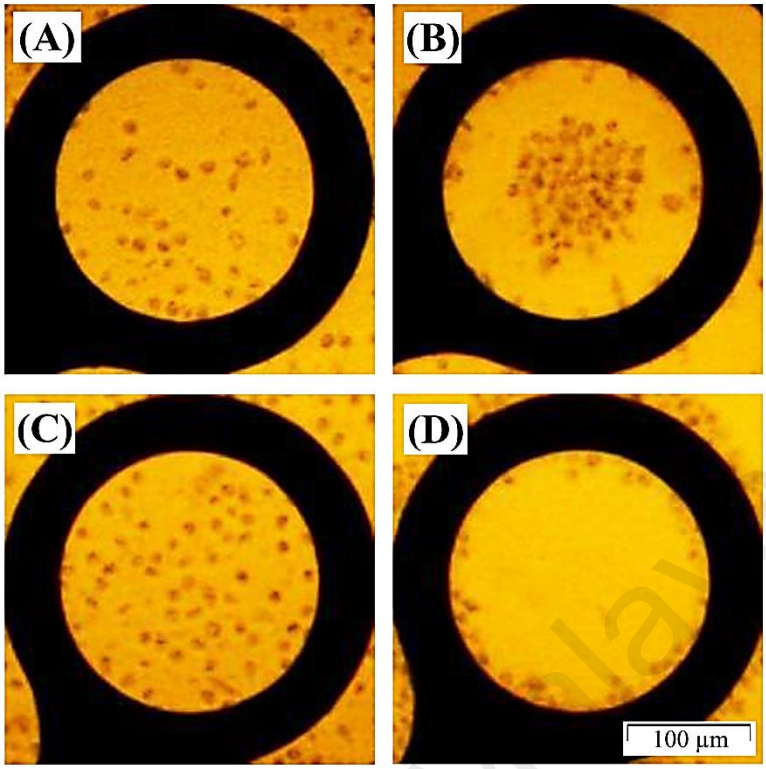

Figure 4.15: Selected images of the n-DEP and p-DEP effects among dengue-infected WRL-68 cells.
(A) and (C) show the cells before the application of the electric field, (B) shows the cells after applying the 5 kHz signal (n-DEP effect), and (D) shows the cells after applying the 5 MHz signal (p-DEP effect).

The n-DEP and p-DEP effects collect the cells in and clear the cells from the ROI, respectively; and hence alter the light intensity in that area. In principle, cells behavior toward n-DEP limits light transmission through the ROI due to cells accumulation at the dot center and therefore will decrease the cumulative pixel value of the ROI image compared with that of the ROI image before electric field application. In contrast, p-DEP increases the cumulative pixel value of the ROI image because the cells are cleared from the dot center, allowing greater light transmission through the ROI region. Accordingly, the shift in the cumulative pixel intensity values of the ROI images should be negative and positive for n-DEP and p-DEP, respectively.

4.5 Image Analysis

The cells' response to DEP influences was quantified by plotting the light intensity shift (the shift in cumulative pixel values, explained in detail in Subsection 3.5.3) versus the frequency at which the images were captured to construct the "DEP spectrum" of each set of cells. Analyzing the DEP spectra of cell populations across a wide frequency range reveals the differences in their electrophysiological properties (Broche *et al.*, 2005).

Figure 4.16 displays selected processed images showing the segmented ROIs and their respected histograms. The values of light intensity shift, calculated using Equation 3.1, shifted to negative in the case of n-DEP and to positive in the case of p-DEP. This finding is in agreement with the previous studies that represented the DEP spectrum as the light intensity shift versus the applied frequency (Fatoyinbo *et al.*, 2011; Labeed *et al.*, 2011; Mulhall *et al.*, 2011).

The DEP spectra of normal WRL-68 cells and dengue-infected WRL-68 cells are plotted in Figure 4.17. It is noted that there is an alteration in the curves of the light intensity shifts of normal and infected cells because of the morphological change (i.e., shrinkage) that occurs in the cells upon the infection due to the cytopathic effect, as explained in Subsection 4.4.1.

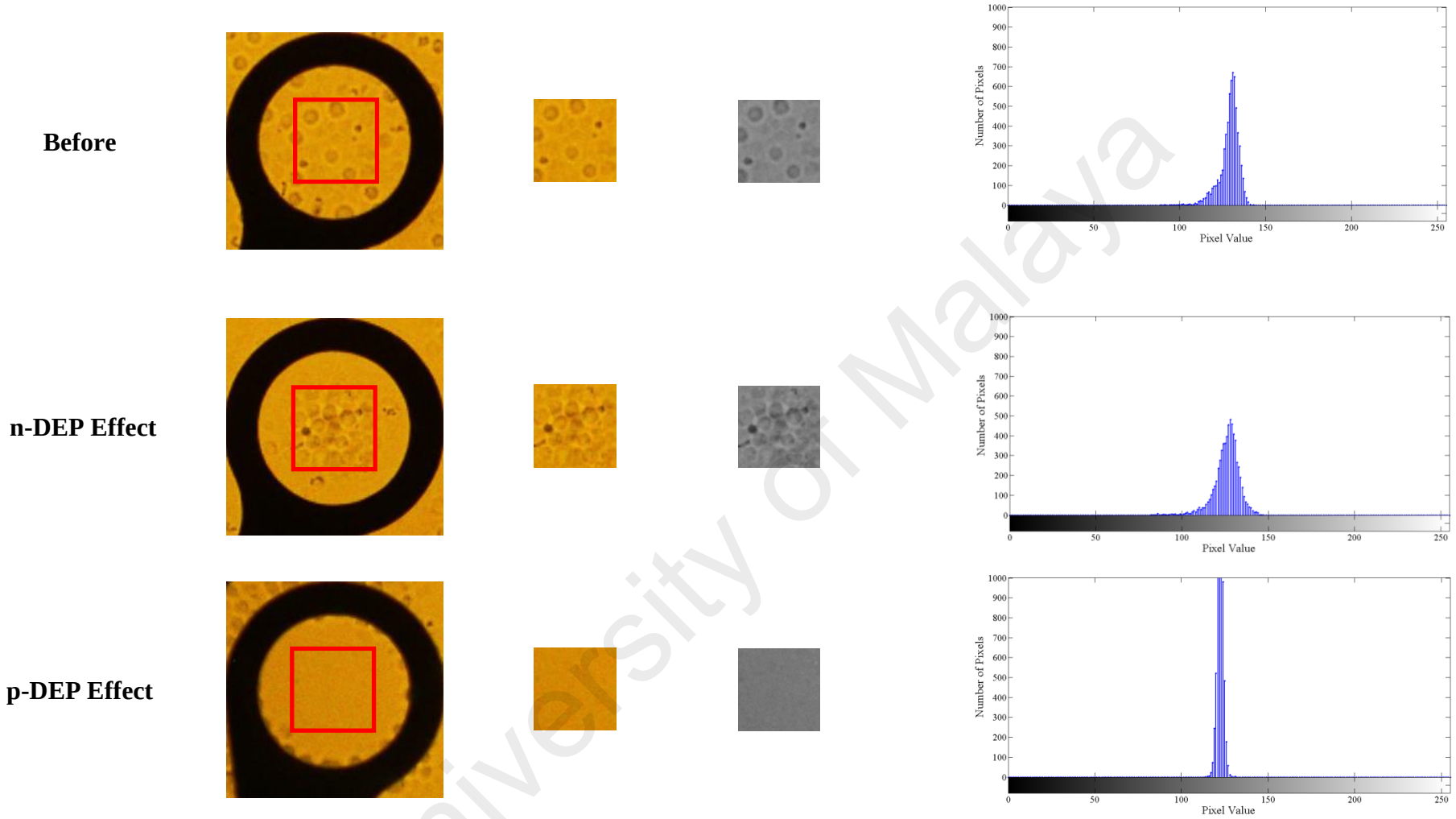

Figure 4.16: Selected processed images along with their segmented ROIs and histograms.

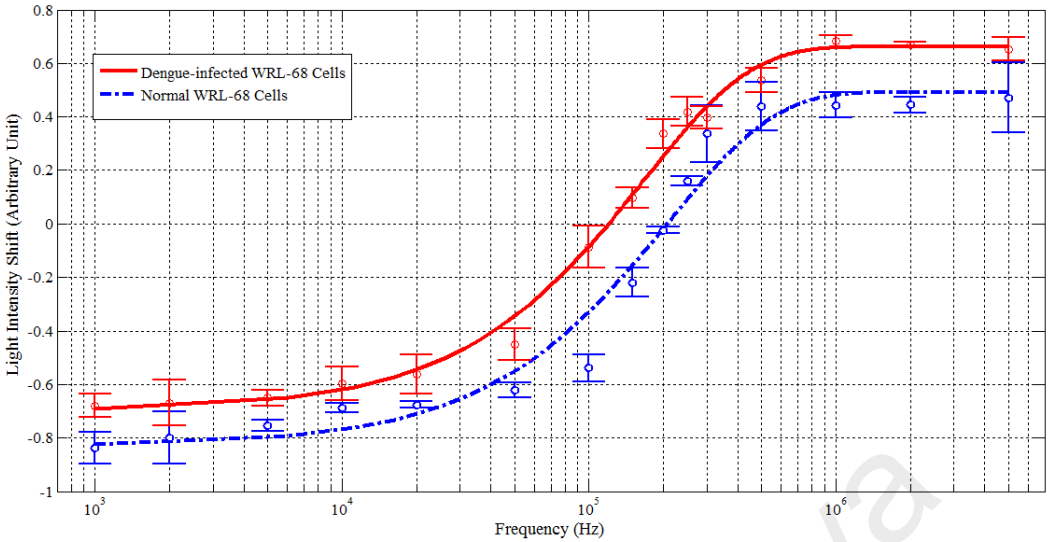

Figure 4.17: DEP spectra of normal and dengue-infected WRL-68 cells plotted using MATLAB® software.
The circles (O) on the graph denote the measured data. Best-fit lines were added to the DEP spectrum of each set of cells using logistic function. The correlation coefficients of the lines were greater than 0.9. The error bars indicate the *standard error* of four experiments conducted at each frequency.

Even though both type of cells experienced p-DEP effect and cleared from the dot center at high frequencies, the light intensity shift is different as shown in Figure 4.17. This is because the light intensity shift is calculated by subtracting the cumulative pixel values of the images before and after the application of the electric field as presented in Equation 3.1 and discussed in Subsection 3.5.3. Therefore, while the cumulative pixel value of the images after the application of the electric signal is same in both normal and infected cells (i.e., cells were cleared from the dot center under p-DEP effect), the cumulative pixel value of the images captured before the application of the electric field is different. This is because the size of the infected cells is smaller compared to the normal cells due to the cells shrinkage after the infection as seen in Figure 4.14 and Figure 4.15.

In order to obtain the crossover frequency, best-fit lines were added to the DEP spectrum of each set of cells. The crossover frequency (at which no DEP force is induced) was then acquired by selecting the frequency at which the light intensity shift

is zero. The measurements were performed by increasing the frequency of the applied signal in small steps from a low value, at which all the cells clearly exhibited n-DEP, until the cells demonstrated no DEP response and did not migrate their initial positions. The obtained crossover frequency decreased from 220 kHz for the normal WRL-68 cells to 140 kHz after infection with the dengue virus. This decrease in the crossover frequency is due to the change in a cell's dielectric properties upon infection. Therefore, the uniqueness of the crossover frequency of cells in a certain physiological or pathological state can reflect any alteration in the cell's normal state (Doh & Cho, 2005; Li & Bashir, 2002). Furthermore, the statistical analysis (explained in Section 3.6) revealed that there is a significant difference between the DEP spectrum of the normal and infected cells, $P < 0.05$.

Besides the discrimination of normal and infected cells, DEP also offers a method of determining the electrophysiological properties of cells (i.e., the conductivity and permittivity of the cytoplasm and the membrane). The extraction of these properties can be performed by fitting the light intensity shifts to the shell model that represents the cell (Broche *et al.*, 2005) and best-fit numerical analysis (Huang *et al.*, 1996) are used to extract the electrophysiological properties of the cells. This approach has been successfully implemented in various DEP characterization studies (Bisceglia *et al.*, 2015; Duncan *et al.*, 2008; Labeed *et al.*, 2011; Mulhall *et al.*, 2011). Interpretation of the extracted properties can provide an evaluation of what state the cells were experiencing and therefore can help in diagnosing diseases.

DEP would eliminate the need for bulky instruments and highly trained personal required to conduct ELISA tests. This technique will pave the way for further studies in miniaturization of non-invasive diagnostic tools, which is applicable not only for virally-infected cells, but also for other types of living organisms. While ELISA

protocols include labeling the antibody/antigen, DEP would eliminate the need for such expensive labels and reduce assay complexity, time and cost. This can lead to expanding the availability of POC diagnostic tests without the use of antigen/antibody coatings or labels.

Furthermore, DEP experiments are conducted when cells are in suspension, so cell adhesion is not needed for measurements. This could allow for a non-invasive collection of cells via oral brush biopsy or simple cotton-tipped swabs of nasal mucosae (Mulhall *et al.*, 2011; Tavakoli *et al.*, 2007).

Moreover, studying the DEP spectrum can be a beneficial tool in drug discovery studies. For instance, if a change in the electrophysiological properties is caused by the existence of an external element, then this change (provided that no other external elements are present) is exclusively generated by that foreign element. Furthermore, the analysis of the DEP spectrum of cells when an external element is present can help to explain the element's mechanism of action on the cellular membrane and the effects that it has on the cytoplasm. For instance, ionophore molecules increase ion transport across cellular membranes (Riddell & Tompsett, 1990). This ion transport will result in alteration of the conductivity values of the cellular membrane and/or cytoplasm because of disruption of the total ionic distribution, hence changing the value of the Clausius-Mossotti factor. This change can be clearly visualized when plotting the DEP spectra of cells before and after introducing external factors.

4.6 Summary

In this chapter, the results of the developed DEP device were presented and evaluated. The simulation results showed that that the dot electrode geometry features a well-defined and enclosed region of analysis, effective electric field penetration, and an axisymmetric electric field distribution around the center of the dot aperture and that the

electric field is higher at the edges of the dots than the center of the dots. Furthermore, the analysis of the numerical modeling confirmed that the electric field strength increases when adding a ground plane between adjacent dots. Furthermore, testing experiments showed the potential of the developed device for manipulating and separating microparticles of different populations rapidly and efficiently. Microparticles migration was controlled merely by adjusting the applied frequency to induce a p-DEP or n-DEP response on the target population in a mixture of various populations. Finally, the DEP device was employed to discriminate between normal and dengue-infected WRL-68 cells based on their electrophysiological properties by exploiting both p-DEP and n-DEP effects. The morphological changes between normal and infected cells were examined, and the DEP responses of the cells were quantified by analyzing the light intensity shift of the captured images before and after the application of the electric field. The results showed that the DEP spectrum of the normal WRL-68 cells shifted after the cells were infected with the dengue virus. Furthermore, a unique DEP crossover frequency was obtained for each cell population.

Results showed that time needed to conduct manipulation and separation experiments based on DEP was reduced significantly in the current project to 5 seconds compared to previous works reviewed in Table 2.2. This is a result of the improvement in the electrode geometry and the LOC design. Furthermore, the results of this project introduced a new approach of discrimination virally-infected cells in a label-free manner without the need to use complex fluorescence microscopy as seen previous works (refer to Table 2.3). The detection of the viral biomarkers was done by studying the change in electrophysiological properties of cells upon the infection with the virus, rather than studying the virus itself using complex methods. This was feasible because of the cytopathic effects that occur on cell upon the viral infection.

CHAPTER 5: CONCLUSION AND FUTURE WORK

5.1 Conclusion

A rapid label-free LOC platform for discriminating dengue-infected cells based on DEP has been developed successfully. The project presents microarray dot electrodes that feature unique advantages over other electrode geometries, including a well-defined and confined region of analysis and effective electric field strength. The simulation results of the designed microarray dot electrode showed that the electric field is axisymmetric around the center of the dot aperture and that it is higher at the edges of the dots than it is at center of the dots. The axisymmetric nature of the electric field facilitates a simple interpretation of the obtained results. Furthermore, the numerical modeling was used to optimize the electrode geometry parameters to generate the highest electric field strength. Moreover, the simple and rapid fabrication processes of planar electrodes make the microarray dot electrode a potential solution to be utilized in research involving the development of cost-effective POC devices; avoiding the use of complex fabrication methods.

Moreover, a novel LOC configuration was developed to be compatible with the microarray dot electrode design. The developed LOC configuration was designed to meet certain standards, including cost effectiveness, ease of fabrication, leakage-free flow, reusability, ability to change any component at any time, and compatibility with different gasket heights. The developed LOC platform showed its capability in implementing microfluidic processes efficiently.

The proposed LOC platform was tested by conducting size-dependent manipulation and separation experiments on different-sized polystyrene microparticles. The experiments' findings confirmed the capability of the proposed LOC platform to rapidly and efficiently manipulate and separate microparticles of various dimensions, utilizing

both p-DEP and n-DEP effects. The time needed to conduct microparticles manipulation and separation experiments was reduced significantly in the current project to 5 seconds compared to previous works as reviewed in Table 2.2. This is a result of the improvement in the electrode geometry and the LOC design. Microparticles migration was controlled merely by adjusting the applied signal frequency. Furthermore, larger size particles were repelled and concentrated in the center of the dot by n-DEP, while the smaller sizes were attracted and collected at the edge of the dot by p-DEP.

Finally, the developed LOC platform was used to distinguish between normal and dengue-infected cells. This project introduced a new approach of discrimination virally-infected cells in a label-free manner without the need to use complex fluorescence microscopy as seen previous works (refer to Table 2.3). The detection of the viral biomarkers was done by studying the change in electrophysiological properties of cells upon the infection with the virus, rather than studying the virus itself using complex methods. This was feasible because of the cytopathic effects that occur on cell upon the viral infection. The results showed that normal and dengue-infected WRL-68 cells can be identified based on their electrophysiological properties by exploiting their DEP effects. The DEP responses of the cells were quantified by analyzing the light intensity shift within the electrode's dot region based on the CMIS image analysis technique. The differences in dielectric properties between infected and uninfected cells were exploited by plotting a unique DEP spectrum for each set of cells. The findings showed that the DEP spectrum of the normal WRL-68 cells shifted after the cells were infected with the dengue virus. Furthermore, a unique DEP crossover frequency was obtained for each cell population. It was concluded that the change in the DEP crossover frequency between dengue-infected cells and their healthy counterparts should allow for direct characterization of these cell types by exploiting their electrophysiological properties.

This work demonstrated the feasibility of using the DEP technique in the identification of viral diseases. The results presented can be interpreted for virally-infected cells. This is due to the physical changes occurring in the cell upon infection with the virus, resulting in a unique DEP response. This study represents a step toward validating DEP in practical settings by proposing LOC designs that combine cost efficiency and ease of fabrication with rapid throughput.

In conclusion, the proposed LOC platform is a rapid, easy to use and low-cost label-free tool to distinguish between normal and virally-infected cells utilizing DEP technology. Automation of the device would render the results free from subjective assessments allowing clinicians with minimal training and expertise to use the technique effectively. Integrating such DEP devices into more complex LOC platforms will be potentially valuable for various POC biomedical applications.

5.2 Contributions

The following is a summary of the original contribution undertaken towards the completion of this project:

i. Proposing a novel approach for detecting viral biomarkers by studying the change in electrophysiological properties of cells upon the infection with the virus, rather than studying the virus itself using complex methods.
ii. Design and development of an optimized version of the microarray dot electrode based on simulation analysis using COMSOL® Multiphysics software.
iii. Development of simple and cost-effective LOC design configuration.
iv. Test the capability of the developed platform for the manipulation and separation of microparticles efficiently.
v. Reduction of the time needed to conduced DEP experiments.

vi. Discrimination between normal and dengue-infected WRL-68 cells in label-free manner using the developed platform.

vii. Processing the DEP images based on CMIS technique to obtain the DEP spectra.

5.3 Limitations

Although the defined objectives of this project have been accomplished successfully, few limitations were faced. One of the problems was the lack of multiple output waveform generator. This could help the project to supply different frequencies to different dots simultaneously and observe the different DEP responses concurrently. However, in the current project, four separate function generators were used to supply four individual dots with different frequencies each time a DEP experiment was run. The availability of multiple output waveform generator would be more practical for POC devices. Another limitation to declare was the un-automation of the system. The DEP experiments were conducted first, and then the images were saved in PC. After that, the images were processed offline, and finally the DEP spectra were obtained. The development of automatic detection and image processing system would certainly speed up the process of obtaining the DEP spectrum of respected cells.

5.4 Future Work

The following is a list of recommendations for possible future work that can be incorporated into the developed LOC platform:

i. Develop a multiple output waveform generator to supply the microarray dot electrode with multiple individual frequencies.

ii. Develop an automatic detection system of dots ROI along with a GUI interface for image processing.

iii. Extract cells' electrophysiological properties by applying an appropriate model to their DEP spectra.

iv. Apply the developed LOC platform to discriminate other types of cells infected with Dengue and other viruses and test the specificity of this technique.

REFERENCES

Alkhalil, A., Hill, D. A., & Desai, S. A. (2007). Babesia and plasmodia increase host erythrocyte permeability through distinct mechanisms. *Cellular Microbiology, 9*(4), 851-860. doi: 10.1111/j.1462-5822.2006.00834.

An, J., Lee, J., Lee, S., Park, J., & Kim, B. (2009). Separation of malignant human breast cancer epithelial cells from healthy epithelial cells using an advanced dielectrophoresis-activated cell sorter (DACS). *Analytical and Bioanalytical Chemistry, 394*(3), 801-809. doi: 10.1007/s00216-009-2743-7

Archer, S., Li, T.-T., Evans, A. T., Britland, S. T., & Morgan, H. (1999). Cell Reactions to Dielectrophoretic Manipulation. *Biochemical and Biophysical Research Communications, 257*(3), 687-698.

Balagaddé, F. K., You, L., Hansen, C. L., Arnold, F. H., & Quake, S. R. (2005). Long-Term Monitoring of Bacteria Undergoing Programmed Population Control in a Microchemostat. *Science, 309*(5731), 137-140. doi: 10.1126/science.1109173

Ball, L. A. (2010). Virus–Host Cell Interactions *Topley & Wilson's Microbiology and Microbial Infections*: John Wiley & Sons, Ltd.

Becker, F. F., Wang, X. B., Huang, Y., Pethig, R., Vykoukal, J., & Gascoyne, P. R. (1995). Separation of human breast cancer cells from blood by differential dielectric affinity. *Proceedings of the National Academy of Sciences, 92*(3), 860-864.

Bisceglia, E., Cubizolles, M., Trainito, C. I., Berthier, J., Pudda, C., Français, O., Mallard, F., & Le Pioufle, B. (2015). A generic and label free method based on dielectrophoresis for the continuous separation of microorganism from whole blood samples. *Sensors and Actuators B: Chemical, 212*(0), 335-343. doi: 10.1016/j.snb.2015.02.024

Bousse, L., Cohen, C., Nikiforov, T., Chow, A., Kopf-Sill, A. R., Dubrow, R., & Parce, J. W. (2000). Electrokinetically controlled microfluidic analysis systems. *Annual Review of Biophysics and Biomolecular Structure, 29*(1), 155-181.

Braff, W. A., Pignier, A., & Buie, C. R. (2012). High sensitivity three-dimensional insulator-based dielectrophoresis. *Lab on a Chip, 12*(7), 1327-1331. doi: 10.1039/c2lc21212a

Braff, W. A., Willner, D., Hugenholtz, P., Rabaey, K., & Buie, C. R. (2013). Dielectrophoresis-based discrimination of bacteria at the strain level based on their surface properties. *PloS one, 8*(10), e76751.

Broche, L. M., Labeed, F. H., & Hughes, M. P. (2005). Extraction of dielectric properties of multiple populations from dielectrophoretic collection spectrum data. *Physics in Medicine and Biology, 50*(10), 2267.

Burgarella, S., Merlo, S., Dell'Anna, B., Zarola, G., & Bianchessi, M. (2010). A modular micro-fluidic platform for cells handling by dielectrophoresis. *Microelectronic Engineering, 87*(11), 2124-2133.

Cao, J., Cheng, P., & Hong, F. (2008). A numerical analysis of forces imposed on particles in conventional dielectrophoresis in microchannels with interdigitated electrodes. *Journal of Electrostatics, 66*(11–12), 620-626.

Castellanos, A., Ramos, A., Gonzalez, A., Green, N. G., & Morgan, H. (2003). Electrohydrodynamics and dielectrophoresis in microsystems: scaling laws. *Journal of Physics D: Applied Physics, 36*(20), 2584.

Çetin, B., Kang, Y., Wu, Z., & Li, D. (2009). Continuous particle separation by size via AC-dielectrophoresis using a lab-on-a-chip device with 3-D electrodes. *Electrophoresis, 30*(5), 766-772. doi: 10.1002/elps.200800464

Cha, M., Yoo, J., & Lee, J. (2011). Bacterial cell manipulation by dielectrophoresis on a hydrophobic guide structure. *Electrochemistry Communications, 13*(6), 600-604. doi: 10.1016/j.elecom.2011.03.020

Chandramohanadas, R., Park, Y., Lui, L., Li, A., Quinn, D., Liew, K., Diez-Silva, M., Sung, Y., Dao, M., & Lim, C. T. (2011). Biophysics of malarial parasite exit from infected erythrocytes. *PloS one, 6*(6), e20869.

Chaudhuri, P. K., Warkiani, M. E., Jing, T., & Lim, C. T. (2015). Microfluidics for research and applications in oncology. *Analyst*.

Cheng, I.-F., Chang, H.-C., Hou, D., & Chang, H.-C. (2007). An integrated dielectrophoretic chip for continuous bioparticle filtering, focusing, sorting, trapping, and detecting. *Biomicrofluidics, 1*(2), 021503. doi: 10.1063/1.2723669

Cheng, I. F., Froude, V. E., Zhu, Y., Chang, H.-C., & Chang, H.-C. (2009). A continuous high-throughput bioparticle sorter based on 3D traveling-wave dielectrophoresis. *Lab on a Chip, 9*(22), 3193-3201. doi: 10.1039/b910587e

Cheng, J., Sheldon, E. L., Wu, L., Uribe, A., Gerrue, L. O., Carrino, J., Heller, M. J., & O'Connell, J. P. (1998). Preparation and hybridization analysis of DNA/RNA from E. coli on microfabricated bioelectronic chips. *Nat Biotech, 16*(6), 541-546.

Chiou, C.-H., Pan, J.-C., Chien, L.-J., Lin, Y.-Y., & Lin, J.-L. (2013). Characterization of Microparticle Separation Utilizing Electrokinesis within an Electrodeless Dielectrophoresis Chip. *Sensors, 13*(3), 2763-2776.

Choi, S., & Park, J.-K. (2005). Microfluidic system for dielectrophoretic separation based on a trapezoidal electrode array. *Lab on a Chip, 5*(10), 1161-1167. doi: 10.1039/b505088j.

Choongho, Y., Vykoukal, J., Vykoukal, D. M., Schwartz, J. A., Li, S., & Gascoyne, P. R. C. (2005). A three-dimensional dielectrophoretic particle focusing channel for microcytometry applications. *Microelectromechanical Systems, Journal of, 14*(3), 480-487. doi: 10.1109/jmems.2005.844839

Chou, C.-F., Tegenfeldt, J. O., Bakajin, O., Chan, S. S., Cox, E. C., Darnton, N., Duke, T., & Austin, R. H. (2002). Electrodeless Dielectrophoresis of Single- and Double-Stranded DNA. *Biophysical Journal, 83*(4), 2170-2179. doi: 10.1016/S0006-3495(02)73977-5

Chuang, H.-S., Raizen, D. M., Lamb, A., Dabbish, N., & Bau, H. H. (2011). Dielectrophoresis of Caenorhabditis elegans. *Lab on a Chip, 11*(4), 599-604. doi: 10.1039/C0LC00532K

Chung, C.-C., Cheng, I. F., Chen, H.-M., Kan, H.-C., Yang, W.-H., & Chang, H.-C. (2012). Screening of Antibiotic Susceptibility to β-Lactam-Induced Elongation of Gram-Negative Bacteria Based on Dielectrophoresis. *Analytical Chemistry, 84*(7), 3347-3354. doi: 10.1021/ac300093w

Cui, L., Holmes, D., & Morgan, H. (2001). The dielectrophoretic levitation and separation of latex beads in microchips. *Electrophoresis, 22*(18), 3893-3901.

del Moral Zamora, B., Álvarez Azpeitia, J. M., Oliva Brañas, A. M., Colomer-Farrarons, J., Castellarnau, M., Miribel-Català, P. L., Homs-Corbera, A., Juárez, A., & Samitier, J. (2015). Dielectrophoretic concentrator enhancement based on dielectric poles for continuously flowing samples. *Electrophoresis*, doi: 10.1002/elps.201400433

Deptech 3DEP Reader. (2015), from http://deptech.com/

Ding, J., Lawrence, R. M., Jones, P. V., Hogue, B. G., & Hayes, M. A. (2016). Concentration of Sindbis virus with optimized gradient insulator-based dielectrophoresis. *Analyst*.

Doh, I., & Cho, Y.-H. (2005). A continuous cell separation chip using hydrodynamic dielectrophoresis (DEP) process. *Sensors and Actuators A: Physical, 121*(1), 59-65. doi: 10.1016/j.sna.2005.01.030

Duncan, L., Shelmerdine, H., Hughes, M. P., Coley, H. M., Hübner, Y., & Labeed, F. H. (2008). Dielectrophoretic analysis of changes in cytoplasmic ion levels due to ion channel blocker action reveals underlying differences between drug-sensitive and multidrug-resistant leukaemic cells. *Physics in Medicine and Biology, 53*(2), N1.

Dürr, M., Kentsch, J., Müller, T., Schnelle, T., & Stelzle, M. (2003). Microdevices for manipulation and accumulation of micro- and nanoparticles by dielectrophoresis. *Electrophoresis, 24*(4), 722-731. doi: 10.1002/elps.200390087

Fang, X., Liu, Y., Kong, J., & Jiang, X. (2010). Loop-Mediated Isothermal Amplification Integrated on Microfluidic Chips for Point-of-Care Quantitative Detection of Pathogens. *Analytical Chemistry, 82*(7), 3002-3006. doi: 10.1021/ac1000652

Fatoyinbo, H. O., Hoettges, K. F., & Hughes, M. P. (2008). Rapid-on-chip determination of dielectric properties of biological cells using imaging techniques in a dielectrophoresis dot microsystem. *Electrophoresis, 29*(1), 3-10. doi: 10.1002/elps.200700586

Fatoyinbo, H. O., Kadri, N. A., Gould, D. H., Hoettges, K. F., & Labeed, F. H. (2011). Real-time cell electrophysiology using a multi-channel dielectrophoretic-dot microelectrode array. *Electrophoresis, 32*(18), 2541-2549. doi: 10.1002/elps.201100033

Ferguson, B. S., Buchsbaum, S. F., Wu, T.-T., Hsieh, K., Xiao, Y., Sun, R., & Soh, H. T. (2011). Genetic Analysis of H1N1 Influenza Virus from Throat Swab Samples in a Microfluidic System for Point-of-Care Diagnostics. *Journal of the American Chemical Society, 133*(23), 9129-9135. doi: 10.1021/ja203981w

Fiorini, G. S., & Chiu, D. T. (2005). Disposable microfluidic devices: fabrication, function, and application. *BioTechniques, 38*(3), 429-446.

Foudeh, A. M., Fatanat Didar, T., Veres, T., & Tabrizian, M. (2012). Microfluidic designs and techniques using lab-on-a-chip devices for pathogen detection for point-of-care diagnostics. *Lab on a Chip, 12*(18), 3249-3266. doi: 10.1039/c2lc40630f

Gascoyne, P., Mahidol, C., Ruchirawat, M., Satayavivad, J., Watcharasit, P., & Becker, F. F. (2002). Microsample preparation by dielectrophoresis: isolation of malaria. *Lab on a Chip, 2*(2), 70-75. doi: 10.1039/b110990c

Gascoyne, P., Pethig, R., Satayavivad, J., Becker, F. F., & Ruchirawat, M. (1997a). Dielectrophoretic detection of changes in erythrocyte membranes following malarial infection. *Biochimica et Biophysica Acta (BBA) - Biomembranes, 1323*(2), 240-252. doi: 10.1016/S0005-2736(96)00191-5

Gascoyne, P. R. C., Shim, S., Noshari, J., Becker, F. F., & Stemke-Hale, K. (2013). Correlations between the dielectric properties and exterior morphology of cells revealed by dielectrophoretic field-flow fractionation. *Electrophoresis, 34*(7), 1042-1050. doi: 10.1002/elps.201200496

Gascoyne, P. R. C., & Vykoukal, J. (2002). Particle separation by dielectrophoresis. *Electrophoresis, 23*(13), 1973-1983.

Gascoyne, P. R. C., Xiao-Bo, W., Ying, H., & Becker, F. F. (1997b). Dielectrophoretic separation of cancer cells from blood. *Industry Applications, IEEE Transactions on, 33*(3), 670-678. doi: 10.1109/28.585856

Gasperis, G., Yang, J., Becker, F., Gascoyne, P. C., & Wang, X.-B. (1999). Microfluidic Cell Separation by 2-dimensional Dielectrophoresis. *Biomedical Microdevices, 2*(1), 41-49. doi: 10.1023/A:1009955200029

Ghallab, Y., & Badawy, W. (2004). Sensing methods for dielectrophoresis phenomenon: from bulky instruments to lab-on-a-chip. *Circuits and Systems Magazine, IEEE, 4*(3), 5-15. doi: 10.1109/mcas.2004.1337805

Gonzalez, R. C., Woods, R. E., & Eddins, S. L. (2004). *Digital image processing using MATLAB*: Pearson Education India.

Green, N. G., & Morgan, H. (1999). Dielectrophoresis of Submicrometer Latex Spheres. 1. Experimental Results. *The Journal of Physical Chemistry B, 103*(1), 41-50. doi: 10.1021/jp9829849

Grom, F., Kentsch, J., Müller, T., Schnelle, T., & Stelzle, M. (2006). Accumulation and trapping of hepatitis A virus particles by electrohydrodynamic flow and dielectrophoresis. *Electrophoresis, 27*(7), 1386-1393.

Guan, W., Joseph, S., Park, J. H., Krstić, P. S., & Reed, M. A. (2011). Paul trapping of charged particles in aqueous solution. *Proceedings of the National Academy of Sciences, 108*(23), 9326-9330. doi: 10.1073/pnas.1100977108

Haeberle, S., Mark, D., von Stetten, F., & Zengerle, R. (2012). Microfluidic Platforms for Lab-On-A-Chip Applications. In Z. Zhou, Z. Wang & L. Lin (Eds.), *Microsystems and Nanotechnology* (pp. 853-895): Springer Berlin Heidelberg.

Haeberle, S., & Zengerle, R. (2007). Microfluidic platforms for lab-on-a-chip applications. *Lab on a Chip, 7*(9), 1094-1110.

Han, S.-I., Joo, Y.-D., & Han, K.-H. (2013). An electrorotation technique for measuring the dielectric properties of cells with simultaneous use of negative quadrupolar dielectrophoresis and electrorotation. *Analyst, 138*(5), 1529-1537. doi: 10.1039/c3an36261b

Hashimoto, M., Kaji, H., & Nishizawa, M. (2009). Selective capture of a specific cell type from mixed leucocytes in an electrode-integrated microfluidic device. *Biosensors and Bioelectronics, 24*(9), 2892-2897.

Ho, J., Tan, M. K., Go, D. B., Yeo, L. Y., Friend, J. R., & Chang, H.-C. (2011). Paper-Based Microfluidic Surface Acoustic Wave Sample Delivery and Ionization Source for Rapid and Sensitive Ambient Mass Spectrometry. *Analytical Chemistry, 83*(9), 3260-3266. doi: 10.1021/ac200380q

Hoettges, K. F., Hübner, Y., Broche, L. M., Ogin, S. L., Kass, G. E. N., & Hughes, M. P. (2008). Dielectrophoresis-Activated Multiwell Plate for Label-Free High-Throughput Drug Assessment. *Analytical Chemistry, 80*(6), 2063-2068. doi: 10.1021/ac702083g

Holzel, R. (2009). Dielectric and dielectrophoretic properties of DNA. *Nanobiotechnology, IET, 3*(2), 28-45.

Hsieh, K., Patterson, A. S., Ferguson, B. S., Plaxco, K. W., & Soh, H. T. (2012). Rapid, Sensitive, and Quantitative Detection of Pathogenic DNA at the Point of Care through Microfluidic Electrochemical Quantitative Loop-Mediated Isothermal Amplification. *Angewandte Chemie, 124*(20), 4980-4984. doi: 10.1002/ange.201109115

Huang, C.-T., Amstislavskaya, T. G., Chen, G.-H., Chang, H.-H., Chen, Y.-H., & Jen, C.-P. (2012). Selectively concentrating cervical carcinoma cells from red blood cells utilizing dielectrophoresis with circular ito electrodes in stepping electric fields. *Journal of medical and biological engineering, 33*(1), 51-58.

Huang, C., Smith, J. P., Saha, T. N., Rhim, A. D., & Kirby, B. J. (2014). Characterization of microfluidic shear-dependent epithelial cell adhesion molecule immunocapture and enrichment of pancreatic cancer cells from blood cells with dielectrophoresis. *Biomicrofluidics, 8*(4), 044107.

Huang, Y., Joo, S., Duhon, M., Heller, M., Wallace, B., & Xu, X. (2002). Dielectrophoretic Cell Separation and Gene Expression Profiling on Microelectronic Chip Arrays. *Analytical Chemistry, 74*(14), 3362-3371. doi: 10.1021/ac011273v

Huang, Y., Wang, X.-B., Becker, F. F., & Gascoyne, P. R. C. (1996). Membrane changes associated with the temperature-sensitive P85gag-mos-dependent transformation of rat kidney cells as determined by dielectrophoresis and electrorotation. *Biochimica et Biophysica Acta (BBA) - Biomembranes, 1282*(1), 76-84. doi: 10.1016/0005-2736(96)00047-8

Hughes, M. P., Morgan, H., & Rixon, F. J. (2002). Measuring the dielectric properties of herpes simplex virus type 1 virions with dielectrophoresis. *Biochimica et Biophysica Acta (BBA) - General Subjects, 1571*(1), 1-8. doi: 10.1016/S0304-4165(02)00161-7

Iliescu, C., Yu, L., Tay, F. E. H., & Chen, B. (2008). Bidirectional field-flow particle separation method in a dielectrophoretic chip with 3D electrodes. *Sensors and Actuators B: Chemical, 129*(1), 491-496.

Imasato, H., Yamakawa, T., & Eguchi, M. (2012). Separation of leukemia cells from blood by employing dielectrophoresis. *Intelligent Automation & Soft Computing, 18*(2), 139-152.

Jaber, F. T., Labeed, F. H., & Hughes, M. P. (2013). *A dielectrophoresis and image processing based system for loading single-neurons per micro-well in planar microelectrode arrays.* Paper presented at the Systems, Signal Processing and their Applications (WoSSPA), 2013 8th International Workshop on.

Jang, L.-S., Huang, P.-H., & Lan, K.-C. (2009). Single-cell trapping utilizing negative dielectrophoretic quadrupole and microwell electrodes. *Biosensors and Bioelectronics, 24*(12), 3637-3644.

Javanmard, M., Emaminejad, S., Gupta, C., Provine, J., Davis, R. W., & Howe, R. T. (2014). Depletion of cells and abundant proteins from biological samples by enhanced dielectrophoresis. *Sensors and Actuators B: Chemical, 193*(0), 918-924.

Jing, T., Ramji, R., Warkiani, M. E., Han, J., Lim, C. T., & Chen, C.-H. (2015). Jetting microfluidics with size-sorting capability for single-cell protease detection. *Biosensors and Bioelectronics, 66*, 19-23.

Jones, P., DeMichele, A., Kemp, L., & Hayes, M. (2014). Differentiation of Escherichia coli serotypes using DC gradient insulator dielectrophoresis. *Analytical and Bioanalytical Chemistry, 406*(1), 183-192. doi: 10.1007/s00216-013-7437-5

Junya, S., & Ronald, P. (1998). The dielectrophoretic movement and positioning of a biological cell using a three-dimensional grid electrode system. *Journal of Physics D: Applied Physics, 31*(22), 3298.

Kadri, N. A. (2010). *Development of near real-time assessment system for cancer cells*. PhD, University of Surrey, Guildford, Surrey.

Kartalov, E. P., Zhong, J. F., Scherer, A., Quake, S. R., Taylor, C. R., & Anderson, W. F. (2006). High-throughput multi-antigen microfluidic fluorescence immunoassays. *BioTechniques, 40*(1), 85.

Khoshmanesh, K., Nahavandi, S., Baratchi, S., Mitchell, A., & Kalantar-zadeh, K. (2011). Dielectrophoretic platforms for bio-microfluidic systems. *Biosensors and Bioelectronics, 26*(5), 1800-1814.

Khoshmanesh, K., Zhang, C., Nahavandi, S., Tovar-Lopez, F. J., Baratchi, S., Mitchell, A., & Kalantar-Zadeh, K. (2010). Size based separation of microparticles using a dielectrophoretic activated system. *Journal of Applied Physics, 108*(3), 034904-034904-034908.

Khoshmanesh, K., Zhang, C., Tovar-Lopez, F. J., Nahavandi, S., Baratchi, S., Kalantar-zadeh, K., & Mitchell, A. (2009a). Dielectrophoretic manipulation and separation of microparticles using curved microelectrodes. *Electrophoresis, 30*(21), 3707-3717. doi: 10.1002/elps.200900079

Khoshmanesh, K., Zhang, C., Tovar-Lopez, F. J., Nahavandi, S., Baratchi, S., Kalantar-zadeh, K., & Mitchell, A. (2009b). Dielectrophoretic manipulation and separation of microparticles using curved microelectrodes. *Electrophoresis, 30*(21), 3707-3717.

Labeed, F. H., Coley, H. M., & Hughes, M. P. (2006). Differences in the biophysical properties of membrane and cytoplasm of apoptotic cells revealed using dielectrophoresis. *Biochimica et Biophysica Acta (BBA) - General Subjects, 1760*(6), 922-929. doi: 10.1016/j.bbagen.2006.01.018

Labeed, F. H., Lu, J., Mulhall, H. J., Marchenko, S. A., Hoettges, K. F., Estrada, L. C., Lee, A. P., Hughes, M. P., & Flanagan, L. A. (2011). Biophysical characteristics reveal neural stem cell differentiation potential. *PloS one, 6*(9), e25458.

Lacaze, P.-C. (2012). *Nanotechnologies: Concepts, Production and Applications*: John Wiley & Sons.

Lapizco-Encinas, B. H., Davalos, R. V., Simmons, B. A., Cummings, E. B., & Fintschenko, Y. (2005). An insulator-based (electrodeless) dielectrophoretic concentrator for microbes in water. *Journal of Microbiological Methods, 62*(3), 317-326. doi: 10.1016/j.mimet.2005.04.027

Li, H., & Bashir, R. (2002). Dielectrophoretic separation and manipulation of live and heat-treated cells of Listeria on microfabricated devices with interdigitated electrodes. *Sensors and Actuators B: Chemical, 86*(2–3), 215-221. doi: 10.1016/S0925-4005(02)00172-7

Li, Q., & Lim, C. (2011). Structure–Mechanical Property Changes in Nucleus arising from Breast Cancer. In A. Gefen (Ed.), *Cellular and Biomolecular Mechanics and Mechanobiology* (Vol. 4, pp. 465-475): Springer Berlin Heidelberg.

Lin, L., Chu, Y.-S., Thiery, J. P., Lim, C. T., & Rodriguez, I. (2013). Microfluidic cell trap array for controlled positioning of single cells on adhesive micropatterns. *Lab on a Chip, 13*(4), 714-721.

Liu, L., Ye, X., Wu, K., Han, R., Zhou, Z., & Cui, T. (2009). Humidity Sensitivity of Multi-Walled Carbon Nanotube Networks Deposited by Dielectrophoresis. *Sensors, 9*(3), 1714-1721.

Madiyar, F. R., Syed, L. U., Culbertson, C. T., & Li, J. (2013). Manipulation of bacteriophages with dielectrophoresis on carbon nanofiber nanoelectrode arrays. *Electrophoresis, 34*(7), 1123-1130. doi: 10.1002/elps.201200486

Martinez-Duarte, R., Camacho-Alanis, F., Renaud, P., & Ros, A. (2013). Dielectrophoresis of lambda-DNA using 3D carbon electrodes. *Electrophoresis, 34*(7), 1113-1122.

Martinez Duarte, R. (2010). *Label-free cell sorting using carbon-electrode dielectrophoresis and centrifugal microfluidics*. 3413010 Ph.D., University of California, Irvine, Ann Arbor.

Masuda, S., Washizu, M., & Nanba, T. (1989). Novel method of cell fusion in field constriction area in fluid integration circuit. *Industry Applications, IEEE Transactions on, 25*(4), 732-737. doi: 10.1109/28.31255

Masuda, T., Maruyama, H., Honda, A., & Arai, F. (2014). Virus Enrichment for Single Virus Infection by Using 3D Insulator Based Dielectrophoresis. *PloS one, 9*(6), e94083.

McCormick, K. D., Liu, S., Jacobs, J. L., Marques, E. T. A., Sluis-Cremer, N., & Wang, T. (2012). Development of a Robust Cytopathic Effect-Based High-Throughput Screening Assay To Identify Novel Inhibitors of Dengue Virus. *Antimicrobial Agents and Chemotherapy, 56*(6), 3399-3401. doi: 10.1128/aac.06425-11

Michael, P. H., & Hywel, M. (1998). Dielectrophoretic trapping of single sub-micrometre scale bioparticles. *Journal of Physics D: Applied Physics, 31*(17), 2205.

Moghimi, N., Decker, D. R., & Tatic-Lucic, S. (2012). *Modeling and measurement of dielectrophoretic force and 2-D trajectories of microspheres in quadrupole electrode configuration.* Paper presented at the 2012 IEEE Sensors Conference, 28-31 Oct. 2012.

Mohamad, A., Jeynes, J., & Hughes, M. (2014). Dielectrophoretic response of DNA shows different conduction mechanisms for poly (dg)-poly (dc) and poly (da)-poly (dt) in solution. *IEEE Transactions on NanoBioscience, 13*(1), 51-54.

Moon, H.-S., Kwon, K., Kim, S.-I., Han, H., Sohn, J., Lee, S., & Jung, H.-I. (2011). Continuous separation of breast cancer cells from blood samples using multi-orifice flow fractionation (MOFF) and dielectrophoresis (DEP). *Lab on a Chip, 11*(6), 1118-1125. doi: 10.1039/c0lc00345j

Morgan, H., & Green, N. G. (2003). *AC electrokinetics: colloids and nanoparticles*: Research Studies Press.

Morgan, H., Hughes, M. P., & Green, N. G. (1999). Separation of Submicron Bioparticles by Dielectrophoresis. *Biophysical Journal, 77*(1), 516-525. doi: 10.1016/S0006-3495(99)76908-0

Mulhall, H. J., Labeed, F. H., Kazmi, B., Costea, D. E., Hughes, M. P., & Lewis, M. P. (2011). Cancer, pre-cancer and normal oral cells distinguished by dielectrophoresis. *Analytical and Bioanalytical Chemistry, 401*(8), 2455-2463. doi: 10.1007/s00216-011-5337-0

Nakano, A., Camacho-Alanis, F., Chao, T.-C., & Ros, A. (2012). Tuning direct current streaming dielectrophoresis of proteins. *Biomicrofluidics, 6*(3), 034108.

Nascimento, E. M., Nogueira, N., Silva, T., Braschler, T., Demierre, N., Renaud, P., & Oliva, A. G. (2008). Dielectrophoretic sorting on a microfabricated flow cytometer: Label free separation of Babesia bovis infected erythrocytes. *Bioelectrochemistry, 73*(2), 123-128.

Park, K., Akin, D., & Bashir, R. (2007). Electrical capture and lysis of vaccinia virus particles using silicon nano-scale probe array. *Biomedical microdevices, 9*(6), 877-883.

Park, S., Koklu, M., & Beskok, A. (2009). Particle Trapping in High-Conductivity Media with Electrothermally Enhanced Negative Dielectrophoresis. *Analytical Chemistry, 81*(6), 2303-2310. doi: 10.1021/ac802471g

Pethig, R. (2010). Review Article—Dielectrophoresis: Status of the theory, technology, and applications. *Biomicrofluidics, 4*(2), 022811.

Pohl, H. (1978). *Dielectrophoresis: the behavior of neutral matter in nonuniform electric fields* (Vol. 80): Cambridge University Press, Cambridge.

Pohl, H. A. (1951). The Motion and Precipitation of Suspensoids in Divergent Electric Fields. *Journal of Applied Physics, 22*(7), 869-871.

Pohl, H. A., & Plymale, C. E. (1960). Continuous Separations of Suspensions by Nonuniform Electric Fields in Liquid Dielectrics. *Journal of The Electrochemical Society, 107*(5), 390-396. doi: 10.1149/1.2427706

Pommer, M. S., Zhang, Y., Keerthi, N., Chen, D., Thomson, J. A., Meinhart, C. D., & Soh, H. T. (2008). Dielectrophoretic separation of platelets from diluted whole blood in microfluidic channels. *Electrophoresis, 29*(6), 1213-1218. doi: 10.1002/elps.200700607

Prasad, S., Zhang, X., Yang, M., Ni, Y., Parpura, V., Ozkan, C. S., & Ozkan, M. (2004). Separation of individual neurons using dielectrophoretic alternative current fields. *Journal of neuroscience methods, 135*(1), 79-88.

Prinz, C., Tegenfeldt, J. O., Austin, R. H., Cox, E. C., & Sturm, J. C. (2002). Bacterial chromosome extraction and isolation. *Lab on a Chip, 2*(4), 207-212.

Ramji, R., Cheong, C. F., Hirata, H., Rahman, A. R. A., & Lim, C. T. (2015). Rapid Quantification of Live Cell Receptors Using Bioluminescence in a Flow-Based Microfluidic Device. *Small, 11*(8), 943-951. doi: 10.1002/smll.201401674

Riddell, F. G., & Tompsett, S. J. (1990). The transport of Na+ and K+ ions through phospholipid bilayers mediated by the antibiotics salinomycin and narasin studied by 23Na- and 39K-NMR spectroscopy. *Biochimica et Biophysica Acta (BBA) - Biomembranes, 1024*(1), 193-197. doi: 10.1016/0005-2736(90)90225-D

Ritzi-Lehnert, M. (2012). Development of chip-compatible sample preparation for diagnosis of infectious diseases. *Expert Review of Molecular Diagnostics, 12*(2), 189-206.

Rosales-Cruzaley, E., Cota-Elizondo, P. A., Sánchez, D., & Lapizco-Encinas, B. (2013). Sperm cells manipulation employing dielectrophoresis. *Bioprocess and Biosystems Engineering, 36*(10), 1353-1362. doi: 10.1007/s00449-012-0838-6

Sabounchi, P., Morales, A., Ponce, P., Lee, L., Simmons, B., & Davalos, R. (2008). Sample concentration and impedance detection on a microfluidic polymer chip. *Biomedical microdevices, 10*(5), 661-670. doi: 10.1007/s10544-008-9177-4

Sabuncu, A. C., Asmar, A. J., Stacey, M. W., & Beskok, A. (2015). Differential dielectric responses of chondrocyte and Jurkat cells in electromanipulation buffers. *Electrophoresis*, n/a-n/a. doi: 10.1002/elps.201500119

Sano, M. B., Caldwell, J. L., & Davalos, R. V. (2011). Modeling and development of a low frequency contactless dielectrophoresis (cDEP) platform to sort cancer cells from dilute whole blood samples. *Biosensors and Bioelectronics, 30*(1), 13-20. doi: 10.1016/j.bios.2011.07.048

Sato, K., Yamanaka, M., Takahashi, H., Tokeshi, M., Kimura, H., & Kitamori, T. (2002). Microchip-based immunoassay system with branching multichannels for simultaneous determination of interferon-γ. *Electrophoresis, 23*(5), 734-739.

Serway, R. (1998). *Principles of Physics* (2nd ed.). Fort Worth, Texas; London: Saunders College Publishing.

Shafiee, H., Sano, M. B., Henslee, E. A., Caldwell, J. L., & Davalos, R. V. (2010). Selective isolation of live/dead cells using contactless dielectrophoresis (cDEP). *Lab on a Chip, 10*(4), 438-445. doi: 10.1039/b920590j

Sin, M., Gao, J., Liao, J., & Wong, P. (2011). System Integration - A Major Step toward Lab on a Chip. *Journal of Biological Engineering, 5*(1), 1-22. doi: 10.1186/1754-1611-5-6

Sista, R., Hua, Z., Thwar, P., Sudarsan, A., Srinivasan, V., Eckhardt, A., Pollack, M., & Pamula, V. (2008). Development of a digital microfluidic platform for point of care testing. *Lab on a Chip, 8*(12), 2091-2104. doi: 10.1039/b814922d

Situma, C., Hashimoto, M., & Soper, S. A. (2006). Merging microfluidics with microarray-based bioassays. *Biomolecular Engineering, 23*(5), 213-231. doi: 10.1016/j.bioeng.2006.03.002

Song, Y., Sonnenberg, A., Heaney, Y., & Heller, M. J. (2015). Device for dielectrophoretic separation and collection of nanoparticles and DNA under high conductance conditions. *Electrophoresis*.

Sonnenberg, A., Marciniak, J. Y., Krishnan, R., & Heller, M. J. (2012). Dielectrophoretic isolation of DNA and nanoparticles from blood. *Electrophoresis, 33*(16), 2482-2490.

Sonnenberg, A., Marciniak, J. Y., Skowronski, E. A., Manouchehri, S., Rassenti, L., Ghia, E. M., Widhopf, G. F., Kipps, T. J., & Heller, M. J. (2014). Dielectrophoretic isolation and detection of cancer-related circulating cell-free DNA biomarkers from blood and plasma. *Electrophoresis, 35*(12-13), 1828-1836. doi: 10.1002/elps.201400016

Stevens, K. A., & Jaykus, L.-A. (2004). Bacterial Separation and Concentration from Complex Sample Matrices: A Review. *Critical Reviews in Microbiology, 30*(1), 7-24. doi: doi:10.1080/10408410490266410

Stulík, K., Amatore, C., Holub, K., Marecek, V., & Kutner, W. (2000). Microelectrodes. Definitions, characterization, and applications (Technical report). *Pure and applied chemistry, 72*(8), 1483-1492.

SuáKim, K., & KwangáHahn, S. (2010). Real-time, step-wise, electrical detection of protein molecules using dielectrophoretically aligned SWNT-film FET aptasensors. *Lab on a Chip, 10*(16), 2052-2056.

Taff, B. M., & Voldman, J. (2005). A Scalable Addressable Positive-Dielectrophoretic Cell-Sorting Array. *Analytical Chemistry, 77*(24), 7976-7983. doi: 10.1021/ac0513616

Tavakoli, N. P., Tobin, E. H., Wong, S. J., Dupuis, A. P., Glasheen, B., Kramer, L. D., & Bernard, K. A. (2007). Identification of dengue virus in respiratory specimens from a patient who had recently traveled from a region where dengue virus infection is endemic. *Journal of clinical microbiology, 45*(5), 1523-1527.

Thomas, R. S., Morgan, H., & Green, N. G. (2009). Negative DEP traps for single cell immobilisation. *Lab on a Chip, 9*(11), 1534-1540. doi: 10.1039/B819267G

van den Driesche, S., Rao, V., Puchberger-Enengl, D., Witarski, W., & Vellekoop, M. J. (2012). Continuous cell from cell separation by traveling wave dielectrophoresis. *Sensors and Actuators B: Chemical, 170*(0), 207-214. doi: 10.1016/j.snb.2011.01.012

Voldman. (2006). ELECTRICAL FORCES FOR MICROSCALE CELL MANIPULATION. *Annual Review of Biomedical Engineering, 8*(1), 425-454. doi: doi:10.1146/annurev.bioeng.8.061505.095739

Voldman, J., Toner, M., Gray, M. L., & Schmidt, M. A. (2003). Design and analysis of extruded quadrupolar dielectrophoretic traps. *Journal of Electrostatics, 57*(1), 69-90. doi: 10.1016/S0304-3886(02)00120-1

Wang, L., Lu, J., Marchenko, S. A., Monuki, E. S., Flanagan, L. A., & Lee, A. P. (2009). Dual frequency dielectrophoresis with interdigitated sidewall electrodes for microfluidic flow-through separation of beads and cells. *Electrophoresis, 30*(5), 782-791. doi: 10.1002/elps.200800637

Wang, X. B., Huang, Y., Wang, X., Becker, F. F., & Gascoyne, P. R. (1997). Dielectrophoretic manipulation of cells with spiral electrodes. *Biophysical Journal, 72*(4), 1887-1899.

Warkiani, M. E., Khoo, B. L., Tan, D. S.-W., Bhagat, A. A. S., Lim, W.-T., Yap, Y. S., Lee, S. C., Soo, R. A., Han, J., & Lim, C. T. (2014). An ultra-high-throughput spiral microfluidic biochip for the enrichment of circulating tumor cells. *Analyst, 139*(13), 3245-3255.

Watarai, H., Sakamoto, T., & Tsukahara, S. (1997). In Situ Measurement of Dielectrophoretic Mobility of Single Polystyrene Microparticles. *Langmuir, 13*(8), 2417-2420. doi: 10.1021/la961057v

Wei Hou, H., Gan, H. Y., Bhagat, A. A. S., Li, L. D., Lim, C. T., & Han, J. (2012). A microfluidics approach towards high-throughput pathogen removal from blood using margination. *Biomicrofluidics, 6*(2), 024115.

Whitesides, G. M. (2006). The origins and the future of microfluidics. *Nature, 442*(7101), 368-373. doi: 10.1038/nature05058

WHO. (2014). Media Center: Dengue and severe dengue. *Fact Sheet No. 117* Retrieved 14th October 2014, from http://www.who.int/mediacentre/factsheets/fs117/en/

Woon-Hong, Y., Hyun-Boo, L., Jong-Hoon, K., Kyong-Hoon, L., & Jae-Hyun, C. (2013). Nanotip analysis for dielectrophoretic concentration of nanosized viral particles. *Nanotechnology, 24*(18), 185502.

Wu, S.-J. L., Grouard-Vogel, G., Sun, W., Mascola, J. R., Brachtel, E., Putvatana, R., Louder, M. K., Filgueira, L., Marovich, M. A., Wong, H. K., Blauvelt, A., Murphy, G. S., Robb, M. L., Innes, B. L., Birx, D. L., Hayes, C. G., & Frankel, S. S. (2000). Human skin Langerhans cells are targets of dengue virus infection. *Nat Med, 6*(7), 816-820. doi: 10.1038/77553

Yafouz, B., Kadri, N., & Ibrahim, F. (2013). Microarray Dot Electrodes Utilizing Dielectrophoresis for Cell Characterization. *Sensors, 13*(7), 9029-9046.

Yafouz, B., Kadri, N., & Ibrahim, F. (2014). Dielectrophoretic Manipulation and Separation of Microparticles Using Microarray Dot Electrodes. *Sensors, 14*(4), 6356-6369.

Yafouz, B., Kadri, N. A., & Ibrahim, F. (2012). The design and simulation of a planar microarray dot electrode for a dielectrophoretic lab-on-chip device. *International Journal of Electrochemical Science, 7*(12), 12054-12063.

Yafouz, B., Kadri, N. A., Rothan, H. A., Yusof, R., & Ibrahim, F. (2015). Discriminating dengue-infected hepatic cells (WRL-68) using dielectrophoresis. *Electrophoresis*.

Yager, P., Edwards, T., Fu, E., Helton, K., Nelson, K., Tam, M. R., & Weigl, B. H. (2006). Microfluidic diagnostic technologies for global public health. *Nature, 442*(7101), 412-418. doi: 10.1038/nature05064

Yahya, W., Kadri, N., & Ibrahim, F. (2014). Cell Patterning for Liver Tissue Engineering via Dielectrophoretic Mechanisms. *Sensors, 14*(7), 11714.

Yeo, L. Y., Chang, H.-C., Chan, P. P. Y., & Friend, J. R. (2011). Microfluidic Devices for Bioapplications. *Small, 7*(1), 12-48. doi: 10.1002/smll.201000946

Yu, Z., Xiang, G., Pan, L., Huang, L., Yu, Z., Xing, W., & Cheng, J. (2004). Negative dielectrophoretic force assisted construction of ordered neuronal networks on cell positioning bioelectronic chips. *Biomedical microdevices, 6*(4), 311-324.

Zhiwei, Z., Soohyun, L., & Ahn, C. H. (2008). A Polymer Microfluidic Chip With Interdigitated Electrodes Arrays for Simultaneous Dielectrophoretic Manipulation and Impedimetric Detection of Microparticles. *Sensors Journal, IEEE, 8*(5), 527-535. doi: 10.1109/jsen.2008.918907

Zhou, R., Wang, P., & Chang, H. C. (2006). Bacteria capture, concentration and detection by alternating current dielectrophoresis and self-assembly of dispersed single-wall carbon nanotubes. *Electrophoresis*, *27*(7), 1376-1385.

LIST OF PUBLICATIONS AND PAPERS PRESENTED

A. Journal Publications

i. **Yafouz, B.**, Kadri, N. A., & Ibrahim, F. (2012). The Design and Simulation of a Planar Microarray Dot Electrode for a Dielectrophoretic Lab-on-Chip Device. *Int. J. Electrochem. Sci*, 7, 12054-12063. (JCR 2011 ISI Q2, Impact Factor: 3.729).

ii. **Yafouz, B.**, Kadri, N., & Ibrahim, F. (2013). Microarray Dot Electrodes Utilizing Dielectrophoresis for Cell Characterization. *Sensors*, 13(7), 9029-9046. (JCR 2012 ISI Q1, Impact Factor: 1.9).

iii. **Yafouz, B.**, Kadri, N., & Ibrahim, F. (2014). Dielectrophoretic Manipulation and Separation of Microparticles Using Microarray Dot Electrodes. *Sensors*, 14(4), 6356-6369. (JCR 2013 ISI Q1, Impact Factor: 2.048).

iv. **Yafouz, B.,** Kadri, N., Rothan, H., Yosuf, R. & Ibrahim, F. (2015) Discriminating Dengue-Infected Hepatic Cells (WRL-68) Using Dielectrophoresis. *Electrophoresis* (JCR 2014 ISI Q1, Impact Factor: 3.028). Accepted.

B. Conference Proceedings

i. **Yafouz, B.**, Kadri, N. A., & Ibrahim, F. (2012). A numerical analysis of electric field strength over planar microarray dot electrode for dielectrophoretic lab-on-chip device. *Paper presented at IEEE EMBS Conference on Biomedical Engineering and Sciences (IECBES)*, 17-19 Dec. 2012, 118 – 121.

ii. **Yafouz, B.**, Kadri, N. A., & Ibrahim, F. (2014). Lab-on-a-chip particles manipulation for point-of-care diagnostic systems utilizing dielectrophoresis. *Paper presented at IEEE Conference on Biomedical Engineering and Sciences (IECBES)*, 8-10 Dec. 2014, 485 – 488.

Int. J. Electrochem. Sci., 7 **(2012)** 12054 - 12063

International Journal of
ELECTROCHEMICAL
SCIENCE
www.electrochemsci.org

The Design and Simulation of a Planar Microarray Dot Electrode for a Dielectrophoretic Lab-on-Chip Device

Bashar Yafouz, Nahrizul Adib Kadri[*]*, Fatimah Ibrahim*

Medical Informatics and Biological Micro-Electro-Mechanical Systems (MIMEMS) Specialized Laboratory, Department of Biomedical Engineering, Faculty of Engineering, University of Malaya, 50603 Kuala Lumpur, Malaysia
[*]E-mail: nahrizuladib@um.edu.my

Received: 1 October 2012 / *Accepted:* 24 October 2012 / *Published:* 1 December 2012

Dielectrophoresis (DEP) has been proven as a method of manipulating and analyzing the electrophysiological properties of bioparticles by applying non-uniform electric fields generated through special electrodes. Various electrode geometries have been developed to address different applications. Electric field simulation over electrodes is essential in order to optimize the generated DEP force for cell manipulation. This paper describes the study of electric field distribution over planar multiple microarray dot electrodes using numerical modeling of Comsol Multiphysics 4.2a®. Electric field evaluation for different dot sizes has been demonstrated by applying a range of frequencies to the designed electrodes. Results show that the electric field is axisymmetrical around the center of the dot aperture and that it is higher at the dot edges than the dot centers. Furthermore, adding ground plane between adjacent dots increases the electric field strength.

Keywords: Dielectrophoresis; Numerical modeling; Dot microarray electrodes

1. INTRODUCTION

Microfluidic devices have the potential to be used for early detection and diagnosis of disease at Point-of-Care (POC). This is aligned with the current trend of miniaturizing laboratory equipment to achieve better reactions efficiency, faster results, portability and lower reagents consumption. One of the platforms used in microfluidic devices is Lab-on-chip, which is a potential solution for an automated bio-microfluidic diagnostic system that requires the minimum quantity of blood and offers fast and high-throughput results.

Many diagnostic techniques have been employed using lab-on-chip platforms; however, dielectrophoresis (DEP) has been proven to offer a number of advantageous features that many of the other techniques available are unable to provide. These include high selectivity and efficacy, non-

Sensors **2013**, *13*, 9029-9046; doi:10.3390/s130709029

OPEN ACCESS

sensors

ISSN 1424-8220

www.mdpi.com/journal/sensors

Review

Microarray Dot Electrodes Utilizing Dielectrophoresis for Cell Characterization

Bashar Yafouz, Nahrizul Adib Kadri * and Fatimah Ibrahim

Medical Informatics and Biological Micro-Electro-Mechanical Systems (MIMEMS) Specialized Laboratory, Department of Biomedical Engineering, Faculty of Engineering, University of Malaya, 50603 Kuala Lumpur, Malaysia; E-Mails: bashar.yafouz@siswa.um.edu.my (B.Y.); fatimah@um.edu.my (F.I.)

* Author to whom correspondence should be addressed; E-Mail: nahrizuladib@um.edu.my; Tel.: +6-037-967-4581; Fax: +6-037-967-4579.

Received: 7 May 2013; in revised form: 30 May 2013 / Accepted: 14 June 2013 / Published: 12 July 2013

Abstract: During the last three decades; dielectrophoresis (DEP) has become a vital tool for cell manipulation and characterization due to its non-invasiveness. It is very useful in the trend towards point-of-care systems. Currently, most efforts are focused on using DEP in biomedical applications, such as the spatial manipulation of cells, the selective separation or enrichment of target cells, high-throughput molecular screening, biosensors and immunoassays. A significant amount of research on DEP has produced a wide range of microelectrode configurations. In this paper; we describe the microarray dot electrode, a promising electrode geometry to characterize and manipulate cells via DEP. The advantages offered by this type of microelectrode are also reviewed. The protocol for fabricating planar microelectrodes using photolithography is documented to demonstrate the fast and cost-effective fabrication process. Additionally; different state-of-the-art Lab-on-a-Chip (LOC) devices that have been proposed for DEP applications in the literature are reviewed. We also present our recently designed LOC device, which uses an improved microarray dot electrode configuration to address the challenges facing other devices. This type of LOC system has the capability to boost the implementation of DEP technology in practical settings such as clinical cell sorting, infection diagnosis, and enrichment of particle populations for drug development.

Sensors **2014**, *14*, 6356-6369; doi:10.3390/s140406356

OPEN ACCESS

sensors

ISSN 1424-8220

www.mdpi.com/journal/sensors

Article

Dielectrophoretic Manipulation and Separation of Microparticles Using Microarray Dot Electrodes

Bashar Yafouz [1,2], Nahrizul Adib Kadri [1,2,*] and Fatimah Ibrahim [1,2]

[1] Department of Biomedical Engineering, Faculty of Engineering, University of Malaya, 50603 Kuala Lumpur, Malaysia; E-Mails: bashar.yafouz@siswa.um.edu.my (B.Y.); fatimah@um.edu.my (F.I.)

[2] Centre for Innovation in Medical Engineering (CIME), Faculty of Engineering, University of Malaya, 50603 Kuala Lumpur, Malaysia

* Author to whom correspondence should be addressed; E-Mail: nahrizuladib@um.edu.my; Tel.: +6-037-967-4581; Fax: +6-037-967-4579.

Received: 15 November 2013; in revised form: 7 March 2014 / Accepted: 14 March 2014 / Published: 3 April 2014

Abstract: This paper introduces a dielectrophoretic system for the manipulation and separation of microparticles. The system is composed of five layers and utilizes microarray dot electrodes. We validated our system by conducting size-dependent manipulation and separation experiments on 1, 5 and 15 µm polystyrene particles. Our findings confirm the capability of the proposed device to rapidly and efficiently manipulate and separate microparticles of various dimensions, utilizing positive and negative dielectrophoresis (DEP) effects. Larger size particles were repelled and concentrated in the center of the dot by negative DEP, while the smaller sizes were attracted and collected by the edge of the dot by positive DEP.

Keywords: dielectrophoresis (DEP); microparticle separation; dot electrode; microfluidics; BioMEMS

1. Introduction

Particle manipulation and separation techniques have been of interest to many research groups worldwide for various biomedical applications, including cell concentration, separation, patterning,

Bashar Yafouz[1,2]
Nahrizul Adib Kadri[1,2]
Hussin A. Rothan[3]
Rohana Yusof[3]
Fatimah Ibrahim[1,2]

[1]Department of Biomedical Engineering, Faculty of Engineering, University of Malaya, Kuala Lumpur, Malaysia
[2]Centre for Innovation in Medical Engineering (CIME), Faculty of Engineering, University of Malaya, Kuala Lumpur, Malaysia
[3]Department of Molecular Medicine, Faculty of Medicine, University of Malaya, Kuala Lumpur, Malaysia

Received June 19, 2015
Revised October 12, 2015
Accepted October 12, 2015

Research Article

Discriminating dengue-infected hepatic cells (WRL-68) using dielectrophoresis

Dielectrophoresis (DEP), the induced movement of dielectric particles placed in a nonuniform electric field, has been used as a potential technique for manipulation and separation of many biological samples without destructive consequences to the cell. Cells of the same genotype in different physiological and pathological states have unique morphological and structural features, therefore, it is possible to differentiate between them using their DEP responses. This paper reports the experimental discrimination of normal and dengue-infected human hepatic fetal epithelial cells (WRL-68 cells) based on their DEP crossover frequency, at which no resultant movement occurs in the cells in response to the DEP force. A microarray dot electrode was used to conduct the DEP experiments. The DEP forces applied to the cells were quantified by analyzing the light intensity shift within the electrode's dot region based on the Cumulative Modal Intensity Shift image analysis technique. The differences in dielectric properties between infected and uninfected cells were exploited by plotting a unique DEP spectrum for each set of cells. We observed that the crossover frequency decreased from 220 kHz for the normal WRL-68 cells to 140 kHz after infection with the dengue virus in a medium conductivity of 100 μS/cm. We conclude that the change in the DEP crossover frequency between dengue-infected cells and their healthy counterparts should allow direct characterization of these cell types by exploiting their electrophysiological properties.

Keywords:
Dengue / Dielectrophoresis / Image processing / Microarray dot electrode / WRL-68 cells
DOI 10.1002/elps.201500282

1 Introduction

Over the last few decades, dengue fever and dengue hemorrhagic fever have been the most dangerous arboviral diseases in humans. More than 2.5 billion people are at risk of infection in tropical countries, and approximately 50–100 million dengue infections occur annually worldwide [1].

Fast and accurate diagnosis of dengue infection is important to determine the severity of the disease and to take suitable action. The currently available diagnostic methods are virus isolation, nucleic acid detection, and antigen (NS1) or antibody (IgG or IgM) detection via ELISA [1]. Virus separation and nucleic acid detection are more sensitive and specific than ELISA, but these examinations are not commonly offered due to their high cost. Furthermore, ELISA requires bulky instruments and highly trained personnel to perform the test, and it takes time to obtain a result [2]. Therefore, the development of an inexpensive, accurate, and rapid tool for diagnosing dengue is in high demand.

With the growth of microfabrication technology, microfluidic platforms have emerged, offering miniaturization and combination of complex tasks [3, 4]. Sample preparation is an essential step in clinical diagnostic applications, which includes centrifugation, extraction, concentration, chemical reactions, washing, and other laborious practices [5]. Various technologies have been developed for sample preparation prior to analysis using microfluidic systems; however, dielectrophoresis (DEP) has proven to be a promising technique for the manipulation of micro/nanoscale objects, including cells, viruses, DNA, bacteria, and proteins, in aqueous suspensions [6–10].

Previous studies have shown that the electrical properties of cells change when cells transform from healthy to a pathological state [11, 12]. This result is in line with the findings confirming a morphological alteration in cells after infection with dengue virus [13, 14]. Cells of the same genotype in different physiological and pathological states have unique morphological and structural features, therefore, it is possible to discriminate between these cells using their

Correspondence: Dr. Nahrizul Adib Kadri, Department of Biomedical Engineering, Faculty of Engineering, University of Malaya, 50603 Kuala Lumpur, Malaysia
E-mail: nahrizuladib@um.edu.my
Fax: +6-037-967-4579

Abbreviations: DEP, dielectrophoresis; **n-DEP**, negative dielectrophoresis; **p-DEP**, positive dielectrophoresis; **ROI**, region of interest; **WRL-68 cells**, human hepatic fetal epithelial cells

Colour Online: See the article online to view Figs. 1, 3–5 in colour.

A Numerical Analysis of Electric Field Strength Over Planar Microarray Dot Electrode for Dielectrophoretic Lab-On-Chip Device

B. Yafouz[1], N.A. Kadri[1], F. Ibrahim[1]

[1] Medical Informatics and Biological Micro-Electro-Mechanical Systems (MIMEMS) Specialized Laboratory, Department of Biomedical Engineering, Faculy of Engineering, University of Malaya, 50603 Kuala Lumpur, Malaysia

***Abstract*—Dielectrophoresis (DEP) has been proven as a method of manipulating and analyzing the electrophysiological properties of bioparticles by applying non-uniform electric fields generated through special electrodes. Various electrode geometries have been developed to address different applications. Simulation of the electric field strength over electrodes is essential in order to optimize the generated DEP force for enhancing cell manipulation. This paper describes the study of electric field distribution over planar multiple microarray dot electrode using numerical modeling of Comsol Multiphysics 4.2a®. Results show that the electric field strength is axisymmetrical around the centre of the dot aperture and that is higher at the dot edges than the dot centers. Further studies will be conducted to investigate the effect of applying different frequencies, varying dots size and adding ground plane in between the electrode dots.**

***Keywords*—Lab-on-Chip, dielectrophoresis, numerical modeling, dot microarray electrodes**

I. INTRODUCTION

Microfluidic devices have the potential to be used for early detection and diagnosis of disease at Point-of-Care (POC). This is aligned with the current trend of miniaturizing laboratory equipment to achieve better reactions efficiency, faster results, portability and lower reagents consumption. One of the platforms used in microfluidic devices is Lab-on-chip, which is a potential solution for an automated bio-microfluidic diagnostic system that requires the minimum quantity of blood and offers fast and high-throughput results.

Many diagnostic techniques have been employed using lab-on-chip platforms; however, dielectrophoresis (DEP) has been proven to offer a number of advantageous features that many of the other techniques available are unable to provide. These include high selectivity and efficacy, non-invasiveness and low cost. DEP has been used as a method for cell manipulation and characterization since its discoverer Pohl [1] launched a novel technique for separating living cells from admixed dead ones, taking advantage of the unique electrical properties of each bioparticle [2].

DEP is the phenomenon that describes the motion of polarizable particles through a non-uniform electric field. One of the core strengths of DEP is that the characterization of different cells depends only on the dielectric properties controlled by the particle's individual phenotype. Hence, the process does not require specific tags or involve chemical reactions [3].

The DEP force depends on the applied frequency and geometry of the electrodes used to generate the electric field. Different electrode geometries have been used in previous studies for different applications. This study provides a numerical analysis of the electric field generated by a 4x4 planar multiple microarray dot electrode, which is a modification of that used by Fatoyinbo *et al.* [4]. This electrode will be used to conduct DEP expirements as a sample preparation prior to the stage of infectious dieases diagnosis.

A. Dielectrophoretic Theory

Applying a non-uniform electric field to polarizable particles that are placed in a conductive medium produces DEP force. The magnitude and direction of the DEP force depend on the relative polarizability of the particle and the surrounding medium [5]. The DEP force acting on a spherical particle can by expressed by the following equation [6]:

$$\langle \vec{F}_{DEP} \rangle = 2\pi r^3 \varepsilon_o \varepsilon_m \,\mathrm{Re}[K(\omega)]\nabla E^2 \tag{1}$$

where ε_o is the permittivity of free space, ε_m is the permittivity of the surrounding medium, r is the particle radius, ∇E is the electric field gradient and $Re[K(\omega)]$ is the real part of Clausius-Mossotti factor which is defined as:

$$K(\omega) = \frac{\varepsilon_p^* - \varepsilon_m^*}{\varepsilon_p^* + 2\varepsilon_m^*} \tag{2}$$

where ε^* is the complex permittivity and subscripts p and m denote particles and medium, respectively. Moreover, the complex permittivity ε^* is described by:

$$\varepsilon^* = \varepsilon - j\frac{\sigma}{\omega} \tag{3}$$

where ε is the permittivity, $j = \sqrt{-1}$, σ is the conductivity and ω is the angular frequency of the applied AC electric field. The value of $Re[K(\omega)]$ for a sphere ranges between -0.5 and 1, and depends on the frequency of the applied AC

978-1-4673-1666-8/12/$31.00 ©2012 IEEE

Lab-on-a-Chip Particles Manipulation for Point-of-Care Diagnostic Systems Utilizing Dielectrophoresis

Bashar Yafouz, *Graduate Student Member, IEEE*, Nahrizul Adib Kadri, and Fatimah Ibrahim, *Member, IEEE*

***Abstract*— Particle manipulation has attracted the attention of many researchers around the globe for various biomedical applications. Although several methods have been utilized to sort particles on lab-on-a-chip platforms, dielectrophoresis (DEP) possess exclusive advantages over other methods. In this paper, we investigated microarray dot electrodes to manipulate microparticles. The geometry of the dot electrode enjoys unique benefits compared to other geometries, including enclosed areas of analysis and strong electric field with axisymmetrical distribution. DEP experiments were conducted to manipulate 1 µm polystyrene particles using the developed DEP system. Results showed that the response of the microparticle populations can be controlled by merely adjusting the applied frequency to induce either positive or negative DEP effects. In negative DEP case, microparticles were gathered at the dot center, while microparticles were collected at the dot edge in the case of positive DEP. Such microarray dot platforms can be utilized to develop economical point-of-care (POC) diagnostic systems by analyzing the transmitted light variations inside the dot regions.**

I. INTRODUCTION

The manipulation of microparticles is essential for various applications in biological and chemical analysis systems [1]. Current procedures require bulky and costly instruments with highly trained personnel. The advancements in microfabrication technology paved the way towards miniaturizing the biomedical instruments aiming for point-of-care (POC) inexpensive devices. This leaded to the implementation of microfluidic systems featuring many advantages include high throughput efficiency, parallelism, low sample size requirement and faster results [2-4].

This research is supported by University of Malaya High Impact Research Grant UM-MOHE UM.C/625/1/HIR/MOHE/05 from the Ministry of Higher Education Malaysia and University of Malaya Research Grant (UMRG: RP009A-13AET).

Bashar Yafouz is with the Department of Biomedical Engineering, Faculty of Engineering, University of Malaya, 50603 Kuala Lumpur, Malaysia, and the Centre for Innovation in Medical Engineering (CIME), Faculty of Engineering, University of Malaya, 50603 Kuala Lumpur, Malaysia (e-mail: bashar.yafouz@siswa.um.edu.my),

Nahrizul Adib is with the Department of Biomedical Engineering, Faculty of Engineering, University of Malaya, 50603 Kuala Lumpur, Malaysia, and the Centre for Innovation in Medical Engineering (CIME), Faculty of Engineering, University of Malaya, 50603 Kuala Lumpur, Malaysia (phone: +6-0379674581; fax: : +6-0379674579; e-mail: nahrizuladib@um.edu.my).

Fatimah Ibrahim is with the Department of Biomedical Engineering, Faculty of Engineering, University of Malaya, 50603 Kuala Lumpur, Malaysia, and the Centre for Innovation in Medical Engineering (CIME), Faculty of Engineering, University of Malaya, 50603 Kuala Lumpur, Malaysia (e-mail: Fatimah@um.edu.my).

Many techniques were explored to manipulate particles in suspending medium, including mechanical [5], chemical [6], optical [7], magnetic [8], thermal [9] and electrical. Dielectrophoresis (DEP), under the latter category, has been used extensively in the last few decades for manipulating and separating microparticles [10].

DEP offers exclusive advantages over other techniques implemented in microfluidics platforms. DEP differentiate cells/particles based simply on their dielectric properties; specifically conductivity and permittivity, which are determined by the phenotype of the respective particles. This feature allows the separation and manipulation of particles on micro and nano levels efficiently.

Since the discovery of DEP, electrodes of different configurations and geometries have been introduced. Each of these electrodes was designed to address a specific task. In this paper, DEP device, based on 4 × 4 microarray dot electrode presented in our previous work in [11], was used to manipulate microparticles by merely changing the applied frequency. Electric field simulations showed that dot electrode features enclosed areas of analysis and strong electric field with axisymmetrical distribution [12, 13]. Furthermore, dot electrodes do not require field mapping or image registration to quantify the force experienced by the target particles. This is because quantifying the DEP force generated by radial electrodes can be done by analyzing the change shifts in the light across the dot electrode before and after switching on the device [14].

II. THEORY

DEP of particles is an electrokinetic phenomenon which takes place when placing a polarizable particle in a non-uniform electric field. In DEP, particles experience a translational force due to the interactions between an applied non-uniform electric field and dipoles generated within polarized particles [15]. The DEP force experienced by a spherical particle with radius r is given by:

$$\langle \vec{F}_{DEP} \rangle = 2\pi r^3 \varepsilon_o \varepsilon_m \, \mathrm{Re}[K(\omega)] \nabla E^2 \quad (1)$$

where ε_o and ε_m is the permittivity of free space and the relative permittivity of the suspending medium; respectively, ∇E indicates the electric field gradient, while $\mathrm{Re}[K(\omega)]$ is the term that reflects the real part of Clausius-Mossotti function which can be described as:

$$K(\omega) = \frac{\varepsilon_p^* - \varepsilon_m^*}{\varepsilon_p^* + 2\varepsilon_m^*} \quad (2)$$

978-1-4799-4084-4/14/$31.00 ©2014 IEEE

APPENDICES

APPENDIX A: MATLAB CODE FOR CALCULATING CUMULATIVE PIXEL INTENSITY VALUES

```
%    This MATLAB code is for calculating the cumulative pixel intensity value of the images before and after the signal application explained in Subsection 3.5.3.

%    Bashar Yafouz, 2015.



close all

clear all

%    (1) Reading the image into MATLAB workplace

color = imread('D:\BASHAR\1kHz\before1.jpg');

%    (2) Converting the colored image to grayscale image

gray = rgb2gray(color);

%    (3) Calculating the histogram of the image

[histogram,x] = imhist(gray);

%    (4) Obtaining the peak pixel

peak_pixels = max(histogram);

peak_pixel = max(peak_pixels);
```

```
%    (5) Obtaining the pixel value of the peak pixel

peak_value = find([histogram(:)] == peak_pixel)-1;

%    (6) Calculating the cumulative pixel values of the
image histogram from the peal value to the maximum light
intensity value of the histogram (i.e., 255)

sum_pixel = 0;

for i = peak_value:255

sum_pixel = sum_pixel + histogram(i+1);

end

%    (7) Displaying the total cumulative pixel values

sum_pixel
```

APPENDIX B: MATLAB CODE FOR PLOTTING DEP SPECTRA

```
%    This MATLAB code is for plotting the DEP spectra of the normal and infected cells as shown in Figure 4.17.

%    Bashar Yafouz, 2015.



close all

clear all

%    (1)   Data   Importing   (f,   i_healthy,   i_infected, e_healthy, e_infected)

importdata('D:\BASHAR\Data_FINAL.mat');

%    (2) Initializing the Figure

f_ = clf;

figure(f_);

ax_ = axes;

set(ax_,'Box','on');

hold on;

%    (3) Plotting the measured intensity shift values of the normal and infected cells versus frequency

h_ = scatter(f,i_healthy);
```

```
h_ = scatter(f,i_infected);

%    (4) Creating best-fit model based on sigmoid function

fo_=fitoptions('method','NonlinearLeastSquares','Normalize'
,'on');

ok_ = isfinite(f) & isfinite(i_healthy);

st_ = [-1.698 0.51600000000000001 0.61899999999999999 ];

set(fo_,'Startpoint',st_);

ft_ = fittype('a*exp(-b*x)+c',...

     'dependent',{'y'},'independent',{'x'},...

     'coefficients',{'a', 'b', 'c'});

%    (5) Fitting the model on the plotted measured values

cf_healthy= fit(f(ok_),i_healthy(ok_),ft_,fo_);

cf_infected= fit(f(ok_),i_infected(ok_),ft_,fo_);

%    (6) Plotting the best-fit curves

h_ = plot(cf_healthy,'fit',0.95);

h_ = plot(cf_infected,'fit',0.95);

set(gca, 'XScale', 'log');
```

```
%     (7) Plotting the error bars

errorbar(f,i_healthy,e_healthy);

errorbar(f,i_infected,e_infected);
```

APPENDIX C: PERFORMANCE EVALUATION OF STATISTICAL ANALYSIS

T-Test

Group Statistics

	Type	N	Mean	Std. Deviation	Std. Error Mean
Normalized_Intensity_Shift	Healthy WRL-68 Cells	60	-1.9086667E-1	.52115330	.06728060
	Dengue-infected WRL-68 Cells	60	.0062000	.54189694	.06995859

Independent Samples Test

		Levene's Test for Equality of Variances		t-test for Equality of Means						
		F	Sig.	t	df	Sig. (2-tailed)	Mean Difference	Std. Error Difference	95% Confidence Interval of the Difference	
									Lower	Upper
Normalized_Intensity_Shift	Equal variances assumed	.219	.640	-2.030	118	.045	-.19706667	.09706124	-.38927435	-.00485899
	Equal variances not assumed			-2.030	117.821	.045	-.19706667	.09706124	-.38927738	-.00485596

APPENDIX D: MATLAB CODE FOR PLOTTING RE[K(ω)] VERSUS FREQUENCY

```
%    This MATLAB code is for plotting Re[K(ω)] versus frequency for 1, 5 and 15 µm polystyrene particles as shown in Figure 4.8 and explained briefly in Subsection 4.3.1.

%    Bashar Yafouz, 2015.



close all

clear all

%    (1) Defining a frequency range (f) from 1 kHz to 10 MHz

f = [1000: 1000: 10000000];

%    (2) Calculating the angular frequency (w)

w = 2*pi*f;

%    (3) Defining the vacuum permittivity (eo)

eo = 8.854187817 * 10^-12;

%    (4) Calculating the complex permittivity (em) of the medium (DI H2O) using Equation 2.3, where Ɛ_H2O = 78 and σ_H2O = 2×10^-4 S/m
```

```
for x=1:10000

em(1,x)=eo*78-i*(2*10^-4/w(1,x));

end
```

% (5) Calculating the complex permittivity of the 1µm polystyrene particles (*ep1*) using Equation 2.3, where $\varepsilon_{1\mu m}$ = 2.5 and $\sigma_{1\mu m}$ = 4.6×10^{-3} S/m

```
for x=1:10000

ep1(1,x)=eo*2.5-i*(4.6*10^-3/w(1,x));

end
```

% (6) Calculating Clausius-Mossotti factor of the 1µm polystyrene particles (*K1*) using Equation 2.2

```
for x=1:10000

K1(1,x)=(ep1(1,x)-em(1,x))/(ep1(1,x)+2*em(1,x));

end
```

% (7) Calculating the complex permittivity of the 5µm polystyrene particles (*ep5*) using Equation 2.3, where $\varepsilon_{5\mu m}$ = 2.5 and $\sigma_{5\mu m}$ = 7.8×10^{-4} S/m

```
for x=1:10000

ep5(1,x)=eo*2.5-i*(7.8*10^-4/w(1,x));

end
```

```
%    (8) Calculating Clausius-Mossotti factor of the 5µm
polystyrene particles (K5) using Equation 2.2

for x=1:10000

K5(1,x)=(ep5(1,x)-em(1,x))/(ep5(1,x)+2*em(1,x));

end

%    (9) Calculating the complex permittivity of the 15µm
polystyrene particles (ep15) using Equation 2.3, where ε15µm
= 2.5 and σ15µm = 2×10^-4 S/m

for x=1:10000

ep15(1,x)=eo*2.5-i*(2*10^-4/w(1,x));

end

%    (10) Calculating Clausius-Mossotti factor of the 15µm
polystyrene particles (K15) using Equation 2.2

for x=1:10000

K15(1,x)=(ep15(1,x)-em(1,x))/(ep15(1,x)+2*em(1,x));

End

%    (11) Plotting K1, K5 and K15 versus f in LOG scale

semilogx(f,K1,f,K5,'m--',f,K15,'g-.','LineWidth',2)
```

APPENDIX E: INTENSITY SHIFT CALCULATIONS FOR NORMAL AND DENGUE-INFECTED CELLS

Intensity shift calculations for normal WRL-68 cells for frequency range from 1 kHz to 5 MHz.

Freq.	Cumulative Pixel Value (Before DEP)	Cumulative Pixel Value (After DEP)	Intensity Shift	Normalized Intensity Shift	Average Intensity Shift	Standard Error
1 kHz	3689	2811	-878	-0.878	-0.83775	0.057690987
	3563	2790	-773	-0.773		
	3126	2320	-806	-0.806		
	3231	2337	-894	-0.894		
2 kHz	3547	2814	-733	-0.733	-0.7995	0.096140522
	3541	2787	-754	-0.754		
	3256	2314	-942	-0.942		
	3014	2245	-769	-0.769		
5 kHz	3475	2745	-730	-0.73	-0.753	0.020379728
	3651	2884	-767	-0.767		
	3387	2614	-773	-0.773		
	2987	2245	-742	-0.742		
10 kHz	3577	2884	-693	-0.693	-0.68625	0.017576025
	3492	2784	-708	-0.708		
	3591	2918	-673	-0.673		
	3867	3196	-671	-0.671		
20 kHz	3125	2450	-675	-0.675	-0.676	0.012516656
	3489	2801	-688	-0.688		
	3304	2645	-659	-0.659		
	3658	2976	-682	-0.682		

50 kHz	3683	3022	-661	-0.661	-0.621	0.027652607
	3394	2792	-602	-0.602		
	3343	2725	-618	-0.618		
	3568	2965	-603	-0.603		
100 kHz	4162	3639	-523	-0.523	-0.5395	0.049695741
	3791	3295	-496	-0.496		
	3588	3060	-528	-0.528		
	3632	3021	-611	-0.611		
150 kHz	3490	3287	-203	-0.203	-0.21875	0.054944669
	3947	3702	-245	-0.245		
	3400	3123	-277	-0.277		
	3159	3009	-150	-0.15		
200 kHz	3862	3834	-28	-0.028	-0.02375	0.01255322
	3104	3094	-10	-0.01		
	3639	3621	-18	-0.018		
	3806	3767	-39	-0.039		
250 kHz	3264	3405	141	0.141	0.159	0.016812694
	3372	3521	149	0.149		
	3027	3196	169	0.169		
	3636	3813	177	0.177		
300 kHz	2885	3221	336	0.336	0.33625	0.105594744
	3924	4239	315	0.315		
	2937	3412	475	0.475		
	3111	3330	219	0.219		

500 kHz	3656	4084	428	0.428	0.4375	0.090632959
	2799	3225	426	0.426		
	2978	3536	558	0.558		
	3429	3767	338	0.338		
1 MHz	3571	3997	426	0.426	0.44375	0.047821718
	2759	3271	512	0.512		
	3407	3843	436	0.436		
	2726	3127	401	0.401		
2 MHz	3214	3632	418	0.418	0.44425	0.029170476
	2951	3395	444	0.444		
	3510	3995	485	0.485		
	3984	4414	430	0.43		
5 MHz	2886	3515	629	0.629	0.47175	0.131345283
	3201	3722	521	0.521		
	3487	3896	409	0.409		
	3589	3917	328	0.328		

Intensity shift calculations for Dengue-infected WRL-68 cells for frequency range from 1 kHz to 5 MHz.

Freq.	Cumulative Pixel Value (Before DEP)	Cumulative Pixel Value (After DEP)	Intensity Shift	Normalized Intensity Shift	Average Intensity Shift	Standard Error
1 kHz	3062	2326	-736	-0.736	-0.68025	0.043115156
	3455	2823	-632	-0.632		
	1548	864	-684	-0.684		
	2845	2176	-669	-0.669		
2 kHz	2314	1749	-565	-0.565	-0.66925	0.085077905
	2813	2041	-772	-0.772		
	2357	1699	-658	-0.658		
	3049	2367	-682	-0.682		
5 kHz	3149	2476	-673	-0.673	-0.65075	0.03081531
	2901	2282	-619	-0.619		
	2764	2134	-630	-0.63		
	2345	1664	-681	-0.681		
10 kHz	3096	2563	-533	-0.533	-0.597	0.063071388
	2512	1828	-684	-0.684		
	2080	1496	-584	-0.584		
	1839	1252	-587	-0.587		
20 kHz	2854	2352	-502	-0.502	-0.562	0.072539644
	2641	1991	-650	-0.65		
	3025	2432	-593	-0.593		
	2654	2151	-503	-0.503		

50 kHz	3255	2776	-479	-0.479	-0.451	0.060332413
	2847	2482	-365	-0.365		
	2803	2300	-503	-0.503		
	1963	1506	-457	-0.457		
100 kHz	2554	2370	-184	-0.184	-0.0865	0.077689553
	3064	3014	-50	-0.05		
	2970	2966	-4	-0.004		
	2568	2460	-108	-0.108		
150 kHz	2980	3071	91	0.091	0.097	0.037876994
	2438	2581	143	0.143		
	3201	3304	103	0.103		
	3571	3622	51	0.051		
200 kHz	3284	3634	350	0.35	0.33725	0.053618249
	3039	3442	403	0.403		
	3600	3921	321	0.321		
	2908	3183	275	0.275		
250 kHz	3106	3580	474	0.474	0.41825	0.054020829
	3741	4110	369	0.369		
	3507	3882	375	0.375		
	2700	3155	455	0.455		
300 kHz	2943	3325	382	0.382	0.39625	0.042460766
	2175	2629	454	0.454		
	2863	3259	396	0.396		
	3326	3679	353	0.353		

500 kHz	3865	4412	547	0.547	0.5365	0.045317399
	2950	3490	540	0.54		
	3866	4341	475	0.475		
	3270	3854	584	0.584		
1 MHz	3019	3670	651	0.651	0.683	0.02258318
	3199	3886	687	0.687		
	3756	4446	690	0.69		
	2746	3450	704	0.704		
2 MHz	2803	3455	652	0.652	0.6685	0.011120552
	2856	3528	672	0.672		
	3159	3835	676	0.676		
	3734	4408	674	0.674		
5 MHz	2670	3369	699	0.699	0.653	0.04433208
	2769	3402	633	0.633		
	2594	3273	679	0.679		
	2573	3174	601	0.601		